ปฏิกิริยาอัลคิลเลชันของโทลูอีนกับเมทานอลบนตัวเร่งปฏิกิริยาซีโอไลต์ชนิดเอ็มเอฟไอที่เติมเหล็กหรือสังกะสี

นาย ธนา พูนทรัพย์สวัสดิ์

วิทยานิพนธ์นี้เป็นส่วนหนึ่งของการศึกษาตามหลักสูตรปริญญาวิศวกรรมศาสตรดุษฎีบัณฑิต
สาขาวิชาวิศวกรรมเคมี ภาควิชาวิศวกรรมเคมี
คณะวิศวกรรมศาสตร์ จุฬาลงกรณ์มหาวิทยาลัย
ปีการศึกษา 2543

ISBN 974-346-315-1

ALKYLATION OF TOLUENE WITH METHANOL ON Fe OR Zn CONTAINING MFI-TYPE ZEOLITE CATALYST

Mr. Thana Punsupsawat

A Dissertation Submitted in Partial Fulfillment of the Requirements
for the Degree of Doctor of Engineering in Chemical Engineering
Department of Chemical Engineering
Faculty of Engineering
Chulalongkorn University
Academic Year 2000

ISBN 974-346-315-1

Thesis Title	ALKYLATION OF TOLUENE WITH METHANOL ON Fe OR Zn CONTAINING MFI-TYPE ZEOLITE CATALYST
By	Mr. Thana Punsupsawat
Department	Chemical Engineering
Thesis Advisor	Dr. Suphot Phatanasri, Dr.Eng.
Thesis Co-advisor	Professor Piyasan Praserthdam, Dr.Ing.

Accepted by the Faculty of Engineering, Chulalongkorn University in Partial Fulfillment of the Requirements for the Doctor's Degree

……...…Dean of Faculty of Engineering
(Professor Somsak Panyakeow, Dr. Eng.)

Thesis Committee

…….Chairman
(Professor Wiwat Tanthapanichakoon, Ph.D.)

…….Thesis Advisor
(Suphot Phatanasri, Dr.Eng.)

…….Thesis Co-advisor
(Professor Piyasan Praserthdam, Dr.Ing.)

……..…Member
(Assistant Professor Tharathon Mongkhonsi, Ph.D.)

……..…Member
(Aticha Chaisuwan, Ph.D.)

ธนา พูนทรัพย์สวัสดิ์ : ปฏิกิริยาอัลคิลเลชันของโทลูอีนกับเมทานอลบนตัวเร่งปฏิกิริยาซีโอไลต์ชนิดเอ็มเอฟไอ ที่เติมเหล็กหรือสังกะสี (ALKYLATION OF TOLUENE WITH METHANOL ON Fe OR Zn CONTAINING MFI-TYPE ZEOLITE CATALYST) อ.ที่ปรึกษา : ดร. สุพจน์ พัฒนะศรี , อ. ที่ปรึกษาร่วม : ศ. ดร. ปิยะสาร ประเสริฐธรรม, 99 หน้า, ISBN 974-346-315-1.

ปฏิกิริยาอัลคิลเลชันระหว่างโทลูอีนกับเมทานอล ได้ศึกษาบนตัวเร่งปฏิกิริยาซีโอไลต์ชนิดเอ็มเอฟไอที่เติมโลหะเหล็กหรือสังกะสีในปริมาณร้อยละ 0 ถึง 2 โดยน้ำหนัก และตัวเร่งปฏิกิริยาที่ใช้จะถูกเตรียมขึ้นด้วยกรรมวิธีที่แตกต่างกัน ได้แก่ วิธีแลกเปลี่ยนไอออน(ion exchanged) และวิธีเติมโลหะเข้าไปในโครงสร้าง(incorporation) และวิเคราะห์คุณลักษณะของตัวเร่งปฏิกิริยาที่เตรียมขึ้นด้วยเทคนิค XRD, XRF, BET, FTIR และศึกษาเทคนิคการดูดซับไพริดีนด้วยวิธี in-situ FTIR ผลการวิจัยที่ได้แสดงให้เห็นว่าตัวเร่งปฏิกิริยาทั้ง H-Fe,Al-silicate ที่มีสัดส่วนอะตอมของ Si/Fe เท่ากับ 150 และตัวเร่งปฏิกิริยา H-Zn,Al-silicate ที่มีสัดส่วนอะตอมของ Si/Zn เท่ากับ 150 จะให้ผลการเลือกเกิด *p*-xylene ได้ดีเท่าเทียมกับที่ได้จากตัวเร่งปฏิกิริยา Fe(0.8)/H-MFI และ Zn(1.0)/H-MFI ที่มีสัดส่วนของโลหะเหล็กหรือสังกะสีใกล้เคียงกัน การเลือกเกิด *p*-xylene ที่ดีขึ้นบนตัวเร่งปฏิกิริยาทั้ง H-Fe,Al-slicate(Si/Fe=150) และ H-Zn,Al-silicate(Si/Zn=150) เป็นเพราะความแรงของกรดแบบบรอนสเตดอ่อนกว่าที่วัดได้จากตัวเร่งปฏิกิริยาทั้ง Fe(0.8)/H-MFI และ Zn(1.0)/H-MFI เป็นผลให้ปฏิกิริยาไอโซเมอไรเซชันของ *p*-xylene ซึ่งเป็นผลิตภัณฑ์ตัวแรกที่เกิดขึ้นถูกยับยั้ง

ภาควิชา .....วิศวกรรมเคมี..... ลายมือชื่อนิสิต .....

สาขาวิชา .....วิศวกรรมเคมี..... ลายมือชื่ออาจารย์ที่ปรึกษา .....

ปีการศึกษา ....2543..... ลายมือชื่ออาจารย์ที่ปรึกษาร่วม .....

C817804: MAJOR CHEMICAL ENGINEERING
KEY WORD: ION-EXCHANGE METHOD / INCORPORATION METHOD / MODIFIED MFI ZEOLITES / TOLUENE METHYLATION
THANA PUNSUPSAWAT: ALKYLATION OF TOLUENE WITH METHANOL ON Fe OR Zn CONTAINING MFI-TYPE ZEOLITE CATALYST. THESIS ADVISOR : SUPHOT PHATANASRI, Dr.Eng., THESIS COADVISOR : PROFESSOR PIYASAN PHASERTHDAM, Dr.Ing., 99 pp.
ISBN 974-346-315-1

Alkylation of toluene with methanol was investigated on MFI-type zeolite catalysts containing Fe or Zn within the range of 0-2 % as an active component. The catalytic performances were compared on catalysts to which Fe or Zn was introduced by different method, i.e. ion-exchanged and incorporation method. The prepared catalysts were characterized by XRD, XRF, BET, FTIR and pyridine adsorption technique on in-situ FTIR. The results show that both H-Fe,Al-silicate (Si/Fe=150) and H-Zn,Al-silicate (Si/Zn=150) exhibited catalyst activity and xylene selectivity approximately comparable with those of Fe(0.8)/H-MFI and Zn(1.0)/H-MFI with nearly the same amount of the corresponding Fe or Zn. The higher *p*-xylene distribution was achieved with H-Fe,Al-silicate (Si/Fe=150) and H-Zn,Al-silicate (Si/Zn=150) because of the weaker Brönsted acid strengths than those of Fe(0.8)/H-MFI and Zn(1.0)/H-MFI. Therefore, the isomerization of *p*-isomer produced primarily was suppressed by H-Fe,Al-silicate(si/Fe=150) and H-Zn,Al-silicate(Si/Zn=150) better than by Fe(0.8)/H-MFI and Zn(1.0)/H-MFI.

ภาควิชา .....วิศวกรรมเคมี..... ลายมือชื่อนิสิต .....
สาขาวิชา .....วิศวกรรมเคมี..... ลายมือชื่ออาจารย์ที่ปรึกษา .....
ปีการศึกษา ....2543..... ลายมือชื่ออาจารย์ที่ปรึกษาร่วม .....

ACKNOWLEDGEMENT

The author would like to express the appreciation to the Thailand Research Fund (TRF) which partly supported this work.

CONTENTS

LIST OF TABLES

LIST OF FIGURES

CHAPTER I

INTRODUCTION

The mixture of xylene from the reformates has three isomer: *ortho*, *para* and *meta*. Separation of this three isomers is difficult, due to the close proximity of their boiling points. It is futher complicated by the relatively low ratio of *para*-xylene (about 24 wt% of the total xylene). *Para*-xylene is the most important intermediate for producing terephtalic acid, which is used for the production of polyesters, the most important synthetic fiber raw materials. Catalytic oxidation of *ortho*-xylene gives phthalic anhydride for the production of platicizers. *Meta*-xylene, although the major component of the xylene mixture from catalytic reforming, is the least utilized of the three isomers for chemical production. It is usually isomerized to the other two isomers [1]. Initially, xylene synthesization from alkylation of toluene with methanol use catalyst such as chlorinated alumina or aluminium chloride, which have high degree of corrosion and symptom of pollutes. Faujasite and mordenite were used later but not worldwide in spite of great *para*-xylene selectivity because high deactivation due to coking [2]. Until 1972, Mobil Oil Corp. published zeolite ZSM-5 (MFI-type) as catalyst which synthesized liquid fuel from methane [3]. Because of the unique catalytic performance, ZSM-5 was wildly used in a lot of commercial processes.

ZSM-5 is an aluminosilicate crystal having the MFI pore structure. The aluminium ingredient in ZSM-5 is responsible for the formation of strong acid sites for various reactions. The pore structure of ZSM-5 leads to various types of shape selectivity, reactant shape selectivity, product shape selectivity and transition state shape selectivity. The three dimensional pore structure of ZSM-5 is considered to be responsible for its long catalyst life. Many researchers tried to modify ZSM-5 in order to alter the selectivities of the alkylaromatics produced. A typical example is the ion-exchanged or incorporation of ZSM-5 with various metals which significantly increases the selectivity of *para*-xylene [4-7].

The influence of the preparation method i.e. ion-exchanged or incorporation method on the location of loading metals and their role for the catalytic properties were briefly reported up to now. Therefore, this research tried to vary the location of loading metals by applying different loading method in order to obtain the relation between the structural properties and the catalytic activity of the modified HZSM-5 catalysts in alkylation of toluene with methanol. Moreover, the effects of reaction temperature, space velocity, and time-on-stream were also studied.

The Objective of This Research

1. To compare the catalytic performances of MFI-type zeolite catalysts containing Fe or Zn within the range of 0-2 % loading as an active component, that introduced by different methods, i.e. ion-exchanged and incorporation method on alkylation of toluene with methanol. Characterization of prepared catalysts are also included.
2. To investigate the effect of reaction temperatures, space velocities and times-on-stream for this reaction.

The Scope of This Research

1. Introducing transition metals such as Fe or Zn into MFI-type zeolite catalysts within the range 0-2 % loading by different methods, i.e. ion-exchanged and incorporation methods.
2. Characterizing the prepared catalysts by following methods:
   - Analyzing structure of catalysts by X-ray Diffraction (XRD).
   - Analyzing bulk concentration of each component by X-ray Fluorescence Spectrometer (XRF).
   - Analyzing morphology of crystals by Scanning Electron Microscope (SEM).
   - Analyzing surface areas of catalysts by Brunauer-Emmett-Teller (BET) Surface Areas Measurement .

- Analyzing zeolite acidity by pyridine adsorption technique on *in-situ* FTIR.

3. Investigating the performances of the prepared catalysts on the alkylation of toluene with methanol under the following conditions:

- Atmospheric pressure
- Reaction temperatures 350-550 ^{o}C
- Space velocities 2,000-10,000 h^{-1}
- Time-on-stream 0-6 h

The reaction feeds and products were analyzed by Gas Chromatograph (GC).

CHAPTER II

LITERATURE REVIEW

In 1972, Mobil Oil Corp. published zeolite "ZSM-5" that is the catalyst which synthesized liquid fuel from methane (The MTG Process) [3]. The investigation of shape-selective zeolite was undertaken in many laboratories. Some of the more prominent studied on modified ZSM-5 for alkylation process are summarized below.

Yashima et al. [8] believed that formaldehyde, formed *in-situ* from methanol dehydrogenation, is the actual alkylating reagent and the major side chain during toluene alkylation over solid bases is the formation of carbon monoxide from decomposition of the alkylating agent. In the sequent paper, they reported that modified HZSM-5 (modified with Mg, P and B) and metallosilicates with MFI zeolite structure (modified with Fe, B Ga, Sb and As) exhibited much higher *para*-selectivities than unmodified HZSM-5 zeolites. The weaker acid sites on the catalysts with ZSM-5 zeolites structure provide the higher *para*-selectivity, because in the narrow pores the isomerization of *para*-isomer which is produced primarily through "restricted transition-state selectivity" is suppressed and required strong acid sites, compared with the alkylation [5].

Itoh et al. [9, 10] described the cooperation of Lewis acid/base pairs in the mechanism of toluene alkylation. A base site activates the methyl group of toluene, whereas the acid site interacts with the aromatic ring.

Kaeding et al. [4] studied selective alkylation of toluene with methanol on ZSM-5 type zeolite. They proposed that the high *para*-selectivity of modified HZSM-5 zeolites (such as impregnation with Mg or Ni) was due to "product selectivity" namely the intracrystalline diffusivity of *para*-isomer was much higher than those of the other two isomers.

A detailed study of the acidity of surface hydroxyls in H-B-ZSM-5, H-Fe-ZSM-5, H-Ga-ZSM-5 and H-ZSM-5 has been carried out by Chu and Chang [11]. They showed the following relation among the acidity strength of the bridged M(OH)Si hydroxyls :

SiOH < B(OH)Si << Fe(OH)Si < Ga(OH)Si < Al(OH)Si

Paparatto et al. [12] reported that *para*-isomer formed selectively inside the ZSM-5 channels, while the isomerization proceeded just on the external surface and modification of the zeolite suppressed the activity of external surface sites resulting in improvement of *para*-alkylated product selectivity.

Chen [13] and Franenkel and Levy [14] reported that large crystal zeolite samples provided higher *para*-selectivity than small crystal samples (with a larger external surface). For this reason, they suggested that undesirable processes occur on the external active site; e.g., *p*-xylene isomerization to other xylenes.

Kim et al. [15, 16] and Lonyi et al. [17] reported that the number of Brönsted acid sites decreased with zeolite modified by isomorphous substitution of Ga, Fe, B and that this decelerates the side reactions more effectively than the formation of primary product, *para*-isomer. This implied that *para*-selectivity is higher on zeolite with lower acidity.

The effect of ion-exchange with transition metal for the protons of HZSM-5 reported by Inui et al. [18]. The protons of H-ZSM-5 having Si/Al atomic ratio 40 were ion-exchanged with an aqueous solution of various kinds of transition metal salts. The amount of metal exchanged was set at 0.5 wt%, the aromatic selectivity increased by :

Zn > Ga > Ni > Cr > Co > V > Mn > H

Mirth and Lercher [19] studied *in-situ* FTIR on the surface species during the methylation of toluene over HZSM-5 in the range 100-400 ^{o}C. They showed that this reaction follows Langmuir-Hinshelwood (LH) kinetics; both the toluene and the alkylating agent molecules form a coadsorption complex over the catalyst surface.

Toluene ethylation with ethanol over Al-MFI, B-, Fe-, Ga-isomorphously substituted zeolites of MFI structure was investigated by Parikh et al. [20]. The acid properties of the metallosilicates increased in the order B < Fe < Ga < Al. This order is reflected in the activity of the zeolites in term of toluene conversion. Influence of crystal size variation on *para*-selectivity was much more than the change in acidity by isomorphous substitution.

The kinetic studied of alkylation of toluene with methanol over Mg modified ZSM-5 was investigated by Sotelo et al. [7]. They reported that the reaction follows the Rideal-Eley mechanism; the methanol is adsorbed on the catalyst surface while the toluene reacts from the gas phase with the adsorbed alkylating agent.

Uguina et al. [21] observed that the selectivity for *p*-xylene was increased by coking with mesitylene because of the shape selectivity enhancement produced by the deposition of coke species on the external surface of ZSM-5 zeolite.

Bhandarkar and Bhatia [22] studied the selective formation of ethyltoluene by alkylation with ethanol over modified (or unmodified) HZSM-5 zeolites. HZSM-5 provided good activity and stability while modified HZSM-5 with P, B and Mg yielded better selectivity and decreased the strength but not the number of acid sites. Modification decreased the strength of strong Brönsted acid sites and increased the number of weak Lewis acid sites.

A comparative study of the alkylation of benzene or toluene with methanol or ethylene over a medium(ZSM-5) pore and a large pore (β) zeolites was studied by Panagiotis and Ruckenstein [23]. They observed that the reaction temperature in combination with the structures of the zeolites play an important role in the reactions. The maximum yield of either the primary or secondary alkylation products may occur at an intermediate temperature, which is lower over β zeolite. Due to its pore structure, β zeolite favors secondary alkylation reactions and also disproportionation reactions of the generated

alkylaromatics to a higher extent than ZSM-5 does. Methanol generated both primary and secondary alkylation products, while ethylene favors oligomerization reactions, primary alkylation reactions, and particularly, disproportionation reactions. Toluene is more reactive for alkylation reactions than benzene.

Mirth et al. [24] studied the role of catalyst acid properties to direct surface chemistry and selectivity in toluene methylation with methanol. The protonic form of Mobil Oil Corp's zeolite ZSM-5 was used in this study. Selectivity depended on the nature of the surface complexes and reactant concentration in the zeolite pores. In the presence of Brönsted acid sites, xylenes were primary products. Methanol was preferentially adsorbed over toluene, the rate of methylation proportional to the surface concentration of chemisorbed methanol. The toluene aromatics ring was weakly adsorbed and interacted with sorbed methanol species.

Wang et al. [25] simulated the alkylation of toluene with alcohol (methanol or ethanol) over ZSM-5 zeolite catalysts. The simulations showed that differences in diffusivity and in the equilibrium adsorption constant for the different product isomers, and in the intrinsic alkylation rate constants, all contribution to the shape selectivity. Both the equilibrium constant and the intrinsic rate constant are known to be dependent on the zeolites' surface acidity, and the intracrystalline diffusivity is dependent on zeolite pore structure.

The enhancement of the *para*-selectivity feature of the zeolite by inactivation of the external surface was studied by Bhat et al. [26]. The morphology and crystal size play an important role in deciding the extent of modification required to achieve a predesired *para*-selectivity. The extent of modification was higher for the zeolite batches containing smaller, spherical shaped crystals, while it was lower for the batches having longer, oblong shaped crystals. Any covering of the oblong crystals by foreign particles such

as silica enhances the extent of inactivation required to achieve a specific *para*-compound selectivity.

Bordiga et al. [27] studied structure and reactivity of framework and extraframework iron in Fe-silicate as investigated by spectroscopic and physicochemical methods. They concluded that thermal treatment at high temperature and in presence of water vapor favor the breaking of the bonds connecting iron with the framework and its migration into extraframework sites.

Berndt et al. [28] promoted zinc into HZSM-5 catalysts by ion exchange and by impregnation. Both methods displayed an increased number of Lewis sites and a decreased number of Brönsted sites. Otherwise, partial pore blocking with increasing zinc loading seems to limit the promoting effect in case of zinc ion exchange samples. The results showed that ionic zinc species determine the catalytic properties, acting as strongly acidic Lewis sites.

The influence of the preparation method i.e. ion-exchanged or incorporation method on the location of loading metals and their role for the catalytic properties were briefly reported up to now. Therefore, this research tried to vary the location of loading metals by applying different loading method in order to obtain the relation between the structural properties and the catalytic activity of the modified HZSM-5 catalysts in alkylation of toluene with methanol. Moreover, the effects of reaction temperature, space velocity, and time-on-stream were also studied.

CHAPTER III

THEORY

3.1 Structural Overview

Zeolites were first identified by Constredt in 1756 [29]. The word "*Zeolite*" from the Greek words meaning "*boiling stones*", alludes to the frothing and bubbling observed by Contredt when he heated several crystals.

Zeolites and molecular sieves are finding applications in many areas of catalysis, generating interest in these materials in industrial and academic laboratories. As catalyst, zeolites exhibit appreciable acid activity with shape-selectivity features not available in the compositional equivalent amorphous catalysts. In addition these materials can act as supports for numerous catalytically active metals. Major advances have occured in the synthesis of zeolites since the initial discovery of the synthetic zeolite's type A, X and Y, and a great number of techniques have evolved for identifying and characterizing these materials. Added to an extensive and ever growing list of aluminosilicate zeolite are molecular sieves containing other elemental compositions. These materials differ in their catalytic acidity relative to the aluminosilicate zeolites and may have potential in customizing or tailoring the molecular sieves catalyst for specific applications. Elements isoeletronic with Al^{+3} or Si^{+4} have been proposed to substitute into the framework lattice during synthesis. These include B^{+3}, Ga^{+3}, Fe^{+3} and Cr^{+3} substituting for Al^{+3} and Ge^{+4} and Ti^{+4} for Si^{+4}. The incorporation of transition elements such as Fe^{+3} for framework Al^{+3} position modifies the acid activity and, in addition, provides a novel means of obtaining high dispersions of these metals within the constrained pores of industrially interesting catalyst materials.

3.1.1 Zeolite

Structurally, the zeolite is a crystalline aluminosilicate with a framework based on an extensive three-dimensional network of oxygen ions. Situated within the tetrahedral sites formed by the oxygen can be either a Si^{+4} or an Al^{+3} ion (Figure 3.1). The AlO_2^- tetrahedra in the structure determine the framework charge. This is balanced by cations that occupy nonframework positions.

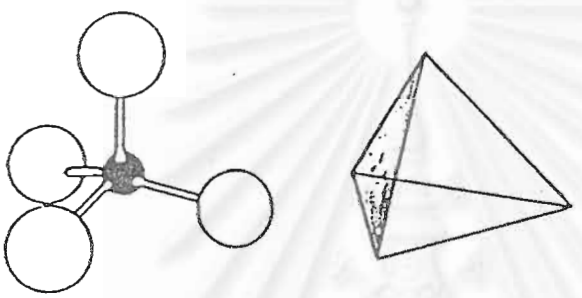

Figure 3.1 SiO_4 or AlO_4 tetrahedra [29].

A representative empirical formula for a zeolite is written as :

$$M_{2/n}O.Al_2O_3.xSiO_2.yH_2O$$

M represents the exchangeable cations, generally from the group I or II ions, although other metal, nonmetal, and organic cations may also be used to balance the framework charge, and n represents the cation valence. These cations are present either during synthesis or through post synthesis ion exchange. The value of x is equal to or greater than 2 because Al^{+3} dose not occupy adjacent tetrahedral sites. The crystalline framework structure contains voids and channels of discrete size. Water molecules present are located in these channels and cavities, as are the cations that neutralize the negative charge created by the present of the AlO_2^- tetrahedra in the structure. Typical cations include : the alkaline (Na^+, K^+, Rb^+, Cs^+) and alkaline earth (Mg^{+2}, Ca^{-2}), NH_4^+ , $H_3O^+(H^+)$ and other nitrogen-containing organic cations. and the rare-earth and noble metal ions.

3.1.2 Molecular Sieves

A molecular sieve framework is based on an extensive three-dimensional network of oxygen ions generally tetrahedral type sites. In addition to the Si^{+4} and Al^{+3} that compositionally define the zeolite molecular sieve, other cations also can occupy these sites. These cations need not be isoelectronic with Si^{+4} or Al^{+3}, but must have the ability to occupy framework sites. Cations presently known to occupy these sites within molecular sieve structures are listed in Table 3.1.

Table 3.1 Cations that may form molecular sieve framework structures and the metal oxide charge possible [29].

	M
$\mathbf{(M^{+2}O_2)^{-2}}$	Be, Mg, Zn, Co, Fe, Mn
$\mathbf{(M^{+3}O_2)^{-1}}$	Al, B, Ga, Fe, Cr
$\mathbf{(M^{+4}O_2)^{0}}$	Si, Ge, Mn, Ti
$\mathbf{(M^{+5}O_2)^{+1}}$	P

3.1.3 When is an aluminosilicate not a zeolite ?

The zeolite structure was thought to require a high proportion of aluminum for its formation. With the discovery of the high-silica molecular sieves such as zeolite ZSM-5 and silicalite, it was realized that aluminum was not a crucial component in the formation of the microporous structures. In these materials aluminum can be present in as little as trace quantities within a given structure. In very high-silica materials, aluminum in homogeneity from one unit cell to another could occur. At these low concentrations of framework aluminum it becomes statistically possible to have unit cells that contain no aluminum at all. This raises a question about the limits on defining these high-silica materials as zeolite. Should they be defined only in the broad sense as molecular sieves ?

Haag et al. [30] have calculated occupancy of aluminum within a unit cell for the high-silica form of zeolite ZSM-5, which has a SiO_2/Al_2O_3 of 190.

Table 3.2 Differentiation between the definition of molecular sieve and zeolite [29].

MOLECULAR SIEVE	ZEOLITE
Microporous crystalline structure	Microporous crystalline
Variable elemental composition	Aluminosilicate
Variable framework charge	Anionic framework

This is equivalent to one aluminum per unit cell. If random aluminum distribution occurs among all the sites, 36% of all unit cells have no aluminum,whereas the others have one, two, three, or more aluminum ions. For a SiO_2/Al_2O_3 of 96, which is an average of two aluminum ions per unit cell, 14% of the cells would still contain no aluminum ions. It is true that defining the chemical composition for high-silica aluminosilicates based on bulk composition appears to hold little meaning at the individual unit cell level. On the other hand, applications of these materials as catalysts and adsorbents generally rely on their bulk or average properties. The aluminosilicate with the ZSM-5 structure, for example, will be considered a zeolite at silica/alumina less than 190. Materials of this structure with silica/alumina above 190 will be considered only as molecular sieves. The same convention will be used for zeolite containing trace amounts of other elements in the framework ion positions. For example, a molecular sieve material containing both aluminum and iron in a silicate matrix will be considered a zeolite if the number of iron ions averages less than one per unit cell. At greater than one iron per unit cell, the material will be referred to as an aluminoferrosilicate molecular sieve.

3.2 Structure of Zeolite

All zeolites that are significant for catalytic and adsorbent applications can be classified by the number of T atoms, where T = Si or Al, that define the pore opening. There are only three pore opening known to date in the aluminosilicate zeolite system that are of practical interest for catalytic applications; they are descriptively refered to as 8-, 10-, and 12-ring openings. Zeolite containing these pore openings may also be refered to as small (8-

member ring), medium (10-member ring) and large (12-member ring) pore zeolites. In this simplified classification system, no indication is given as to exact dimension of the pore opening or whether the zeolite contains a one-, two-, or three-dimentional pore system. The different ring sizes, based on the different number of T atoms defining the opening, are shown in Figure 3.2 for three representative zeolites: erionite, ZSM-5, and type Y. Zeolites of known structure are listed in table 3.3, classified in terms of their largest pore opening. Generally one can consider any of the zeolites in the individual classes to provide similar shape-selective behavior.

Table 3.3 Known zeolite structures listed by pore opening, as defined as the number of T (or TO_4) units that shape the channels [29].

12-RING	10-RING	8-RING
Faujasite (Type X, Y)	ZSM-5 (Silicalite)	Type A, ZK-5
Mordenite	ZSM-11	Bikitaite
Cancrinite	Dachiardite	Brewsterite
Gmelinite	Epistilbite	Chabazite
Type L	Ferrierite	TMA-E (AB)
Mazzite	Laumontite	Edingtonite
Offertite	Stilbite	Erionite
Omega	ZSM-23	Gismondine
ZSM-12	Theta-1 (ZSM-22)	Heulandite
Beta	Eu-1 (ZSM-50)	Levyne
	ZSM-48 (Eu-2)	Merlinoite
		Natrolite
		Phillipsite
		Paulingite
		Rho
		Thomsonite
		Yugawaralite

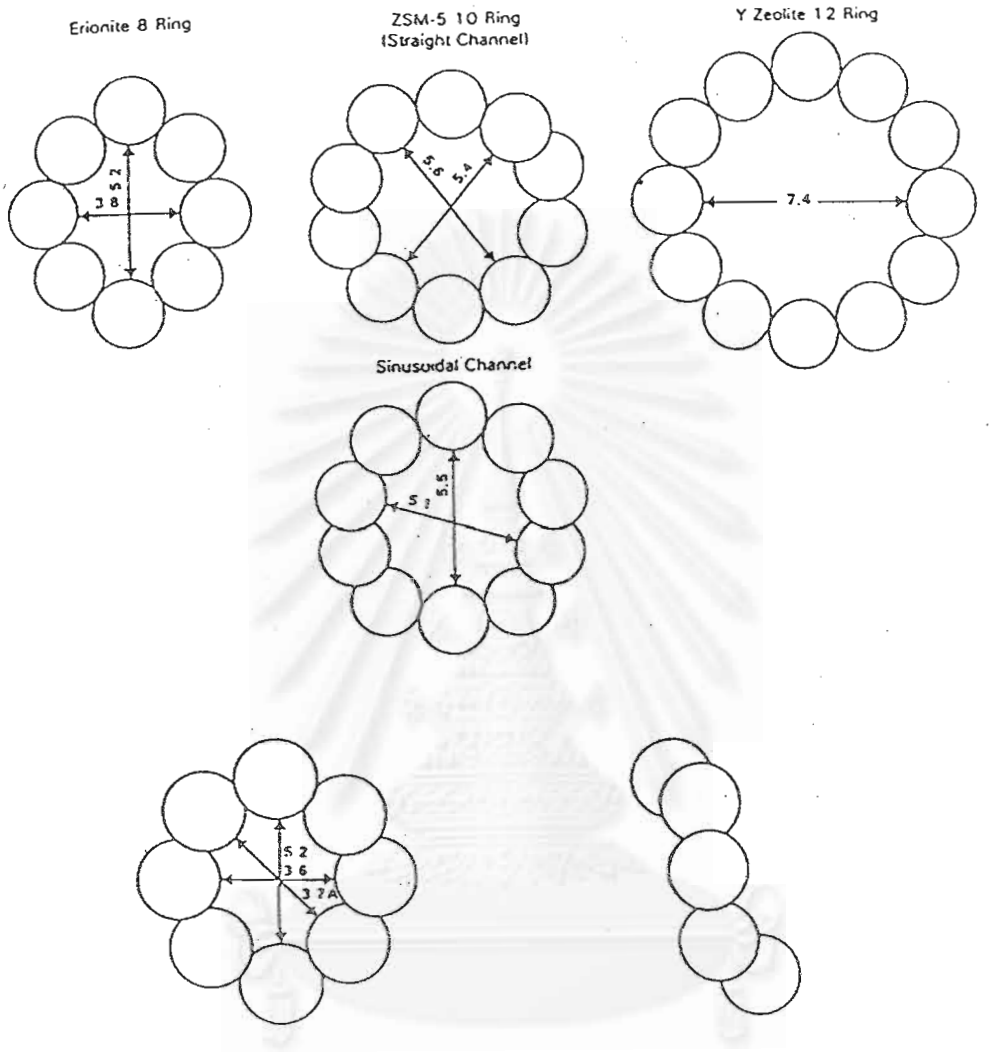

Figure 3.2 Examples of the three types of pore opening in the zeolite molecular sieves. (a) Erionite contains an 8 ring pore opening; ZSM-5, two 10 ring systems differing in the shape of the opening; and type Y zeolite. a 12-ring pore system. (b) A front and side view of the pore opening for erionite [31].

The primary building unit of a zeolite structure is the individual tetrahedral TO_4 unit, where T is either Si or Al. A secondary building unit (SBU) consists of selected geometric groupings of those tetrahedra. There are nine such building units, which can be used to describe all of known zeolite structures. These secondary building units consist of 4or (S4R), 6 or (S6R), and 8 or (S8R)-member single ring, 4-4 or (D4R), 6-6 or (D6R), 8-8 or (D8R)-member double rings, and 4-1, 5-1, and 4-4-1 branched rings [31]. The topologies of these units are shown in Figure 3.3. Also listed are the symbols used to describe them. Most zeolite framework can be generated from several different SBU's. Descriptions of known zeolite structures based on their SBU's are listed in Table 3.4. Both zeolite ZSM-5 and ferrierite are described by their 5-1 building units. Offretite, zeolite L, cancrinite, and erionite are generated using only single 6-member rings. Some zeolite structures can be described by several building units. The sodalite framework can be built from either the single 6-member ring or the single 4-member ring. Faujasite (type X or type Y) and zeolite A can be constructed using 4-ring or 6-ring building units. Zeolite A can also be formed using double 4-ring building units, whereas faujasite cannot.

3.3 Silicalite and ZSM-5

Silicalite-1 or Silicalite, is a name proposed by Flanigen et al. [34] to identify the pure silica polymorph of zeolite ZSM-5. In silicalite and ZSM-5, the tetrahedra are linked to form the chain-type building block in Figure 3.4. The chain can be connected to form a layer, as shown in Figure 3.5. Rings consisting of five O atoms are evident in this structure; the name pentasil is therefore used to describe it. Also evident in Figure 3.5 are rings consisting of 10 oxygen atoms; these are important because they provide opening in the structure large enough for passage of even large molecules. The layers can link in two ways, the former pertains to the zeolite ZSM-11, the later to silicalite or ZSM-5; intermediate structure constitute the pentasil series.

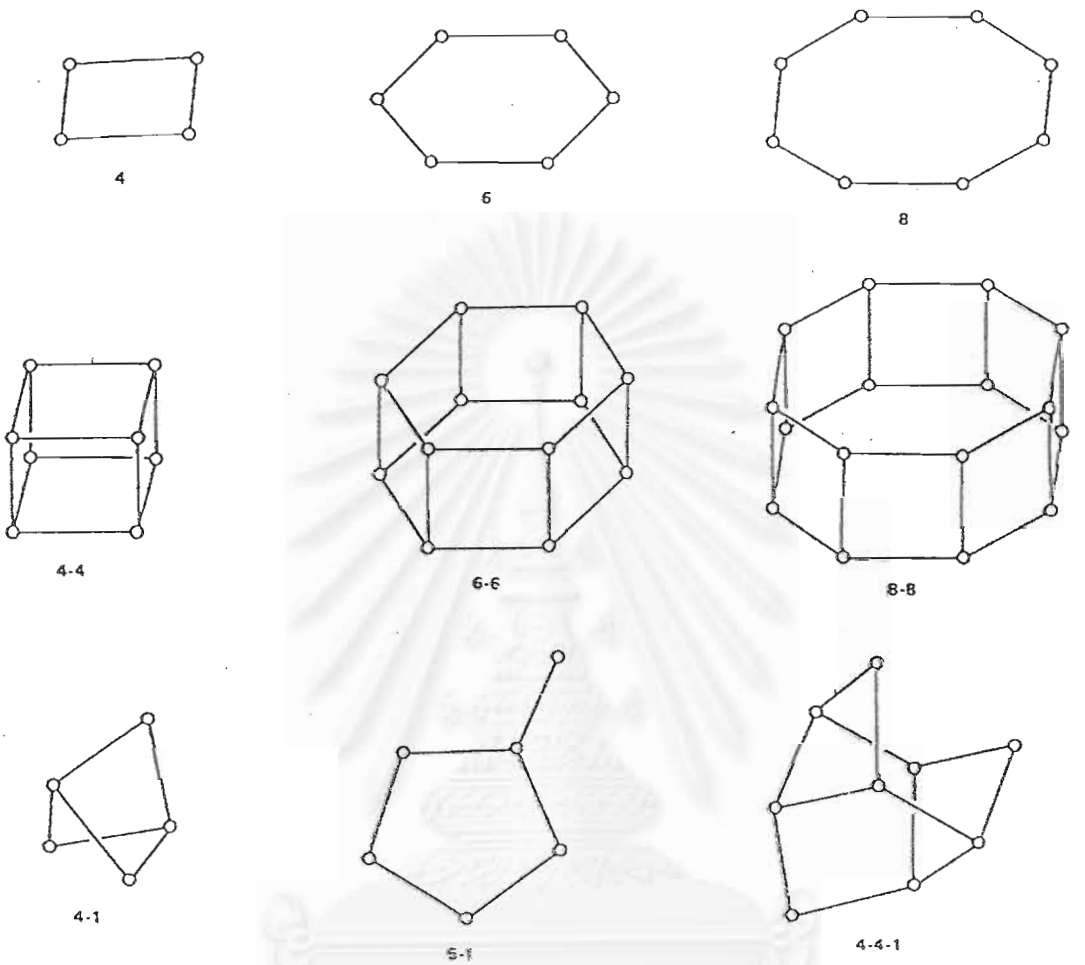

Figure 3.3 Secondary building units (SBU's) found in zeolite structures [32].

Table 3.4 Zeolites and their secondary building units. The nomenclature used is consistent with that presented in Figure 3.3 [33].

	SECONDARY BUILDING UNITS								
ZEOLITE	4	6	8	4-4	6-6	8-8	4-1	5-1	4-4-1
Bakitaite								X	
Li-A (BW)	X	X	X						
Analcime	X	X							
Yugawaralite	X		X						
Epistilbite								X	
ZSM-5								X	
ZSM-11								X	
Ferrierite								X	
Dachiardite								X	
Brewsterite	X								
Laumontile		X							
Mordenite								X	
Sodalite	X	X							
Heulandite									X
Stilbite									X
Natrolite							X		
Thomsonite							X		
Edingtonite							X		
Cancrinite		X							
Zeolite L		X							
Mazzite	X								
Merlinoite	X		X			X			
Phillipsite	X		X						
Zeolite losod		X							
Erionite	X	X							
Paulingite	X								
Offretite		X							
TMA-E (AB)	X	X							
Gismondine	X		X						
Levyne		X							
ZK-5	X	X	X			X			
Chabazite	X	X				X			
Gmelinite	X	X	X			X			
Rho	X	X	X				X		
Type A	X	X	X	X					
Faujasite	X	X				X			

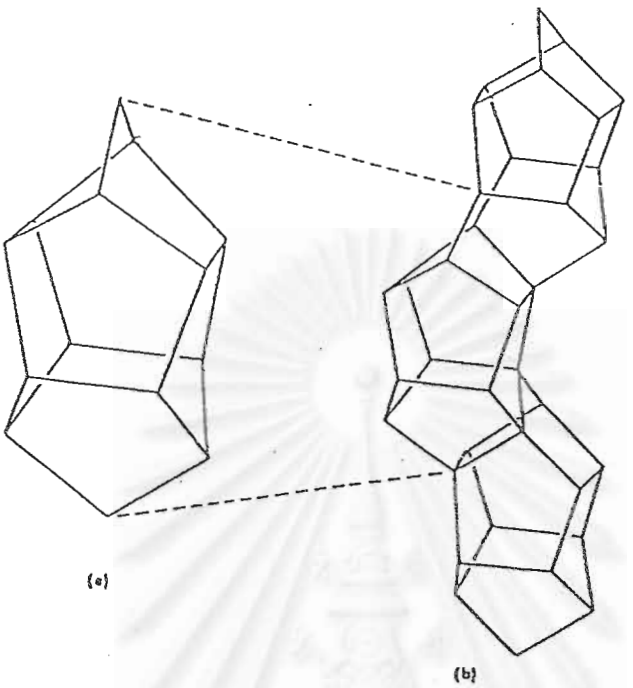

Figure 3.4 Building the chain units (b) found in the ZSM-5 and ZSM-11 structures from the smaller 5-1 secondary building unit (a) [29].

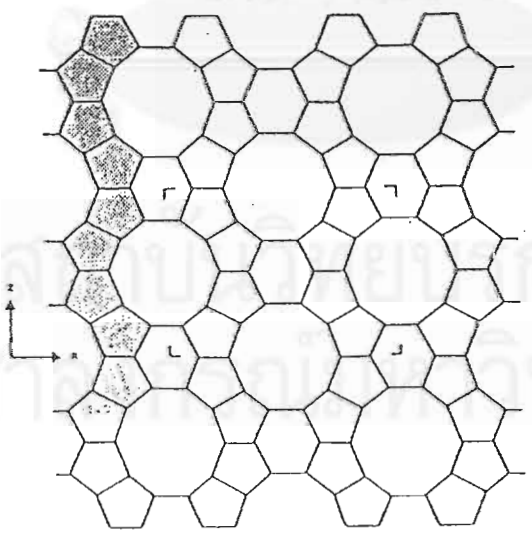

Figure 3.5 Sheet projection of ZSM-5 (or ZSM-11) showing the chain building units (shaded) used to generate these structures [29].

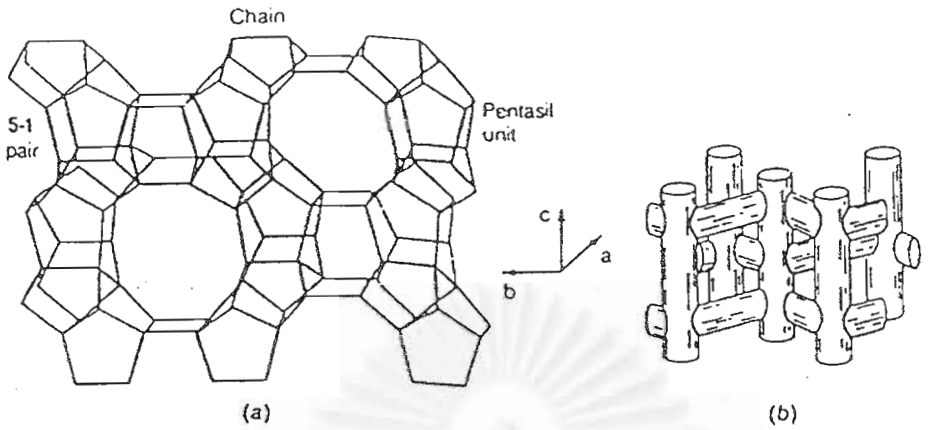

Figure 3.6 Three dimensional structure of silicalite (and ZSM-5) [29].

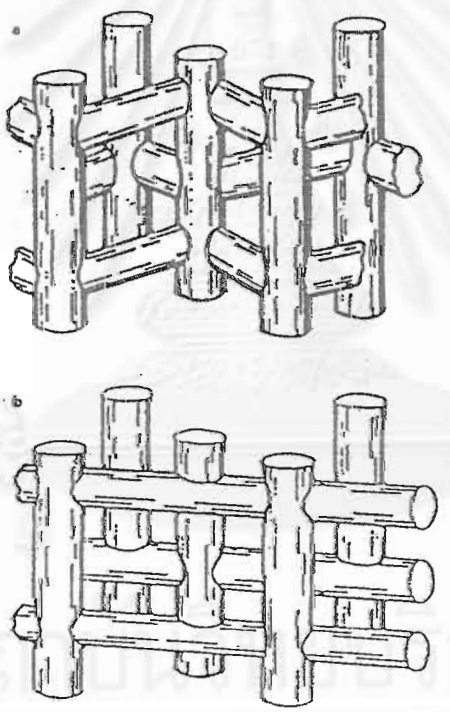

Figure 3.7 ZSM-5 and ZSM-11 channel system [29].

The three dimensional structure of silicalite (and ZSM-5) is presented in Figure 3.6. The 10-membered rings provide access to a network of intersecting pores within the crystal. The pore structure is depicted schematically in Figure 3.7: there is a set of straight, parallel pores intersected by set of perpendicular zigzag pores. many molecules are small enough to penetrate into this intracrystalline pore structure, where they may catalytically converted.

3.4 Zeolite Active Sites

The reactivity and the selectivity of molecular sieve zeolites as catalysts are determined by active sites provided by an imbalance in charge between the silicon and the aluminum ions in the framework. Each aluminum atom contained within the framework structure induces a potential active acid site [35]. Classical Brönsted and Lewis acid models of acidity have been used to classify the active sites on zeolites. Brönsted acidity is proton-donor acidity; this occur in the zeolites when the cations balancing the framework anionic charge are protons (H^+). Lewis acidity is electron acceptor acidity; a trigonally co-ordinated aluminum atom is an electron-deficient and can accept an electron pair, therefor behaves as a Lewis acid.

In general, the increase in Si/Al ratio will increase acidic strength and thermal stability of zeolite [36]. Since the number of acidic OH groups depend on the number of aluminum atom in the zeolite's framework, decrease in Al content is expected to reduce catalytic activity of zeolite. It has been reported the mean charge on the proton was shifted regularly towards higher values as the Al content decrease [37]. Simultaneously the total number of acidic hydroxyls, governed by the Al toms, were decrease. This evidence emphasized that the entire acid strength distribution (weak, medium, strong) was shifted towards stronger values. That is, weaker acid sites become stronger with the decrease in Al content.

3.4.1 Generation of Acid Centers

Protonic acid centers of zeolite are generated in various ways Figure 3.8 depicts the thermal decomposition of ammonium exchanged zeolites yielding the hydrogen form. The Brönsted acidity due to water ionization on polyvalent cations, described below, is depicted in Figure 3.9.

$$M^{n+} + xH_2O \rightarrow M(OH)_x^{(n-X)+} + xH^+ \quad \text{..... (3.1)}$$

The exchange of monovalent ions by polyvalent cations could improve the catalytic property. Those highly charged cations create very acidic centers by hydrolysis phenomena.

Brönsted acid sites are also generated by the reduction of transition metal cations. The concentration of OH groups of zeolite containing transition metals was noted to increase by reduction with hydrogen at 250-450 ^{o}C to increase with the rise of the reduction temperature [38].

$$Cu^{2+} + H_2 \rightarrow Cu^0 + 2H^+ \quad \text{..... (3.2)}$$

$$Ag^+ + 1/2\ H_2 \rightarrow Ag^0 + H^+ \quad \text{..... (3.3)}$$

The formation of Lewis acidity from Brönsted acid sites is depicted in Figure 3.10. The dehydration reaction decrease the number of protons and increase that of Lewis sites. Then Brönsted (OH) and Lewis (-Al-) sites can be present simultaneously in the structure of zeolite at high temperature.

Dehydroxylation (loss of structural water from the lattice) is thought to occur on zeolite ZSM-5 above 500 ^{o}C which causes a small decrease in the degree of crystallinity and some dealumination [39]. Calcination at 800 to 900 ^{o}C produces irreversible dehydroxylation.

Dealumination is believed to occur during dehydroxylation which may result from the steam generation within the sample. The dealumination is indicated by an increase in the surface concentration of aluminum on the crystal. The dealumination process is expressed in Figure 3.11. Progressive dealumination occurs with the severity and duration of steaming [40, 41].

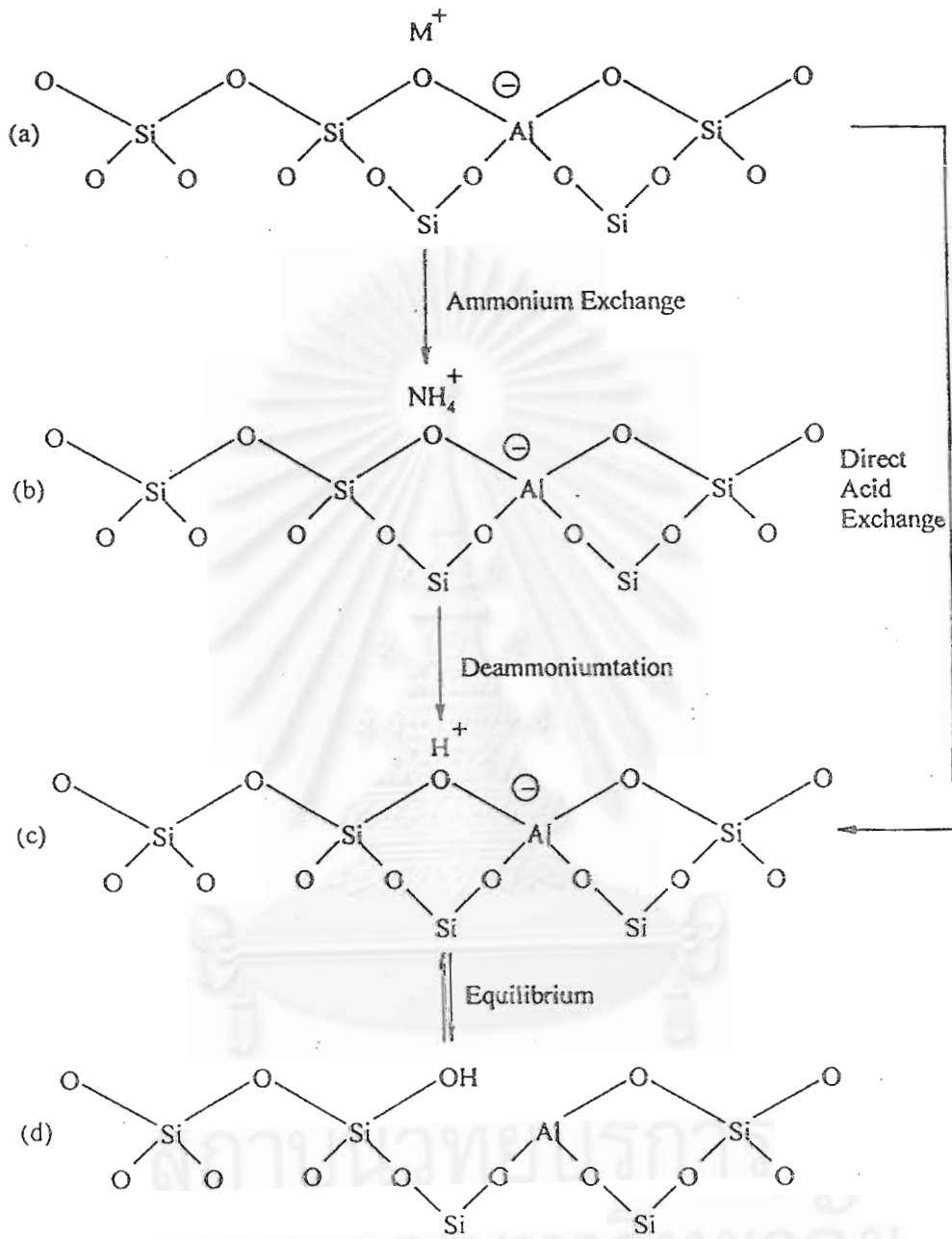

Figure 3.8 Diagram of the surface of a zeolite framework [29].

(a) In the as-synthesized form M^+ is either an organic cation or an alkali metal cation.

(b) Ammonium in exchange produces the NH_4^+ exchanged form.

(c) Thermal treatment is used to remove ammonium, producing the H^+ form.

(d) The acid form in (c) is in equilibrium with the form shown in (d) where there is a silanol group adjacent to a tricoordinate aluminum.

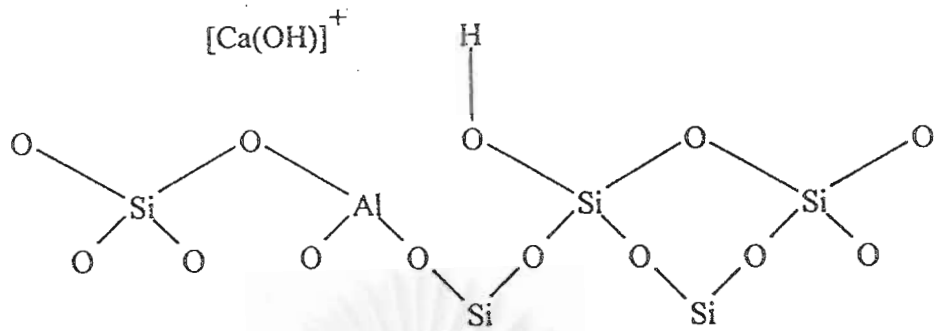

Figure 3.9 Water molecules coordinated to polyvalent cation are dissociated by heat treatment yielding Brönsted acidity [38].

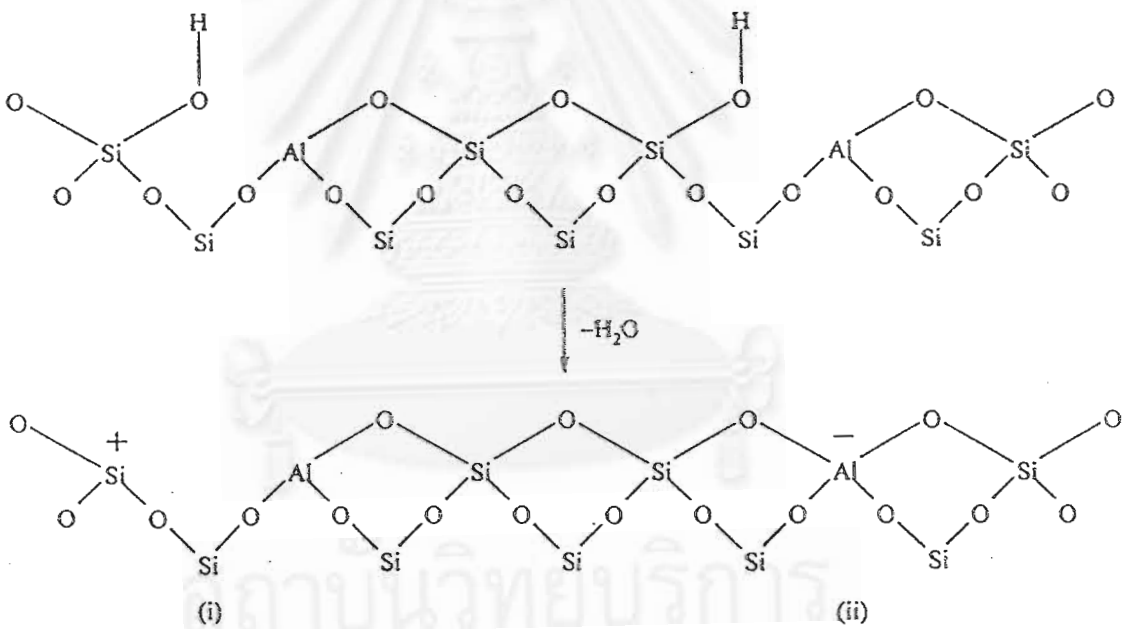

Figure 3.10 Lewis acid site developed by dehydroxylation of Brönsted acid site [38].

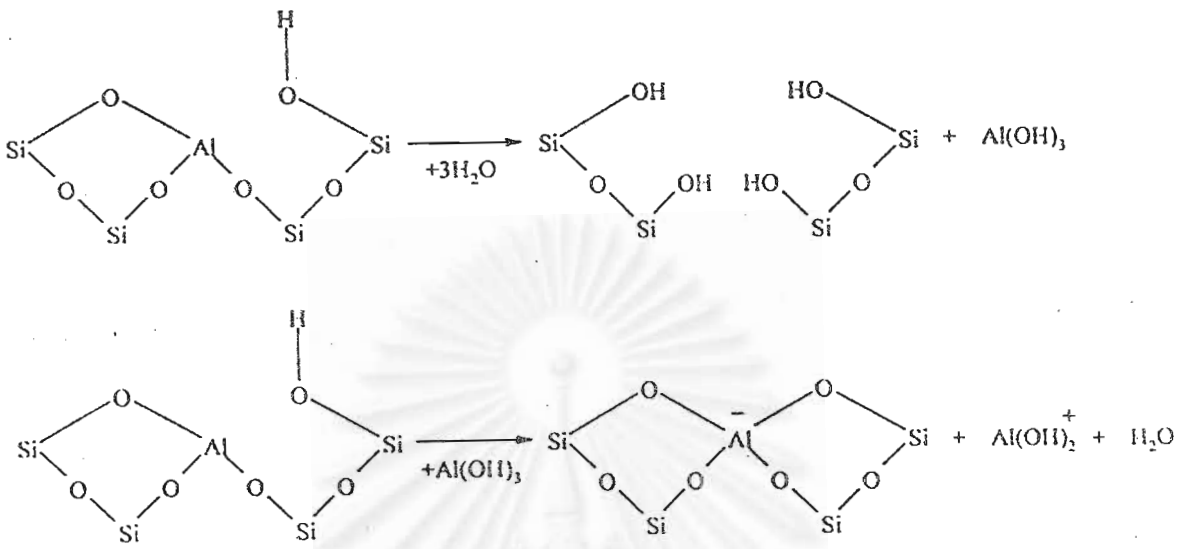

Figure 3.11 Steam dealumination process in zeolite [38].

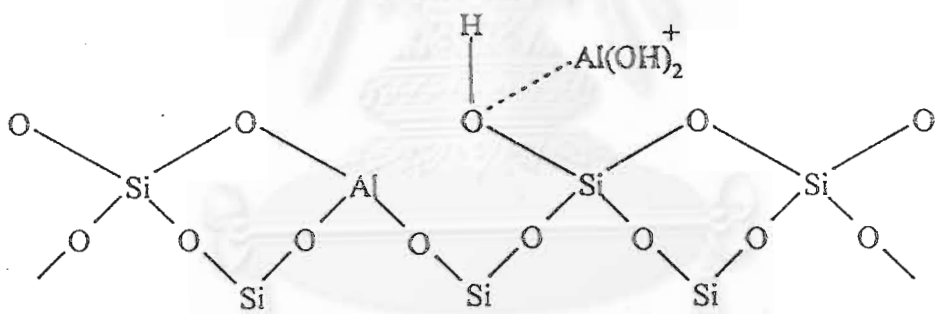

Figure 3.12 The enhancement of the acid strength of OH groups by their interaction with dislodged aluminum species [38].

3.5 Shape Selectivity

Many reactions involving carbonium ions intermediates are catalyzed by acidic zeolites. With respect to a chemical standpoint the reaction mechanisms are not fundamentally different with zeolites or with any other acidic oxides. The shape selective characteristics of zeolites influence their catalytic

phenomena by three modes; reactants, products, and transition states shape selectivity [42]. These types of selectivity are depicted in Figure 3.12.

Reactant or charge selectivity results from the limited diffusibility of some of the reactants, which cannot effectively enter and diffuse inside crystal pore structures of the zeolites.

Product shape selectivity occurs as slowly diffusing product molecules cannot escape from the crystal and undergo secondary reactions. This reaction path is established by monitoring changes in product distribution as a function of varying contact time.

Restricted transition state shape selectivity is a kinetic effect arising from local environment around the active site, the rate constant for a certain reaction mechanism is reduced if the necessary transition state is too busy to form readily.

The critical diameter (as opposed to the length) of the molecules and the pore channel diameter of zeolite are important in predicting shape selective effects. However, molecules are deformable and can pass through openings which are smaller than their critical diameters. Hence, not only size but also the dynamics and structure of the molecules must be taken into account. Table 3.5 present values of selected critical molecular diameters and Table 3.6 present values of the effective pore size of various zeolites. Correlation between pore size(s) of zeolites and kinetics diameter of some molecules are depicted in Figure 3.14.

(a) Reactant Selectivity

(b) Product Selectivity

(c) Transient State Selectivity

Figure 3.13 Diagram depicting the three type of selectivity [42].

Figure 3.14 Correlation between pore size(s) of various zeolites and kinetic diameters of some molecules [43].

(a) Reactant Selectivity

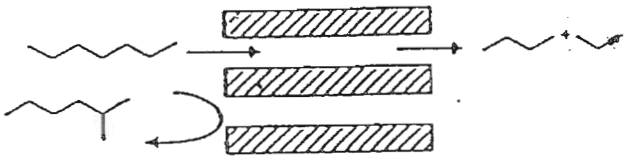

(b) Product Selectivity

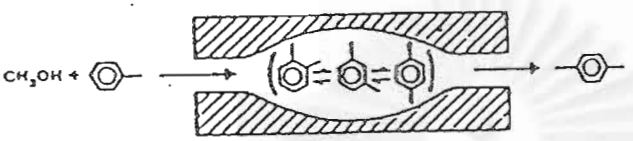

(c) Transient State Selectivity

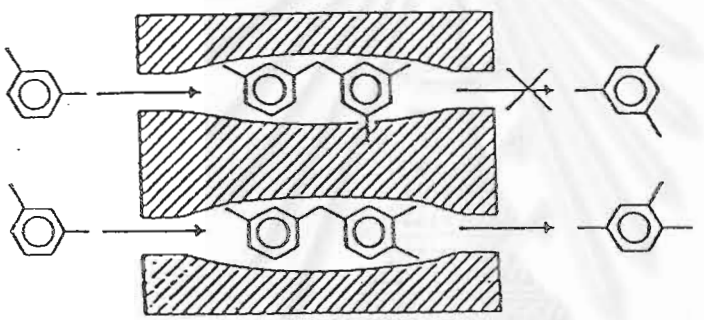

Figure 3.13 Diagram depicting the three type of selectivity [42].

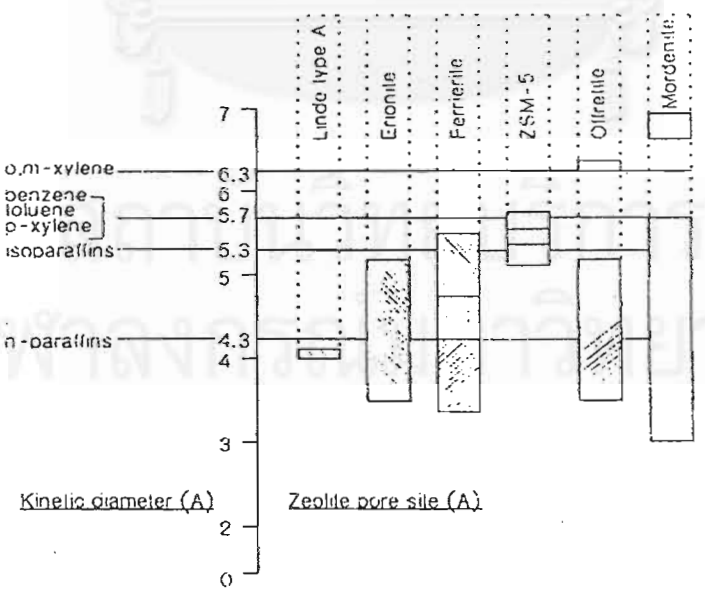

Figure 3.14 Correlation between pore size(s) of various zeolites and kinetic diameters of some molecules [43].

Table 3.5 Kinetics diameters of various molecules based on the Lennard-Jones relationship [44].

	KINETIC DIAMETER (ANGSTROMS)
He	2.60
H_2	2.89
O_2	3.46
N_2	3.64
NO	3.17
CO	3.76
CO_2	3.30
H_2O	2.65
NH_3	2.60
CH_4	3.80
C_2H_2	3.30
C_2H_4	3.90
C_3H_8	4.30
n-C_4H_{10}	4.30
Cyclopropane	4.23
i-C_4H_{10}	5.00
n-C_5H_{12}	4.90
SF_6	5.50
Neopentane	6.20
$(C_4F_9)_3N$	10.20
Benzene	5.85
Cyclohexane	6.00
m-xylene	7.10
o-Xylene	7.40
p-Xylene	6.75
1,3,5 trimethylbenzene	8.50
1,3,5 triethylbenzene	9.20
1-methylnapthalene	7.90
$(C_4H_9)_3N$	8.10

Table 3.6 Shape of the pore mouth openings of known zeolite structures. The dimensions are based on two parameters, the number of T atoms forming the channel opening (8-, 10-, 12-rings) and the crystallographic free diameters of the channels. The channels are parallel to the crystallographic axis shown in brackets(e.g.<100>) [33].

STRUCTURE	8 MEMBER RING	10 MEMBER RING	12 MEMBER RING
Bikitaite	3.2 x 4.9[001]		
	2.3 x 5.0[100]		
	2.7 x 4.1[001]		
Cancrinite			6.2[001]
Chabazite	3.6 x 3.7[001]		
Dachiardite	3.6 x 4.8[001]	3.7 x 6.7[010]	
TMA-E	3.7 x 4.8[001]		
Edingtonite	3.5 x 3.9[110]		
Epistillbite	3.7 x 4.4[001]	3.2 x 5.3[100]	
Erionite	3.6 x 5.2[001]		
Faujasite			7.4<111>
Ferrierite	3.4 x 4.8[010]	4.3 x 5.5[001]	
Gismondine	3.1 x 4.4[100]		
	2.8 x 4.9[010]		
Gmelinite	3.6 x 3.9[001]		7.0[001]
Heulandite	4.0 x 5.5[100]	4.4 x 7.2[001]	
	4.1 x 4.7[001]		
ZK-5	3.9<100>		
Laumontite		4.0 x 5.6[100]	
Levyne	3.3 x 5.3[001]		
Type A	4.1<100>		
Type L			7.1[001]
Mazzite			7.4[001]
ZSM-11		5.1 x 5.5[100]	
ZSM-5		5.4 x 5.6[010]	
		5.1 x 5.5[100]	
Mordenite	2.9 x 5.7[010]		6.7 x 7.0[001]
Natrolite	2.6 x 3.9<101>		
Offretite	3.6 x 5.2[001]		6.4[001]
Paulingite	3.9<100>		

3.6 Alkylation Processes

The term alkylation has generally been used to describe the catalyzed reaction between isobutane and various light olefins. The producer is a highly branched paraffinic hydrocarbon used a blend to improve the octane number of gasoline. A more specific explanation of the term alkylation is the attachment of one or more alkyl groups to a hydrocarbon compound or to a hydrocarbon derivative. This may take place by an electrophilic attack of a carbonium ion species (whether formal or ion-pair) or by a nucleophlic attack of a carbonion or carbonion-like species. When a carbonium ion is the intermediate, alkylation can occur either by addition, as the case of the reaction between a carbonium ion and an alkene, e.g.

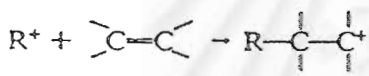

or by substitution as in the case of Friedel-Crafts type reactions e.g.

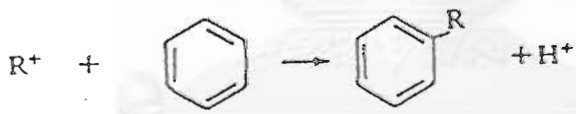

Alkylation reactions are useful in organic synthetic research as well as in industrial applications for the production of important chemicals. Examples of alkylates of commercial importance are ethylbenzene, cumene, linear alkylbenzene, alkylamines and 2,2,4-trimethylpentane. These alkylates are produced by the aid of acidic-type catalysts. many types of alkylating agents are used, but those that easily form carbonium ions are the most important. Olefins, alcohols and alkyl halides are the most commonly used alkylating agents.

3.6.1 Alkylation Catalysts

Catalysts for alkylation reactions used essentially to be of the homogeneous type. However, due to the discovery that certain molecular sieves (zeolites) are not only acidic enough to promote carbonium ion or ion-pair formation, but are also more selective than homogeneous catalysts, they are now used in some new alkylation processes.

Homogeneous alkylation catalysts may be Brönsted acids such as HF and H_2SO_4 etc. using alkenes as alkylating agents, a proton is donated by the acid to the substrate.

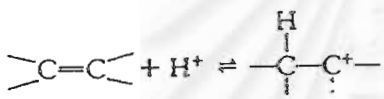

When alkenes are treated with a Lewis acid such as $AlCl_3$, a small amount of a proton acid is normally added as a co-catalyst to promote the formation of carbonium ions.

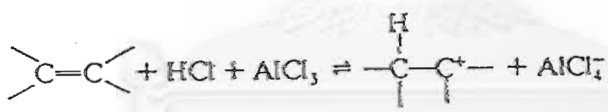

If alcohols are the alkylating agents in the presence of Brönsted acids, they are protonated and carbonium ions may be formed.

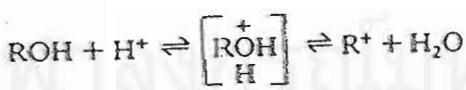

In presence of Lewis acids, such as $AlCl_3$, a complex is first formed with the alcohol and HCl is released. The complex then donates the carbonium ion.

Alkylation with heterogeneous catalysts has been carried out using a variety of acidic oxides such as Al_2O_3 and Al_2O_3/SiO_2. These catalysts also promote carbonium ion-type reactions. Depending on the method of preparation, silica/alumina catalyst may be amorphous or crystalline. These compounds have been both Brönsted and Lewis acid sites. When alkylating benzene with ethylene, on a zeolite catalyst for example, adsorbed ethylene is protonated at a Brönsted acid site on the catalyst surface forming an ethylcarbonium ion.

$$Zeol—O^-H^+ + CH_2{=}CH_2 \rightarrow CH_3—CH_2^+ + Zeol—O^-$$

The carbonium ion then attacks the benzene ring giving ethylbenzene and the proton is regained by the zeolite.

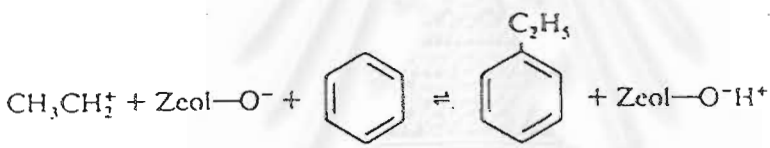

Zeolites were found to be more suitable alkylation catalysts than the amorphous types because of their higher activities and selectivities toward certain reactions.

3.6.2 Alkylation of Toluene with Methanol (Production of Xylenes)

Xylenes are mainly produced by a distillation-extraction scheme from reformed gasolines. Xylene are important precursors for many chemicals. The ration of the isomers, *para : ortho : meta* is approximately 1 : 1 : 2, which is very close to the thermodynamic equilibrium values for the three isomers at the reforming temperature (Table 3.7).

Table 3.7 Thermodynamic equilibrium values for xylene isomers[1].

Aromatics wt.%	**Composition**		
	200 ^{o}C	300 ^{o}C	500 ^{o}C
p-Xylene	21.8	21.1	18.9
o-Xylene	20.6	21.6	23.0
m-Xylene	53.5	51.1	47.1
Ethylbenzene	4.1	6.2	11.0

Para-xylene is the most important intermediate for producing terephtalic acid, which is used for the production of polyesters, the most important synthetic fiber raw materials. Catalytic oxidation of *ortho*-xylene gives phthalic anhydride for the production of plasticizers. *Meta*-xylene although the major component of the xylene mixture from catalytic reforming, is the least utilized of the three isomers for chemical production. It is usually isomerized to the other two isomers. Figure 3.15 shows the most important chemical based on xylene. A process that selectively produces *p-x*ylene may be economically competitive to the currently used scheme. Recent work for alkylation of toluene with methanol using HY zeolite and ZSM-5 at a temperature range of 300-700 ^{o}C was investigated.

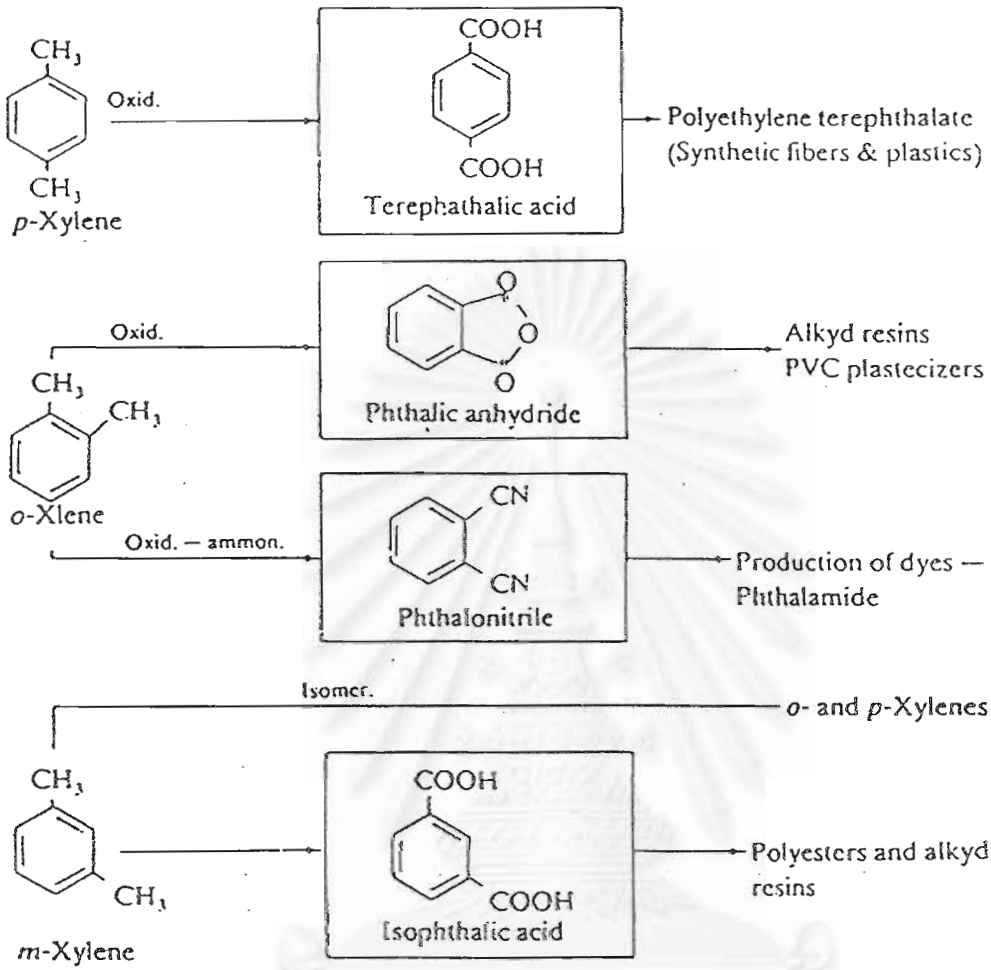

Figure 3.15 Important chemicals from xylenes[1].

CHAPTER IV

EXPERIMENTS

The catalyst study for alkylation of toluene with methanol over metal containing MFI-type zeolite catalysts and reaction method as well as catalysts characterization were explained in the following section.

4.1 Catalyst Preparation

The MFI-type catalysts were prepared by adopting the rapid crystallization method [45, 46]. H-MFI incorporated with Fe(Fe,Al-silicate) or Zn(Zn,Al-silicate) were prepared by rapid crystallization method similar to H-MFI synthesis but adding both Al and Fe or Zn during the stage of gel preparation. While H-MFI ion-exchanged with Fe(Fe/MFI) or Zn(Zn/MFI) catalyst were prepared by ion-exchange H-MFI with an aqueous solution of $Fe(NO_3)_3.9H_2O$ or $Zn(NO_3)_2.6H_2O$. The preparation procedures and the reagents used are shown in Figure 4.1 and Table 4.1, respectively. (For calculation see Appendix A-1).

4.1.1 Preparation of Gel Precipitation and Decantation Solution

Firstly, a gel mixture was prepared by adding A1 and B1 into C1 solution with vigorous stirring using a magnetic stirrer at room temperature as shown in Figure 4.2. A1 and B1 were added from burettes by manual control to keep PH of the mixed solution in the range of 9-11 because it was expected that this PH range was suitable for precipitation. The gel mixture was separated from the supernatant liquid by a centrifugal separator. The precipitated gel mixture was

milled for 1 hr by a powder miller(Yamato-Notto, UT-22). The milling procedure was as follow: milled 15 min. → centrifuge (to remove the liquid out) → milled 15 min. → centrifuge → milled 30 min. Milling before the hydrothermal treatment was the essential step to obtain the uniform and fine crystals. On the other hand, another decantation solution was prepared by adding A2 and B2 into C2 solution. The method and condition of mixing were similar to the preparation of the gel mixture. The colorless supernatant liquid was separated from the mixture by centrifugation.

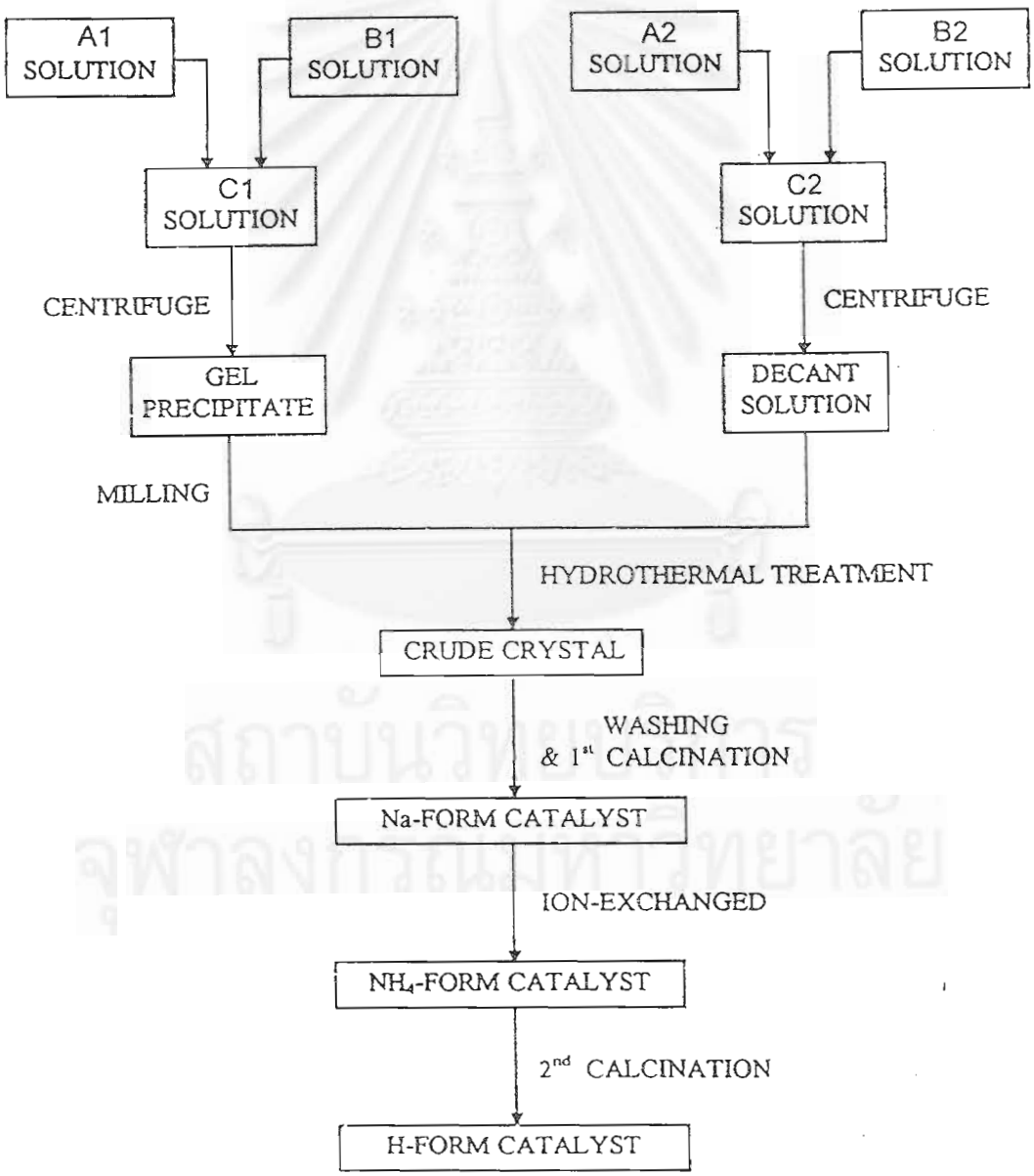

Figure 4.1 Preparation Procedure of MFI Catalysts by Rapid Crystallization Method.

Table 4.1 Reagents Used for The MFI-type Zeolite Catalyst Preparation

Reagents for the gel preparation		Reagents for decant-solution preparation	
Solution A1		**Solution A2**	
$AlCl_3$ (g)	A	$AlCl_3$ (g)	A
$Fe(NO_3)_3.9H_2O$, or	B	$Fe(NO_3)_3.9H_2O$, or	B
$Zn(NO_3)_2.6H_2O$	C	$Zn(NO_3)_2.6H_2O$	C
Tetrapropylamonium bromide		Tetrapropylamonium bromide	
TPABr (g)	5.75	TPABr (g)	7.53
De-ionized water (ml)	60.00	De-ionized water (ml)	60.00
conc. H_2SO_4 (ml)	3.40	conc. H_2SO_4 (ml)	3.40
Solution B1		**Solution B2**	
De-ionized water (ml)	45.00	De-ionized water (ml)	45.00
Sodium Silicate (g)	69.00	Sodium Silicate (g)	69.00
($Na_2O.SiO_2.H_2O$)		($Na_2O.SiO_2.H_2O$)	
Solution C1		**Solution C2**	
NaCl (g)	40.59	NaCl (g)	26.27
NaOH (g)	2.39	De-ionized water (ml)	104.00
TPABr (g)	2.61		
De-ionized water (ml)	208.00		
conc. H_2SO_4 (ml)	1.55		

* A, B, and C : based on Si/Al, Si/Fe and Si/Zn charged atomic ratio, respectively.
(For calculation see Appendix A-1)

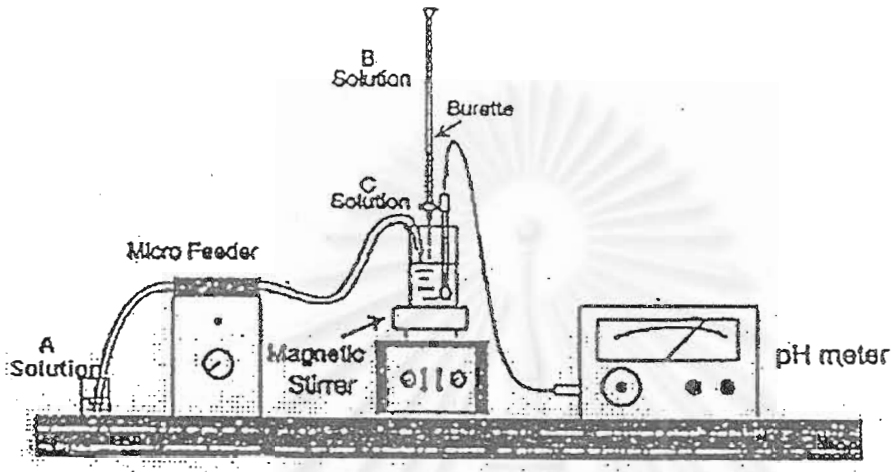

Figure 4.2 Apparatus Used for The Preparation of Na-MFI

4.1.2 Crystallization

The mixture of the milled precipitate and the supernatant of decant solution was mixed together in a 500 ml pyrex glass container. The glass container was placed in a stainless steel autoclave. Then the mixture was heated for crystallization in an autoclave from room temperature to 160 °C in 90 min and up to 210 °C in 4.2 hrs under an initial pressure of 3 kg/cm^2 (gauge) of nitrogen gas. The hot mixture was cooled down to room temperature in an autoclave overnight. The product crystals were washed with deionized water about 8 times by using the centrifugal separator (about 15-20 min for each time) to remove chloride ions out of the crystals and dry in an oven at 110-120 °C for at least 12 hrs.

4.1.3 First Calcination

A portion of dry crystals in a porcelain container was heated in a furnace under an air ambient from room temperature to 540 ^{o}C in 60 min and then kept at this temperature for 3.5 hrs. At this step, TPABr was burned out and left the cavities and channels in the crystals. The calcined crystal was cooled to room temperature and kept in a desiccator. After this step the obtained catalyst was called “Na-form catalyst (Na-MFI)”.

4.1.4 Ammonium Ion-exchange

About 2.0 g of the Na-form catalyst was mixed with 60 ml of 1 M NH_4NO_3 and heated on a stirring hot plate at 80 ^{o}C for 1 h and then the mixture was cooled down to room temperature and centrifuged to remove the used solution. The ion-exchange step was repeated 4 times. The ion-exchanged crystal was then washed twice with deionized water by using a centrifugal separator. Subsequently, the ion-exchanged crystal was dried at 110-120 ^{o}C for 12 hrs in an oven. The Na-form crystal was changed to “NH_4-form catalyst (NH_4-MFI)”.

4.1.5 Second Calcination

The removed species, i.e. NH_3, NO_x were decomposed by thermal treatment of the NH_4-form catalyst in a furnace at 540 ^{o}C, with the same condition as the first calcination. After this step the obtained catalyst was called “H-form catalyst (H-MFI)”.

4.2 Metal Loading by Ion-exchange

A 2.0 g of catalyst was immersed in 60 ml of distilled water and treating catalyst with metal salt aqueous solution at 100 °C for 3 hrs and then the mixture was cooled down to room temperature and centrifuged to remove the used solution(For calculation see Appendix A-2). Then the catalyst was washed with deionized water about 8 times by using the centrifugal separator (about 15-20 min for each time) and dried overnight at 110-120 °C for 12 hrs in an oven. Finally, dry crystal was heated in air with constant heating rate of 10 °C/min up to 350 °C and maintained at this temperature for 2 hrs in a furnace.

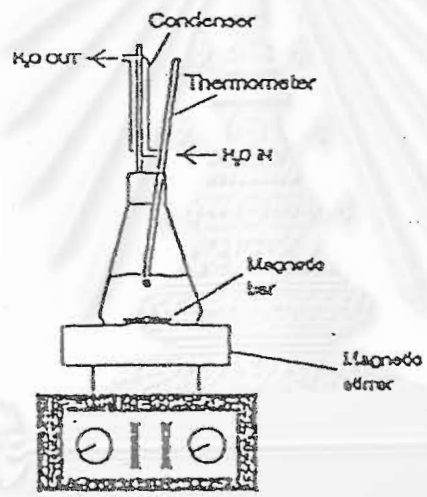

Figure 4.3 Apparatus Used for Ion-exchanged MFI Catalysts

4.3 Prepared Catalyst Bed

The catalysts that used for running the reaction were tableted by a tablet machine at 4500-5000 kg/m^2. After tableting, the catalysts were crushed and sieved to the range of 8-16 mesh to provide the same diffusion rate and to reduce pressure drop.

4.4 Apparatus and Reaction Method

4.4.1 Chemical and Reagents

Toluene and Methanol (Analytical Grade) were provided by AJAX Chemical.

4.4.2 Instruments and Apparatus

4.4.2.1 Reactor

The reactor is a conventional microreactor made from quartz tube with 6.0 mm inside diameter, so it can be operated at high temperature. The reaction was carried out under ordinary gas flow and atmospheric pressure.

4.4.2.2 Automation Temperature Controller

The temperature controller apparatus consists of a magnetic switch connected to a variable voltage transformer and RKC temperature controller connected to a thermocouple attached to the catalyst bed in a reactor. A dial setting establishes a set point at any temperature within the range between 0 ^{o}C to 600 ^{o}C.

4.4.2.3 Electrical Furnace

This supplied the required heat to the reactor for reaction. The reactor can be operated from room temperature up to 650 ^{o}C at maximum voltage.

4.4.2.4 Gas Controlling System

Nitrogen cylinder is equipped with a pressure regulator (0-250 psig), an on-off valve and needle valve were used to adjust flow rate of gas.

4.4.2.5 Gas Chromatographs

Flame ionization detector-type gas chromatographs, Shimadzu GC-14A is used to analyze feeds and products. The Operation conditions used are shown in Table 4.2.

Table 4.2 Operating Conditions for Gas Chromatograph.

Gas Chromatographs	Shimadzu GC-14A	Shimadzu GC-14A
Detector	FID	FID
Column	Silicon OV-1	5% AT-1200 + 1.75%
	∅ 0.25 mm x 50.00 m	Bentone 34 on 100/120
		Chromosorb W-AW
		∅ 4.00 mm x 1.80 m
Carrier gas	N_2 (99.99 %)	N_2 (99.99 %)
Flow rate of carrier gas	25 ml/min	35 ml/min
Column temperature - initial	35 ^oC	80 ^oC
- final	140 ^oC	80 ^oC
Injector temperature	50 ^oC	70 ^oC
Detector temperature	150 ^oC	120 ^oC
Analyzed gas	gasoline range,	aromatics,
	aromatics	xylene isomers

4.4.3 Reaction Method

The alkylation of toluene with methanol reaction was carried out in a fixed bed tubular flow quartz reactor under atmospheric pressure. (See the Figure 4.4)0.25 g of the catalyst was packed in 6.0 mm inner diameter quartz reactor. Nitrogen gas was supplied from a cylinder as carrier gas to adjust flow rate of the system. (For calculation see Appendix A-3) The alkylation of toluene with methanol reaction was carried out under the following conditions: atmospheric pressure; gas hourly space velocity (GHSV), 2000-10000 h^{-1}; reaction temperature, 350-550 ^oC.

The procedures used to operate this reactor were as follow;

(1) Adjust the outlet pressure of N_2 gas to 1 kg/cm^2, and allow the gas to flow through a needle valve.

(2) Adjust 2 three way valves to allow gas to pass through the lower line through the reactor and measure the outlet gas flow rate by using a bubble flow meter.

(3) Heat the reactor from room temperature to 300 ^{o}C and maintain at this temperature for 30 min. Then the reactor was heated to the required temperature and wait until the required temperature becomes constant.

(4) At the same time switch on the heating line, magnetic stirrer and water-bath

(5) Set the water bath temperature at 45 ^{o}C to keep methanol/toluene feed ratio about 2.5-3.5 by wt.

(6) Start to run the reaction by adjusting 2 three way valves to allow nitrogen gas to pass through methanol and toluene mixture inside the saturator set in the water bath. The methanol/toluene feed ratio was controlled by the water-bath temperature.

(7) Take feeds for analysis at 30 min and take products to analyze at 1 and 2 h on stream. The reaction feeds and products were analyzed by gas chromatograph; capillary column. Then, the reaction was repeated at the same condition and take products to analyze at 1 and 2 h on stream by gas chromatograph; packed column, to investigate p-xylene/m-xylene ratio by wt. (For calculation see Appendix A-4)

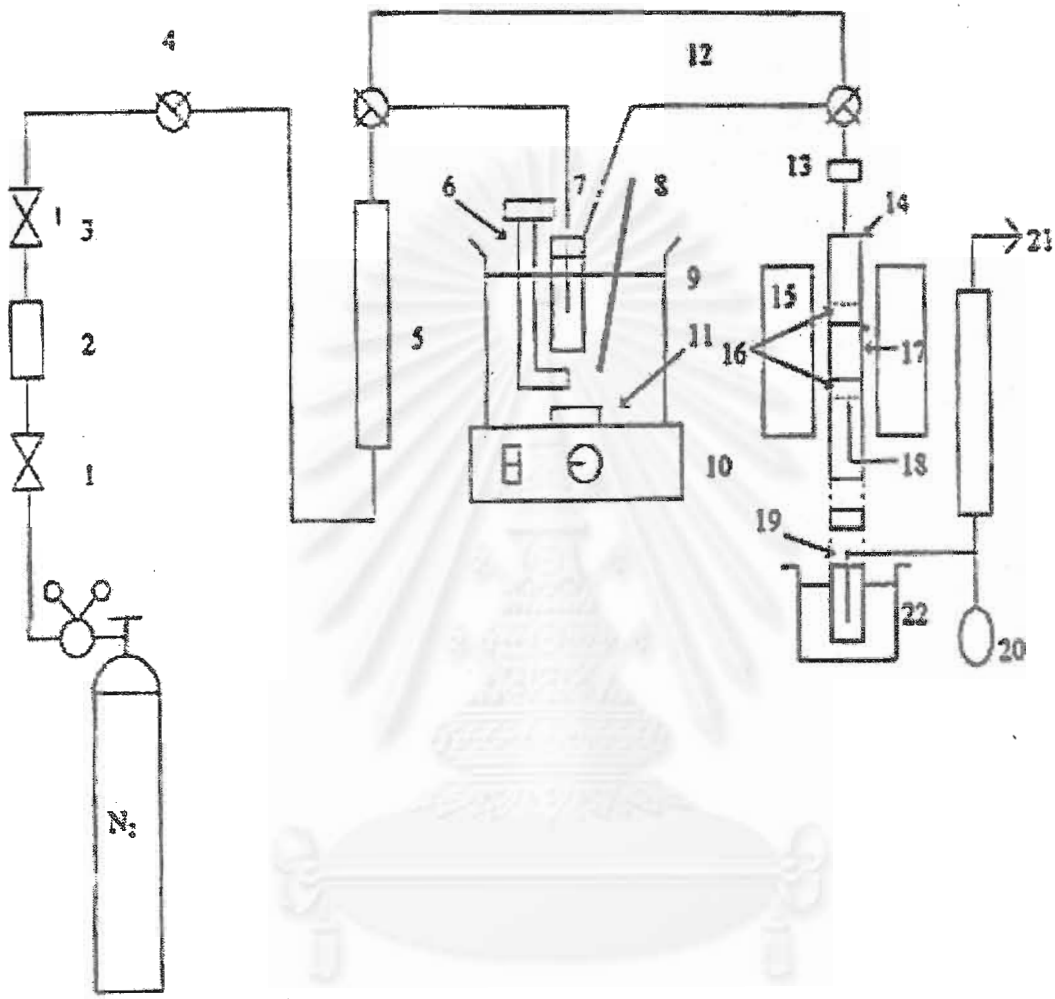

1. On-off valve, 2. Gas filter, 3. Needle valve, 4. Three-way valve, 5. Flow meter, 6. Water bath heater, 7. Saturator set, 8. Thermocouple, 9. Water bath, 10. Stirring controller, 11. Magnetic bar, 12. Heating line, 13. Sampling port, 14. Tubular reactor, 15. Electric furnace, 16. Quartz wool, 17.Catalyst, 18. Thermocouple, 19. Ribbon heater, 20. Soap-film flowmeter, 21. Purge, 22. Trap

Figure 4.4 Schematic Diagram of The Reaction Apparatus for The Alkylation of Toluene with Methanol

4.5 Characterization of Prepared Catalysts

4.5.1 X-ray Diffraction

X-ray powder diffraction (XRD) was used to confirm the MFI structure of prepared catalysts. XRD patterns were performed by using Rigakn-Denki Geigerflex-2013 with Ni-filtrated monochromatic CuK_{α} radiation at the Scientific and Technological Research Equipment Center, Chulalongkorn University (STREC).

4.5.2 Scanning Electron Microscope

The morphology of the prepared catalysts was observed by scanning electron microscope (SEM) using JEOL JSM-35 CF at the Scientific and Technological Research Equipment Center, Chulalongkorn University (STREC).

4.5.3 Chemical Analysis

The chemical compositions of prepared catalysts were measured by X-ray fluorescence (XRF) using Fisons spectrometer ARL-8410 with Uniquant 2 software at the Department of Science Service, Ministry of science, Technology and Environment.

4.5.4 BET Surface Area Measurement

The BET surface areas, micro pore areas, external surface areas and average pore diameter of the prepared catalysts were measured by the BET method, with nitrogen as the adsorbent using a Micromeritics model ASAP 2000 at the Analysis Center of Department of Chemical Engineering, Faculty of Engineering, Chulalongkorn University.

4.5.5 Temperature Programmed Oxidation (TPO)

Temperature Programmed Oxidation of catalyst was carried out in quartz tubular reactor (8 mm. OD) placed inside an electric furnace. The furnace temperature was controlled by a temperature controller (PC 600, Shinko) using 1% oxygen in helium as an oxidizing agent. The effluent was analyzed by gas chromatograph (SHIMADZU 8 AIT).

4.5.6 FTIR Spectroscopy

The acidity measurements was confirmed by using pyridine adsorption technique on *in-situ* FTIR at Petrochemical Engineering Research Laboratory, Chulalongkorn University.

Pyridine adsorption technique on *in-situ* FTIR was described as following procedure: The prepared catalysts were pressed into self-supporting wafer, mounted in a vacuum apparatus, containing cell for IR measurements fitted with potassium bromide windows. The wafer was pretreated by heating to 300 ^{o}C for 1 h under vacuum. Then pyridine was allowed to expose the wafer for 2 h at room temperature. The wafer was then evacuated at 50 ^{o}C for 10 min and heated from 50 ^{o}C to 500 ^{o}C at the rate 5 ^{o}C/min to desorb the absorbed pyridine. In order to measure acid concentration and compare acid strength, the spectra were corrected at 150, 200, 250, 300, 350, 400, 450 and 500 ^{o}C, respectively. The apparatus is shown in Figure 4.5.

Infrared spectra were corrected on a Nicolet Impact 400 spectrometer using OMNIC's software version 1.2a with a resolution of 4 cm^{-1} and typically 500 interferograms were used as an average value.

4.5.7 UV Diffuse Reflectance

Diffuse reflectance UV-visible spectra were analyzed to confirm tetrahedral framework using CARY 5E UV-Vis-NIR at Yokohama National University

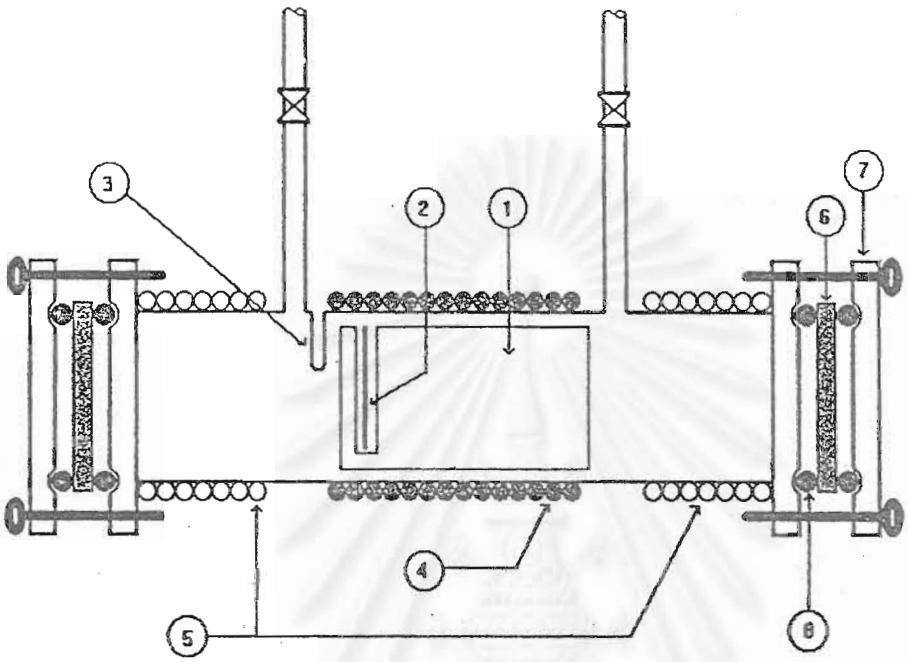

1. Sample Holder
2. Sample Disk
3. Thermocouple Position
4. Heating Rod
5. Water Cooling Line
6. KBr Window
7. Flange
8. O-ring

Figure 4.5 IR Gas Cell Used for The Pyridine Adsorption Technique

CHAPTER V

RESULTS AND DISCUSSIONS

The characteristics of prepared catalysts and catalytic performances on alkylation of toluene with methanol were investigated. The results and discussions are shown as follows.

5.1 Characterization of Prepared Catalysts

All catalysts used in this study were first characterized to overview the difference of their characteristics and properties.

5.1.1 X-ray Diffraction Pattern

The X-ray diffraction patterns of typical ZSM-5 and all the prepared catalysts are shown in Figures 5.1 and 5.2. It was found that the prepared catalysts have the highly crystalline MFI-type zeolite structure, with well-defined characteristic peaks compared with calcined ZSM-5 from patent shown in Figure 5.1. While other non-zeolite phases such as ferro-aluminate, zinco-aluminate and oxide phases of Fe, or Zn were not detected. This indicated that a little amount of metal loaded did not change the main structure of MFI-type zeolite catalysts.

5.1.2 FTIR and UV-Diffuse Reflectance

The MFI-type framework structure has been further confirmed by FTIR spectra using potassium bromide (KBr) (0.5 % by weight catalyst) for studying vibrational modes in the structural sensitive region [49, 50] and UV- Diffuse

Diffuse Reflectance. From Figure 5.3, it has been found that all the prepared catalysts provided the similar asymmetric stretching vibration at 1220-1230 and 1100-1110 cm^{-1}; symmetric stretching vibration at 795-800 cm^{-1}; double ring vibration at about 540-555 cm^{-1}; and the T-O stretching vibration at 440-450 cm^{-1}. These are characteristic features of IR spectra for typical MFI structure. From Figure 5.4, the UV diffuse reflectance peaks around 200-225 nm were found in both H-Fe,Al-silicate and H-Zn,Al-silicate but not observed in Fe_2O_3 and ZnO. Yong and Wha reported the UV diffuse reflectance peak of tetrahedral TiO_4 at around 210 nm [47]. Therefore, it may be suggested that at least some part of Fe or Zn was incorporated into the MFI framework. However, the broad peaks obtained in both cases may be ascribed to some metal oxides formed in case of high loading amount.

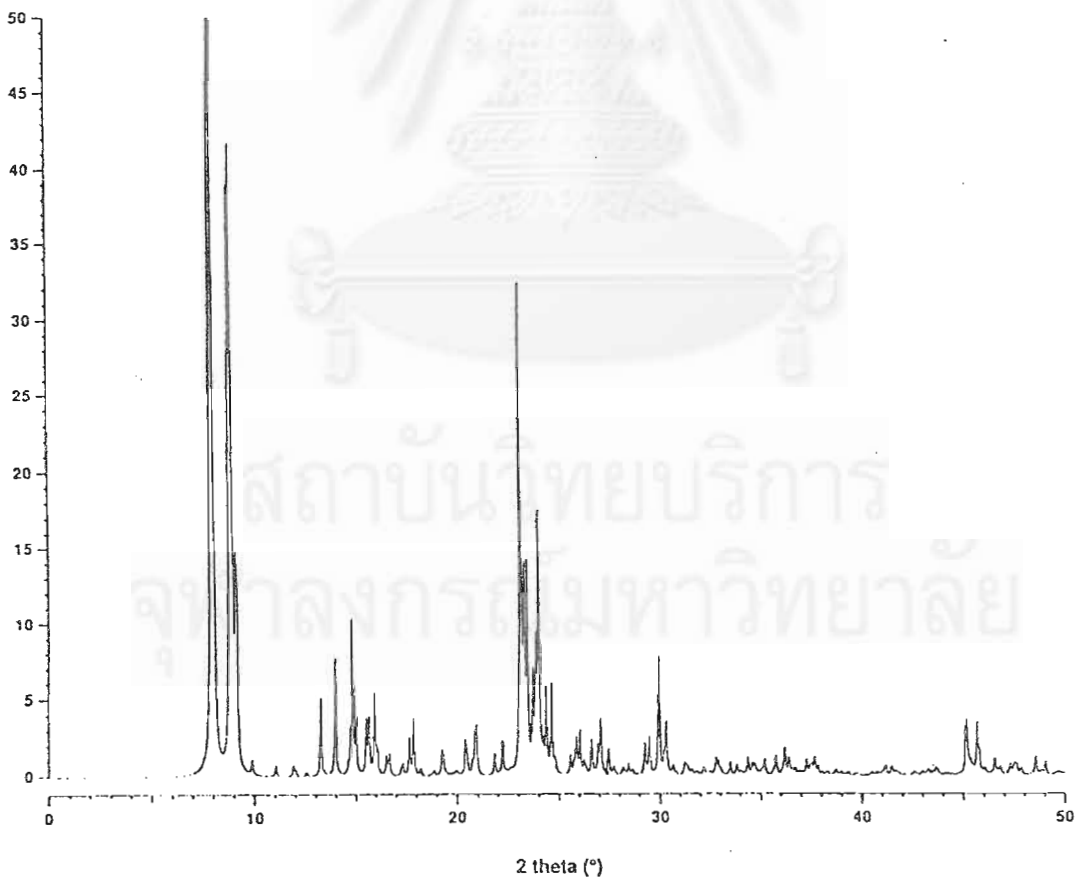

Figure 5.1 X-ray Diffraction Pattern of Calcined ZSM-5 from Patent [48]

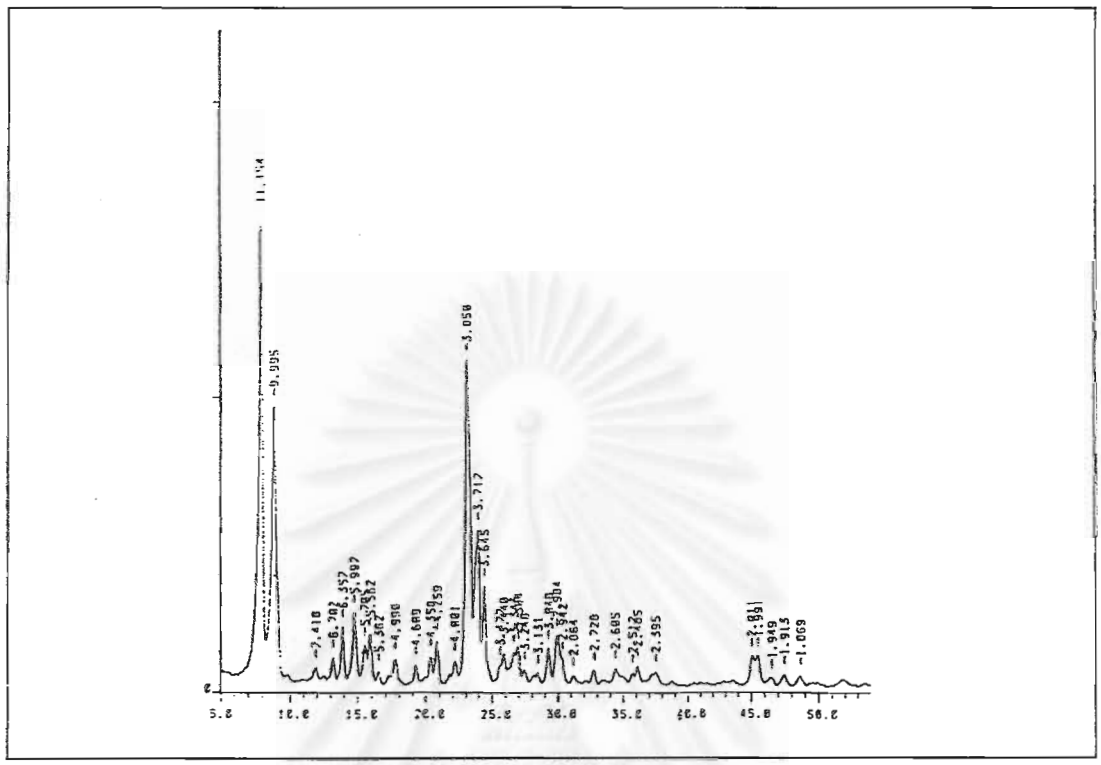

Na-MFI; % Crystallization = 86.61

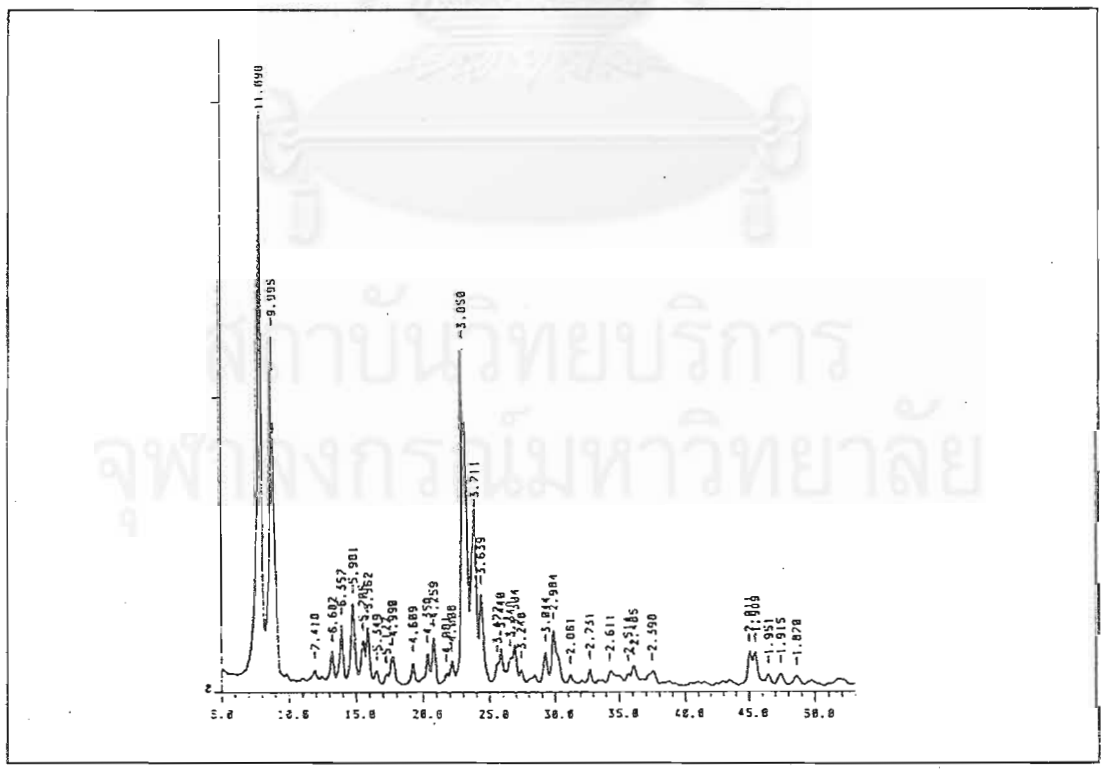

H-MFI; % Crystallization = 78.60

Figure 5.2 X-ray Diffraction Patterns of Prepared Catalysts

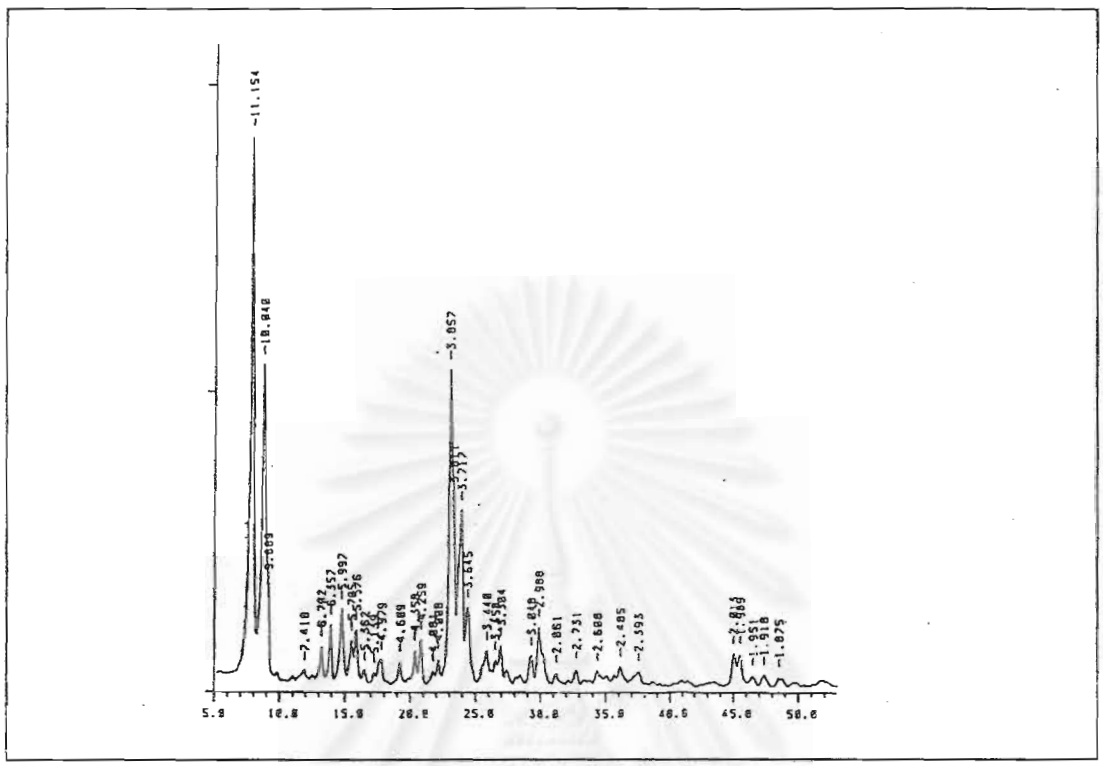

Fe(0.8 %)/H-MFI; % Crystallization = 85.88

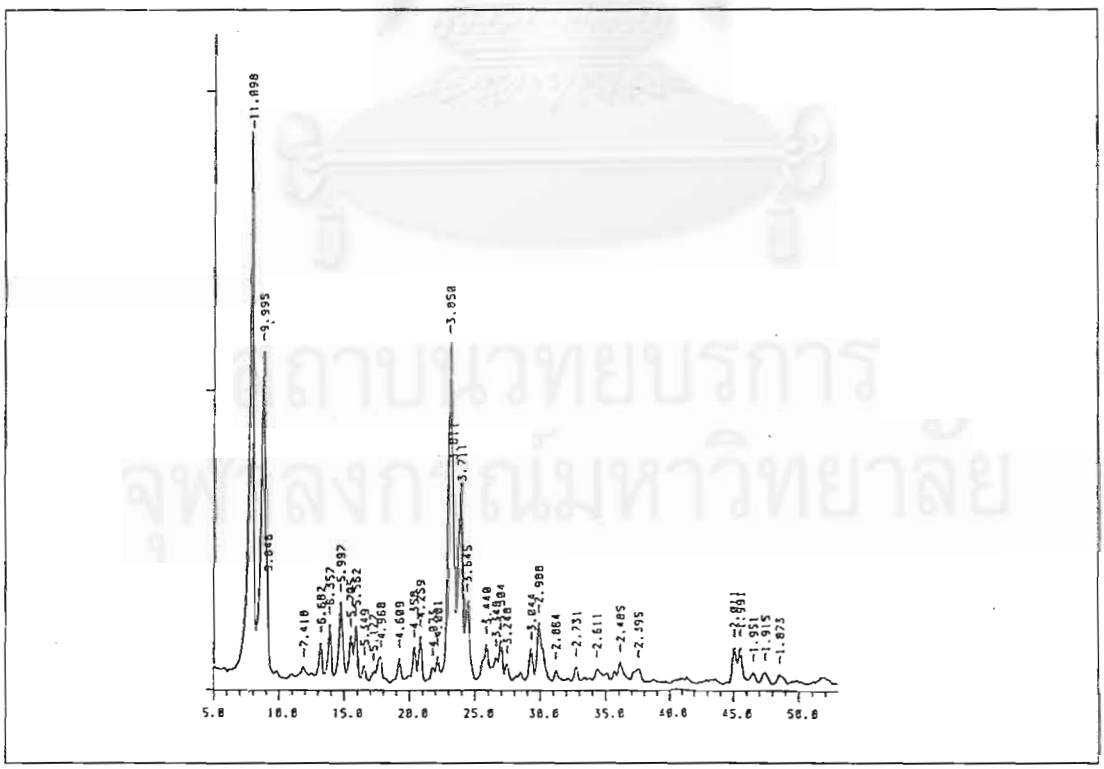

Zn(1.0 %)/H-MFI; % Crystallization = 90.07

Figure 5.2 X-ray Diffraction Patterns of Prepared Catalysts (continued)

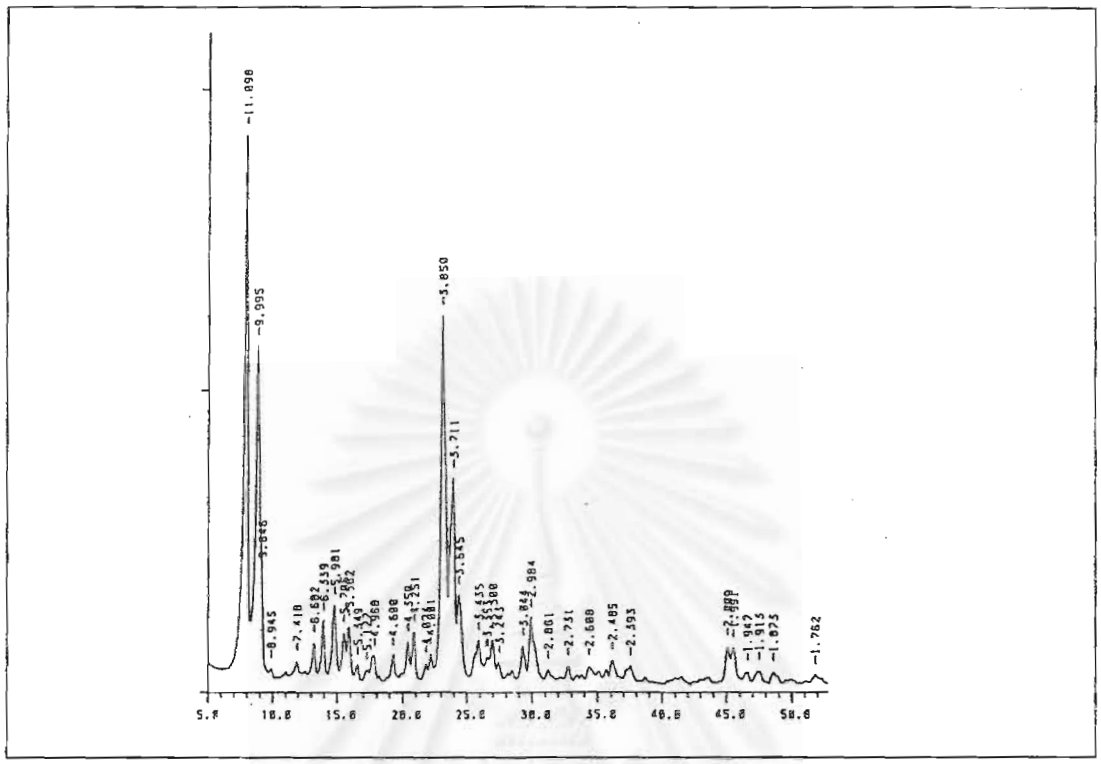

H-Fe,Al-silicate (Si/Fe=150); % Crystallization = 89.70

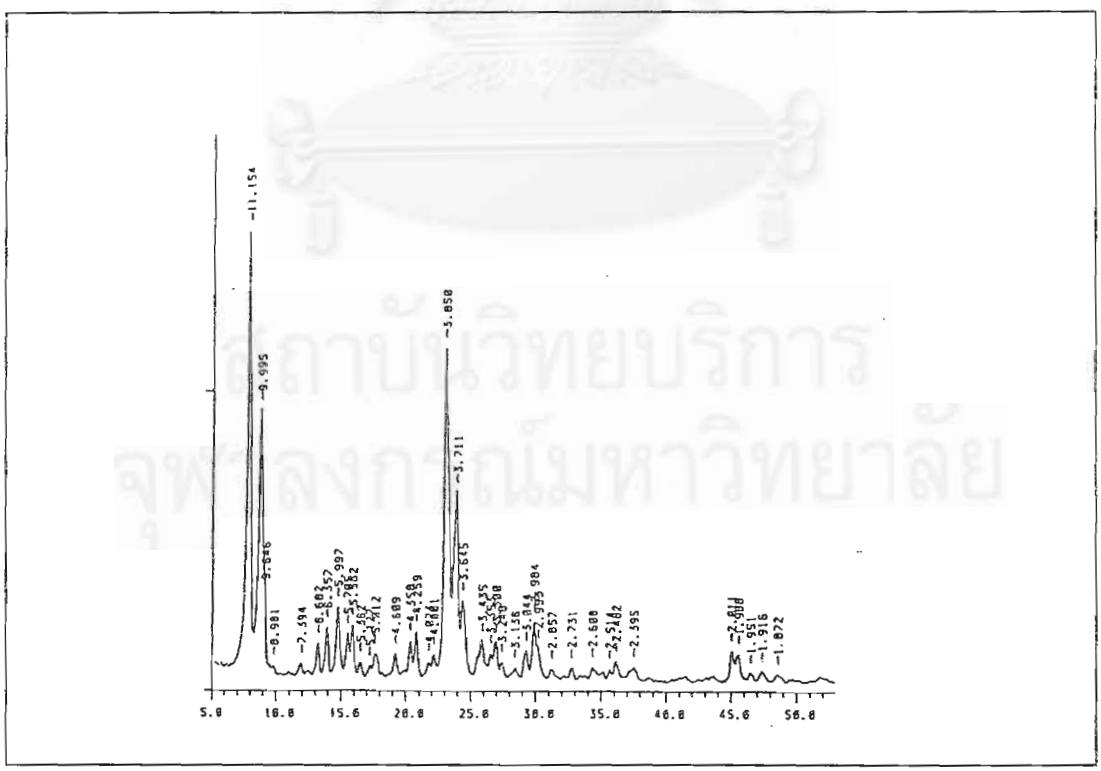

H-Zn,Al-silicate (Si/Zn=150); % Crystalinity = 99.53

Figure 5.2 X-ray Diffraction Patterns of Prepared Catalysts (continued)

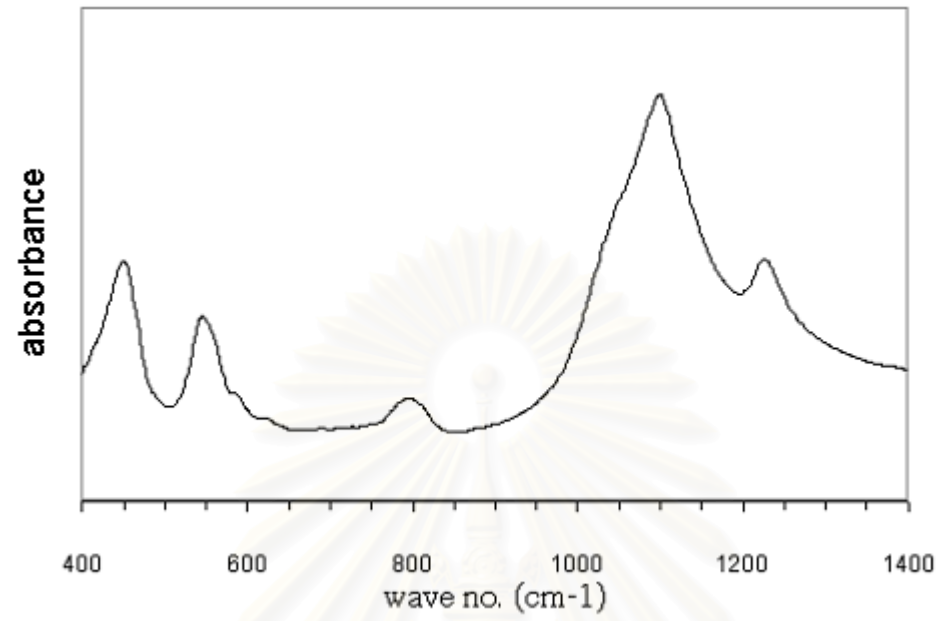

Na-MFI

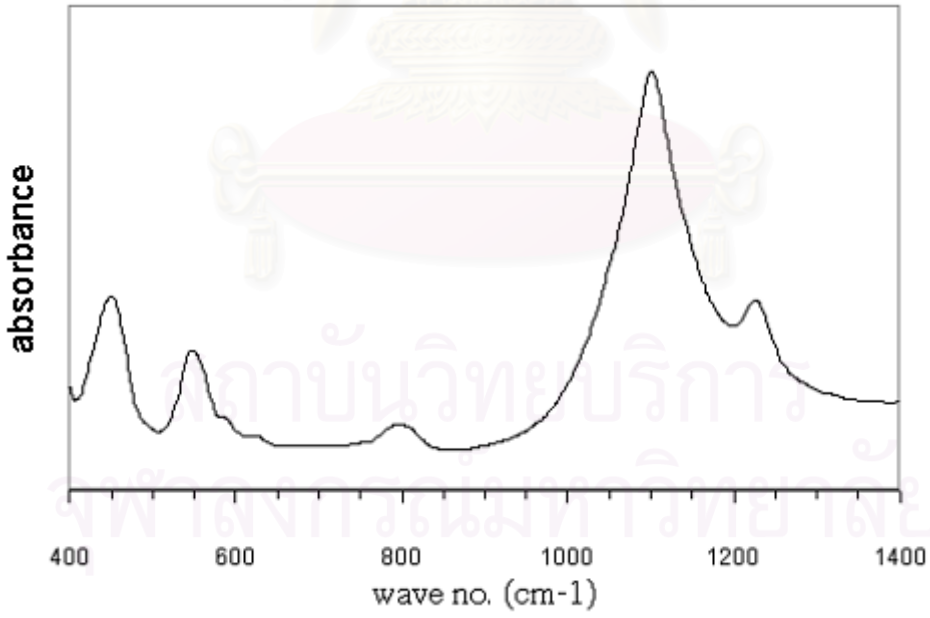

H-MFI

Figure 5.3 FTIR Spectra of Prepared Catalysts

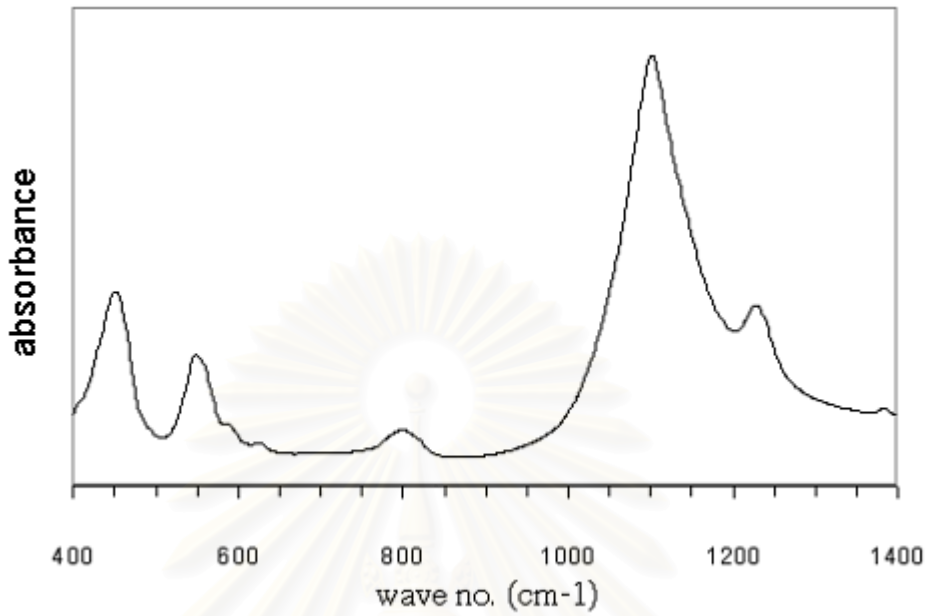

Fe(0.8 %)/H-MFI

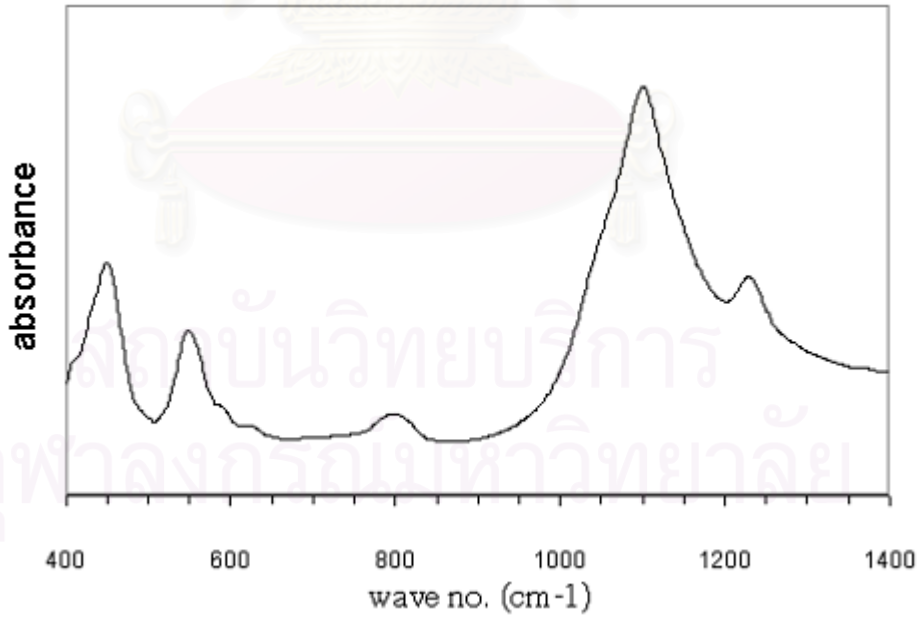

Zn(1.0 %)/H-MFI

Figure 5.3 FTIR Spectra of Prepared Catalysts (continued)

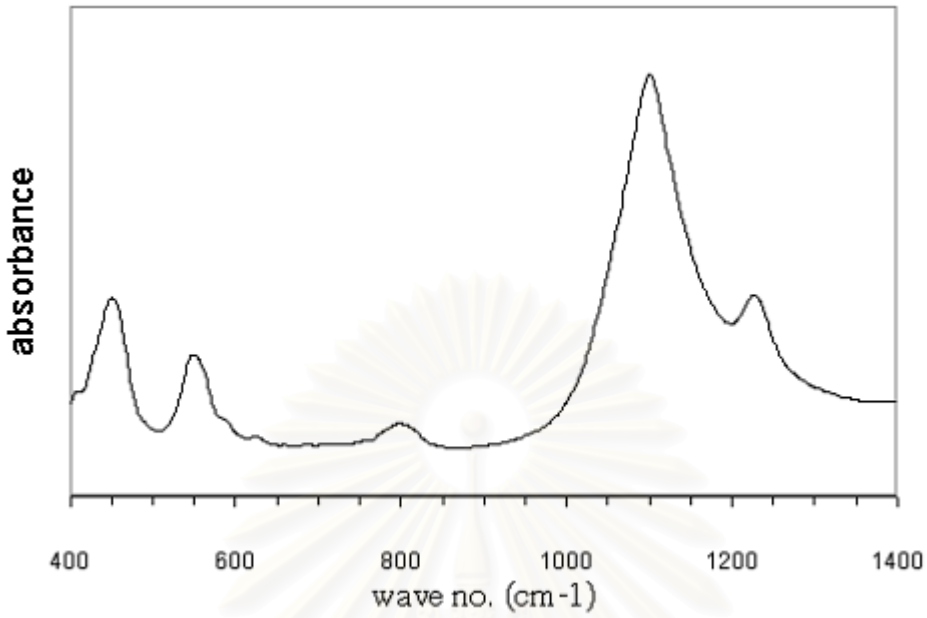

H-Fe,Al-silicate (Si/Fe=150)

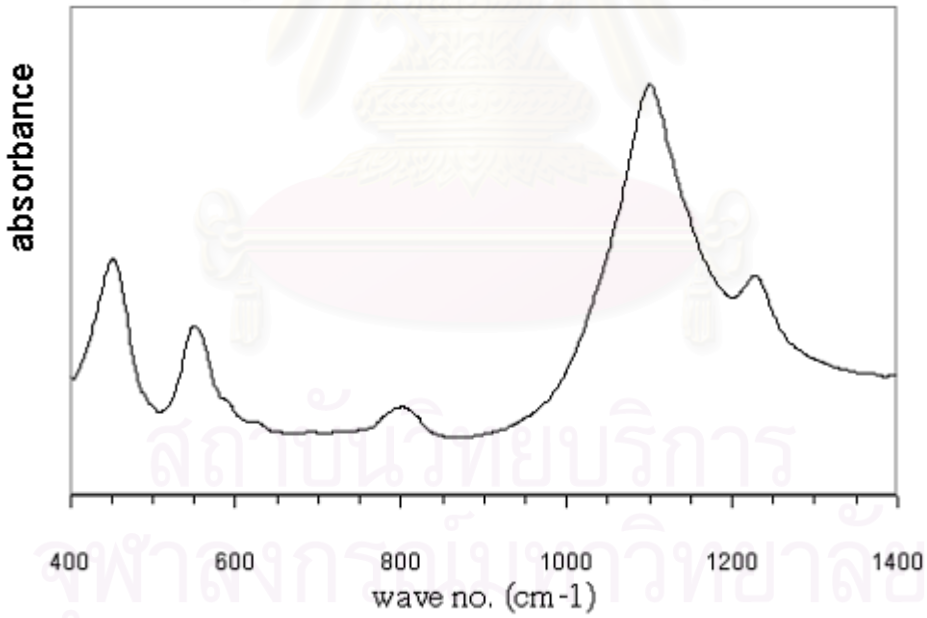

H-Zn,Al-silicate (Si/Zn=150)

Figure 5.3 FTIR Spectra of Prepared Catalysts (continued)

(a) H-Fe,Al-silicate(Si/Fe=150)

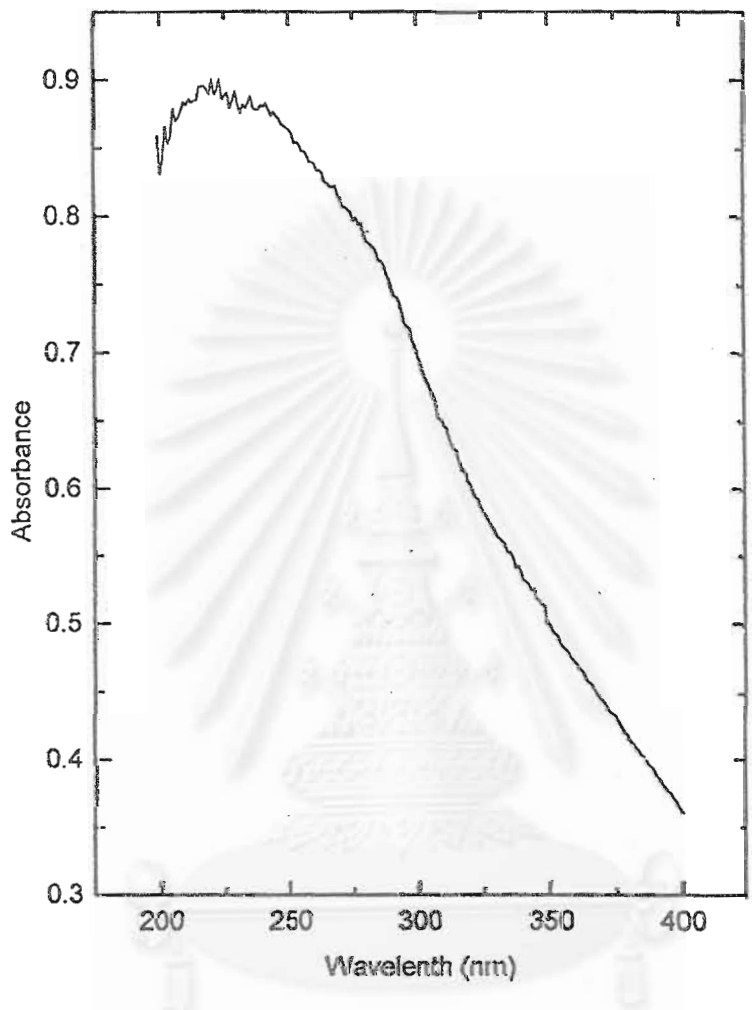

Figure 5.4 UV-Diffuse Reflectance of (a) H-Fe,Al-silicate(Si/Fe=150).

(b) Ref. Fe_2O_3 Powder

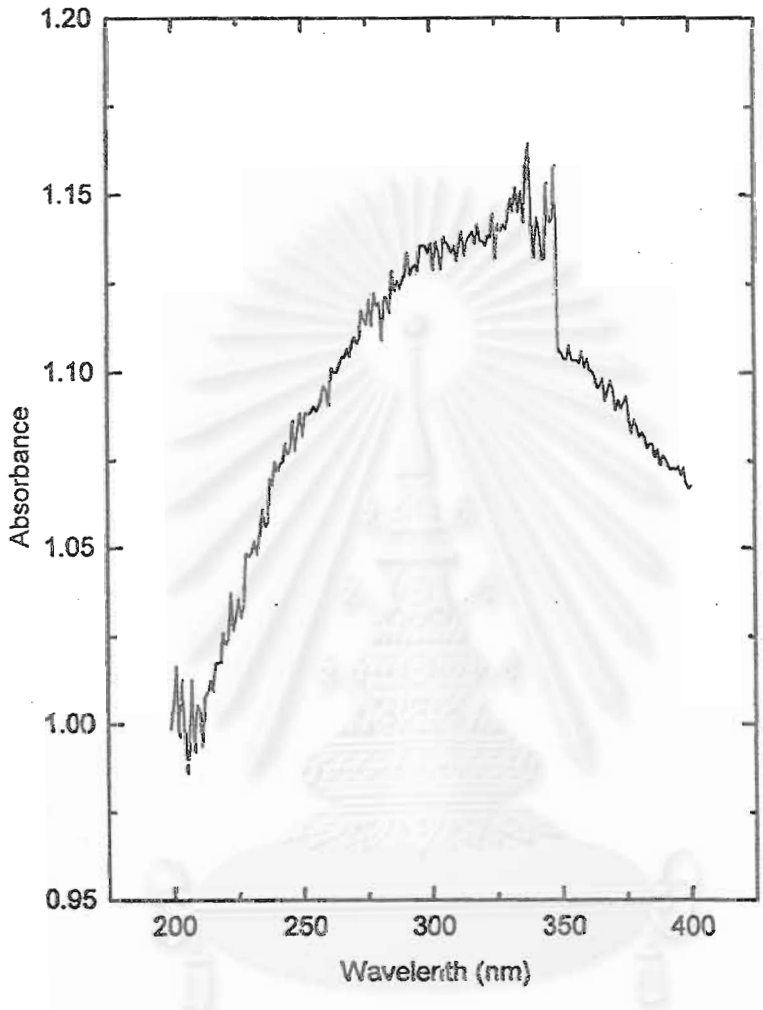

Figure 5.4 UV-Diffuse Reflectance of (b) Ref. Fe_2O_3 Powder.

(c) H-Zn,Al-silicate(Si/Zn=150)

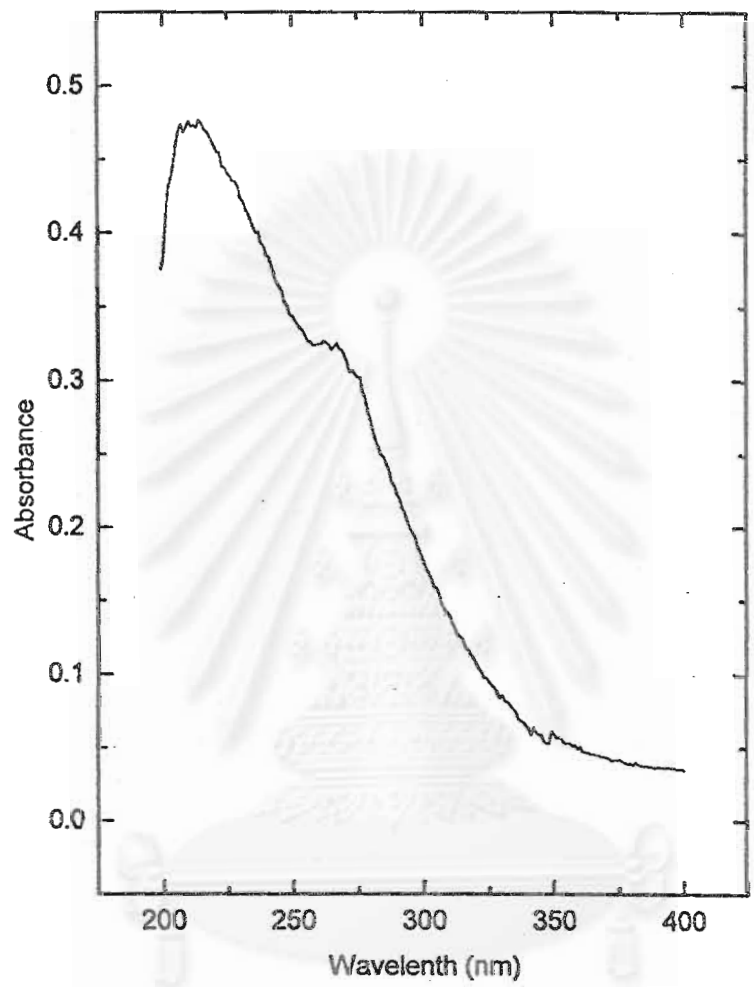

Figure 5.4 UV-Diffuse Reflectance of (c) H-Zn,Al-silicate(Si/Zn=150).

(d) Ref. ZnO Powder

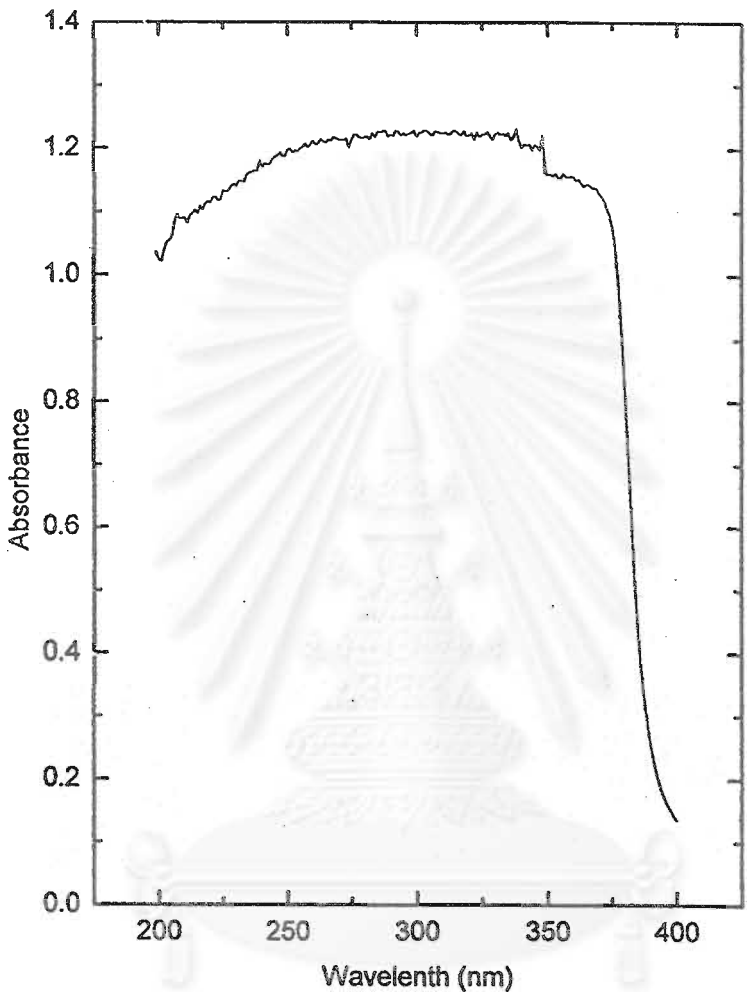

Figure 5.4 UV-Diffuse Reflectance of (d) Ref. ZnO Powder.

5.1.3 Scanning Electron Microscope

SEM photographs of prepared catalysts are shown in Figure 5.5. It is found that all particles are spherical in shape and they are composed of tiny unit crystallites. The crystal surfaces are not clean, some particles adhere to the surfaces making them rough.

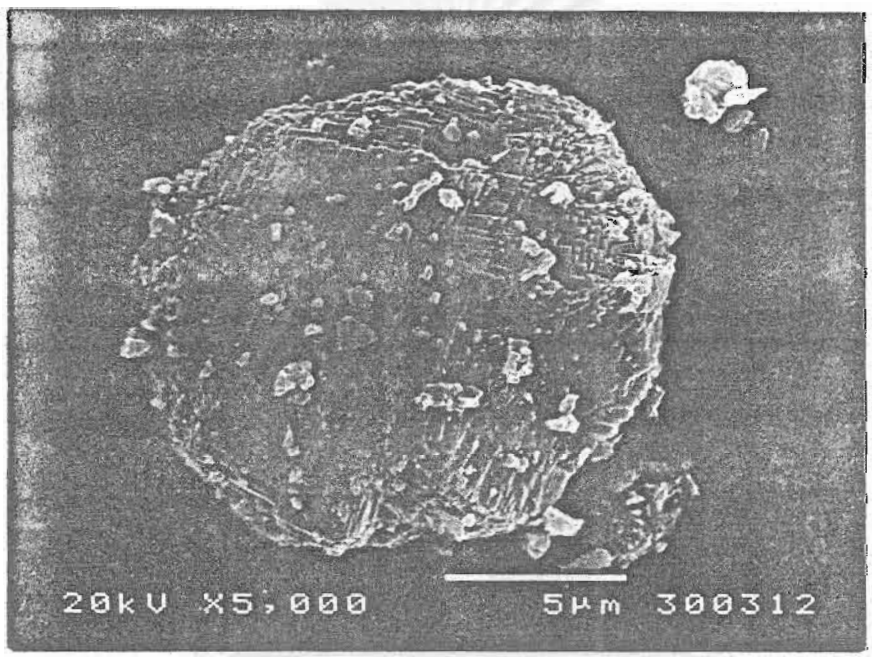

H-MFI

Figure 5.5 SEM Photographs of Prepared Catalysts

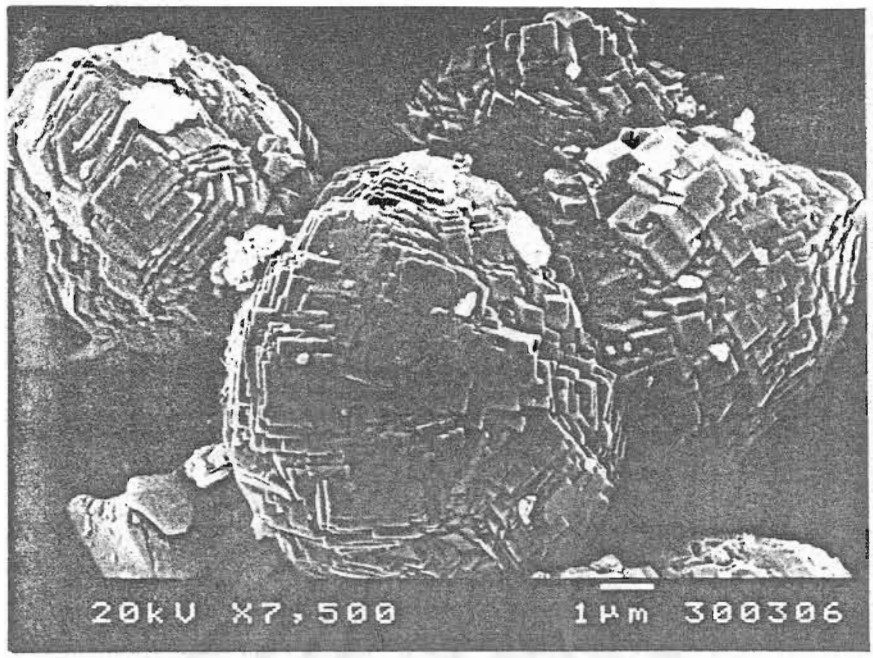

Fe(0.8 %)/H-MFI

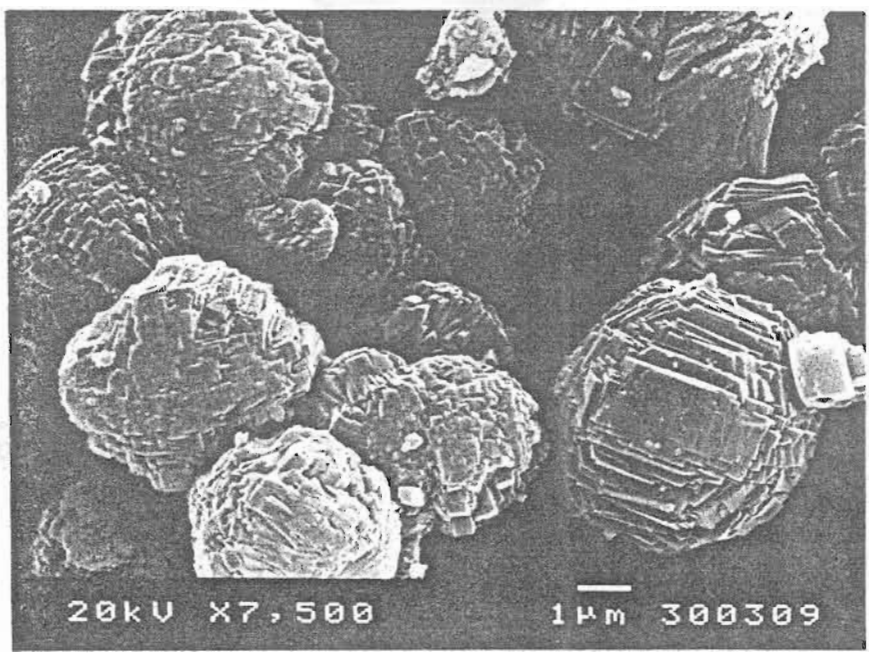

Zn(1.0 %)/H-MFI

Figure 5.5 SEM Photographs of Prepared Catalysts (continued)

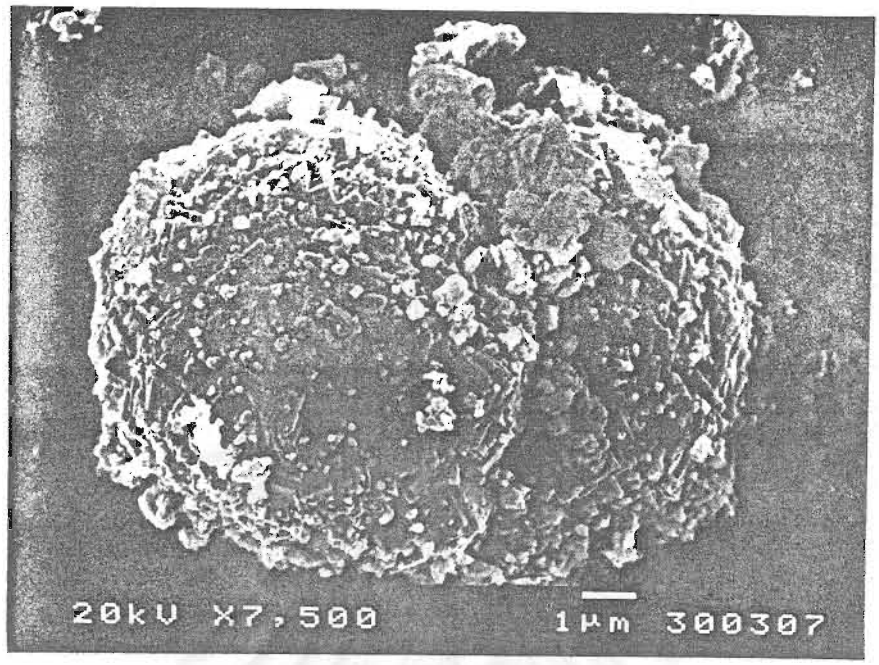

H-Fe,Al-silicate (Si/Fe=150)

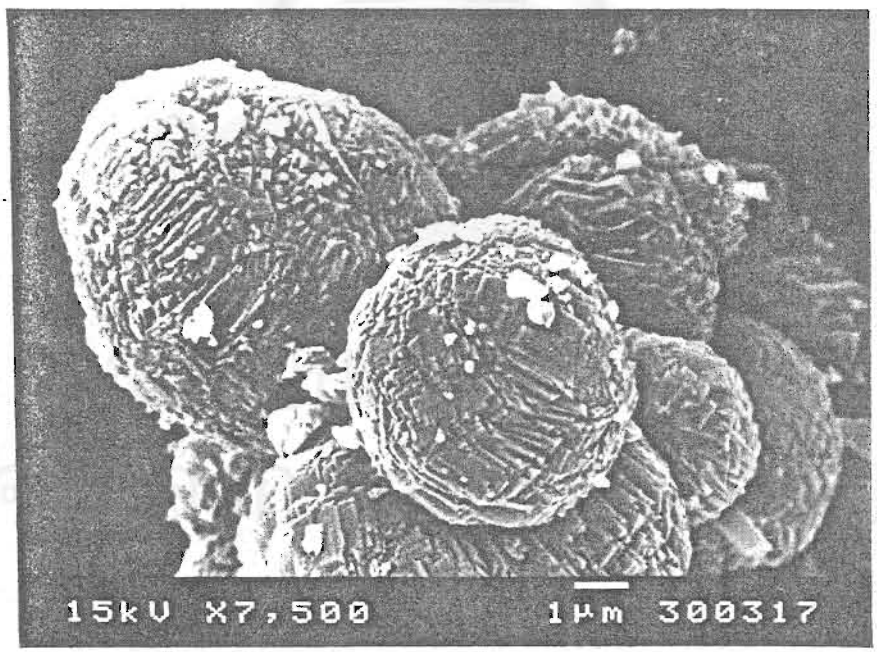

H-Zn,Al-silicate (Si/Zn=150)

Figure 5.5 SEM Photographs of Prepared Catalysts (continued)

5.1.4 Chemical Analysis

The contents of Fe or Zn in ion-exchanged H-MFI and incorporated H-MFI are shown in Table 5.1 and Table 5.2, respectively.

Table 5.1 Fe or Zn Contents in Ion-exchanged H-MFI

(a) Fe/H-MFI with Si/Al atomic ratio about 33.7

% Fe loaded (by wt.)	% Fe observed (by wt.)
0.2	0.25
0.5	0.39
0.8	0.46
1.0	0.76
2.0	1.16

(b) Zn/H-MFI with Si/Al atomic ratio about 32.1

% Zn loaded (by wt.)	% Zn observed (by wt.)
0.2	0.19
0.5	0.34
0.8	0.55
1.0	0.74
2.0	1.12

Table 5.2 Fe or Zn Contents in incorporated H-MFI

Catalyst	Si/Al observed	% Fe observed (by wt.)	% Zn observed (by wt.)
H-Fe,Al-silicate (Si/Fe=150)	34.93	0.50	-
H-Zn,Al-silicate (Si/Zn=150)	31.72	-	0.76

The observed contents of loading metal increase with an increase in charged contents and mainly depend on the nature of loading metal.

5.1.5 BET Measurement

BET surface areas of prepared catalysts are shown in Table 5.3.

Table 5.3 BET Surface Areas of Prepared Catalysts

Catalyst	BET surf. area (m^2/g)
H-MFI	376
Fe(0.2)/H-MFI	386
Fe(0.8)/H-MFI	380
H-Fe,Al-silicate (Si/Fe=150)	378
Zn(0.2)/H-MFI	369
Zn(1.0)/H-MFI	386
H-Zn,Al-silicate (Si/Zn=150)	379

* All the prepared catalysts have bulk Si/Al atomic ratio in the range of 31-35.

From Table 5.3, the BET surface areas of prepared catalysts were assessed by a surface area analyzer (Micromeritics model ASAP 2000). All the samples had BET surface areas in the range of 375-385 m^2/g approximately as commonly found in MFI-type catalyst.

5.1.6 Pyridine Adsorption Technique on *in-situ* FTIR

From the previous studies [51-53], the bands at about 1540 cm^{-1} and 1450 cm^{-1} were assigned to pyridine adsorbed on Brönsted and Lewis acid sites, respectively. The FTIR spectra of pyridine adsorbed on the prepared catalysts are shown in Figs. 5.6-5.12.

The number of Brönsted and Lewis acid site of each zeolite sample was determined by measurement of peak areas of these bands at 150 ^oC as summarized in Table 5.4 while the relative acid strength was determined from the trend of pyridine desorbed in the range of 150 ^oC - 400 ^oC as shown in Figs 5.7-5.12.

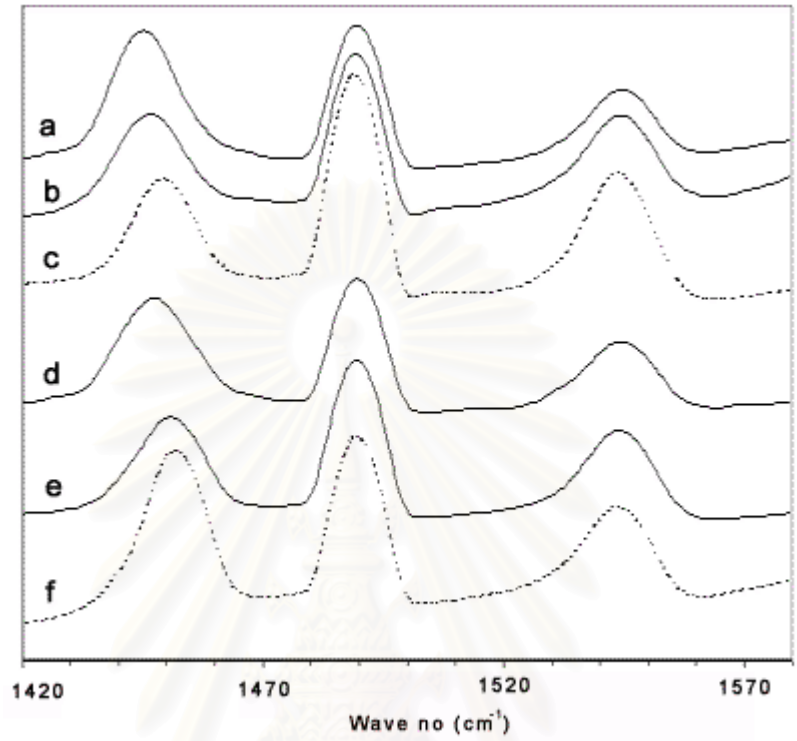

Figure 5.6 FTIR spectra of pyridine adsorbed on prepared catalysts at 150 ^{o}C: (a) Fe(0.2)/H-MFI, (b) Fe(0.8)/H-MFI, (c) H-Fe,Al-silicate (Si/Fe=150), (d) Zn(0.2)/H-MFI, (e) Zn(1.0)/H-MFI and (f) H-Zn,Al-silicate (Si/Zn=150)

Table 5.4 The number of Brönsted and Lewis acid sites

Catalyst	A_B	A_L
Fe(0.2)/H-MFI	36.8	90.1
Fe(0.8)/H-MFI	60.0	63.5
H-Fe,Al-silicate (Si/Fe=150)	79.6	61.9
Zn(0.2)/H-MFI	36.7	73.1
Zn(1.0)/H-MFI	54.9	66.0
H-Zn,Al-silicate (Si/Zn=150)	46.0	93.6

* A_B and A_L refer to areas by weight of band at 1540 cm^{-1} due to Brönsted acid sites and at 1450 cm^{-1} due to Lewis acid sites, respectively.

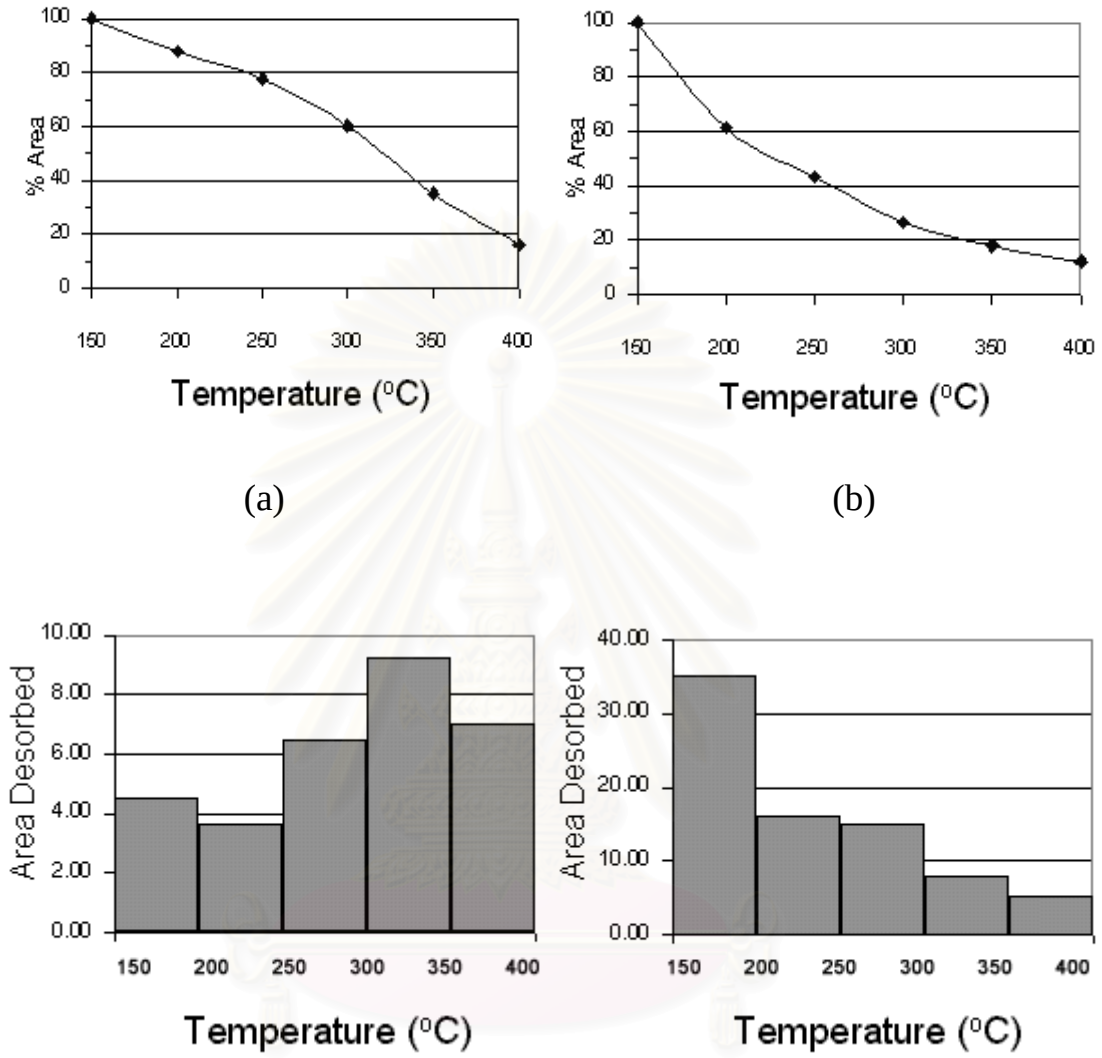

Figure 5.7 The percentage of peak areas of pyridine desorbed on (a) Brönsted or (b) Lewis and the amount of pyridine desorbed from (c) Brönsted or (d) Lewis at various temperature on Fe(0.2)/H-MFI

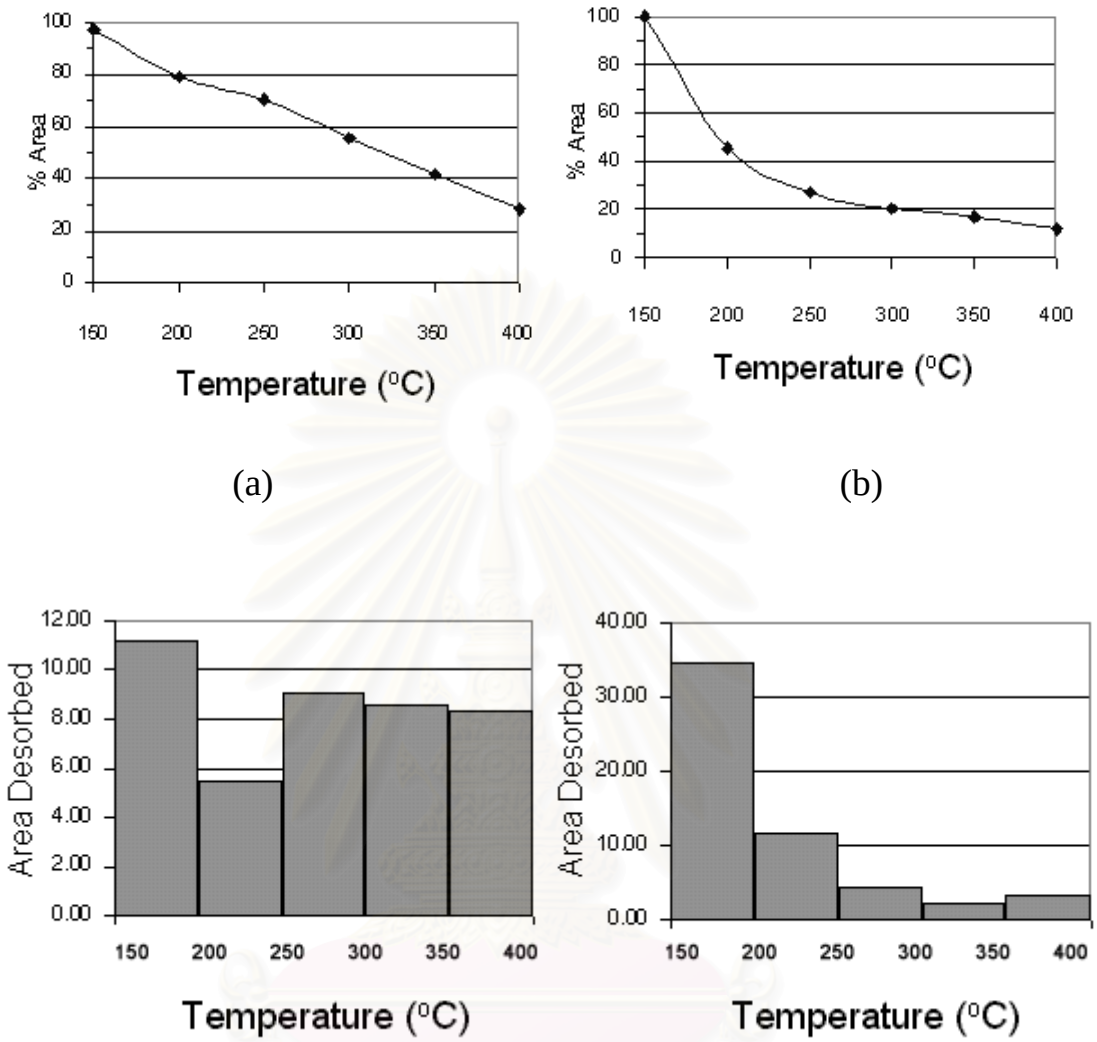

Figure 5.8 The percentage of peak areas of pyridine desorbed on (a) Brönsted or (b) Lewis and the amount of pyridine desorbed from (c) Brönsted or (d) Lewis at various temperature on Fe(0.8)/H-MFI

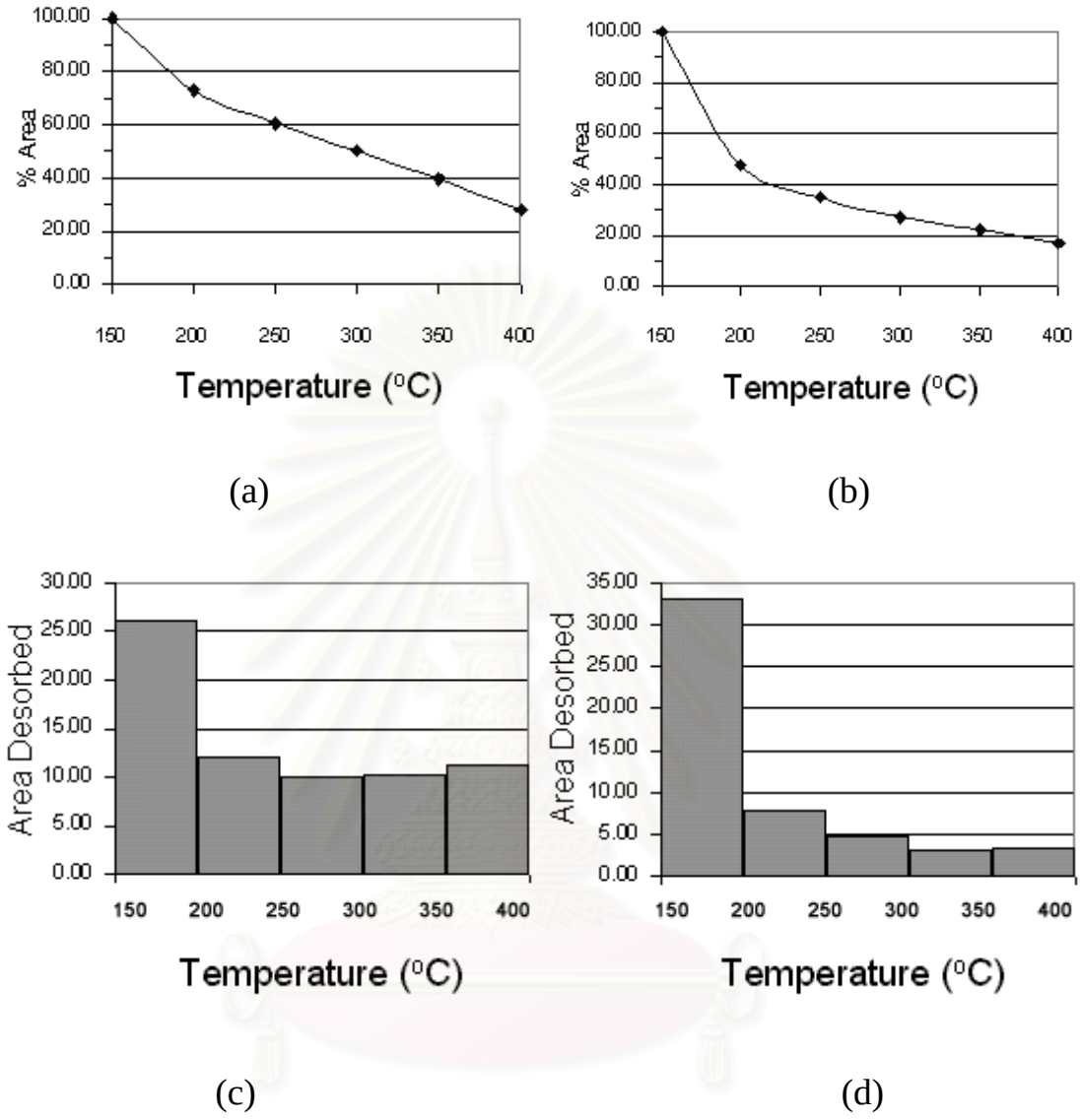

Figure 5.9 The percentage of peak areas of pyridine desorbed on (a) Brönsted or (b) Lewis and the amount of pyridine desorbed from (c) Brönsted or (d) Lewis at various temperature on H-Fe,Al-silicate (Si/Fe=150)

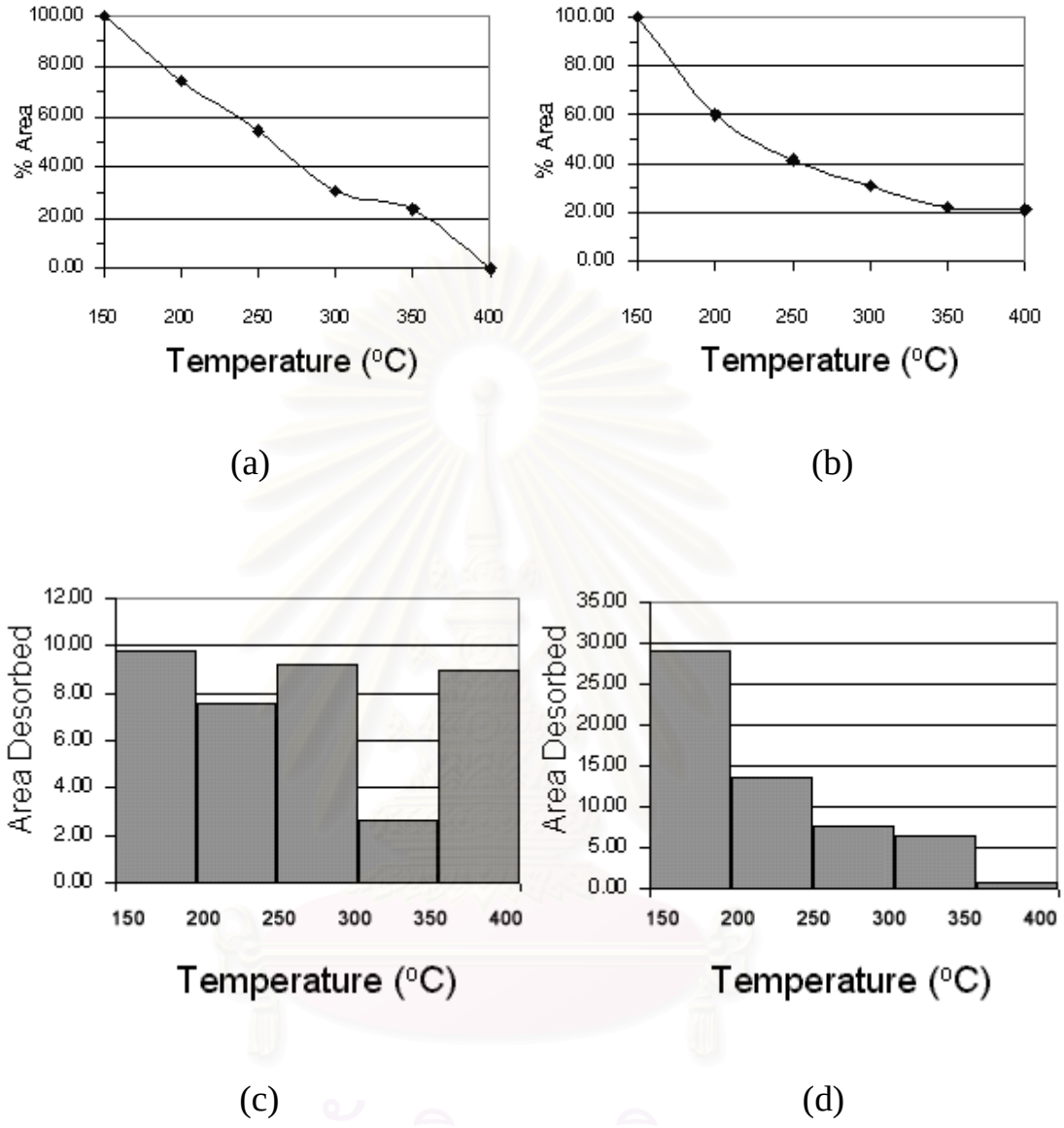

Figure 5.10 The percentage of peak areas of pyridine desorbed on (a) Brönsted or (b) Lewis and the amount of pyridine desorbed from (c) Brönsted or (d) Lewis at various temperature on Zn(0.2)/H-MFI

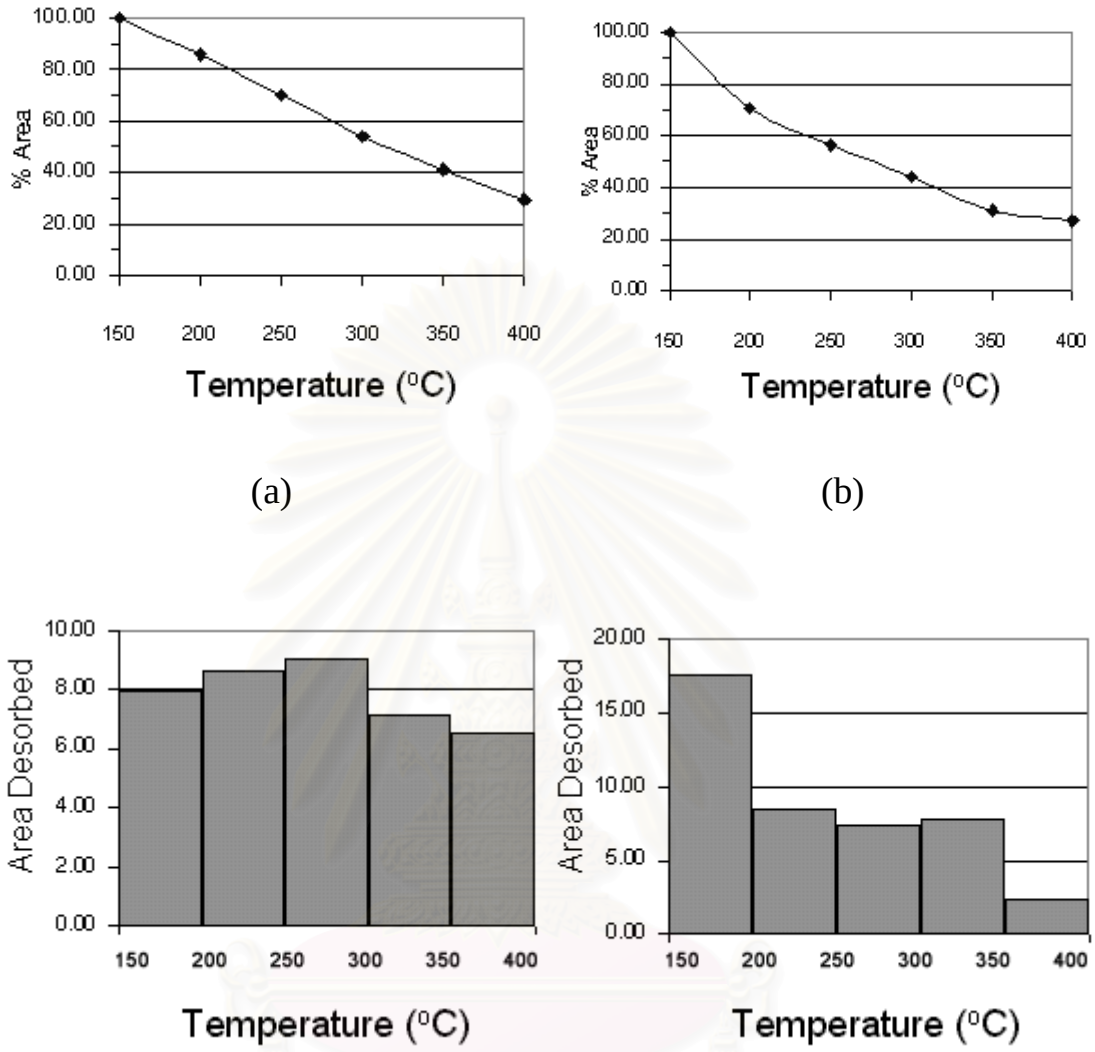

Figure 5.11 The percentage of peak areas of pyridine desorbed on (a) Brönsted or (b) Lewis and the amount of pyridine desorbed from (c) Brönsted or (d) Lewis at various temperature on Zn(1.0)/H-MFI

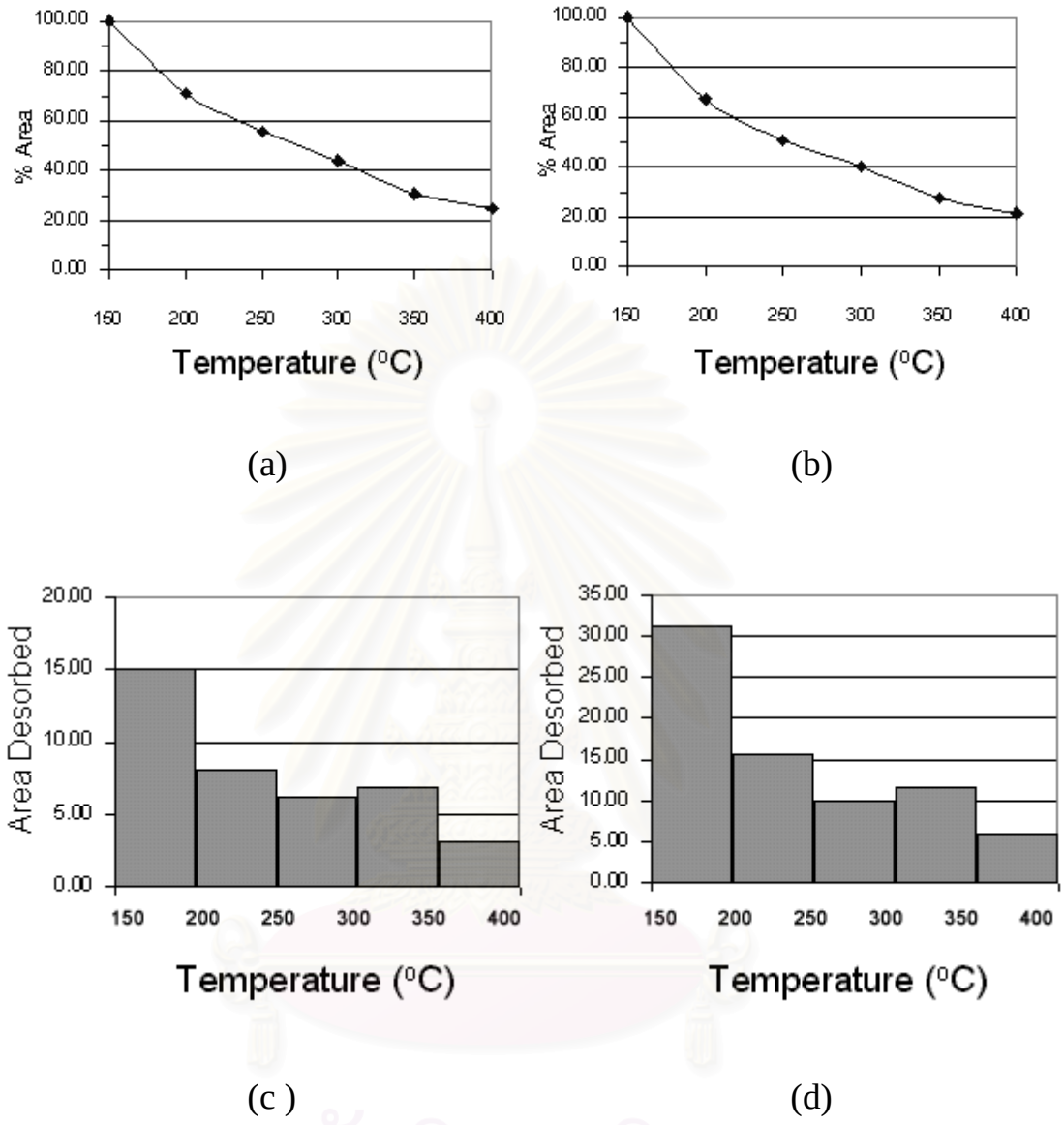

Figure 5.12 The percentage of peak areas of pyridine desorbed on (a) Brönsted or (b) Lewis and the amount of pyridine desorbed from (c) Brönsted or (d) Lewis at various temperature on H-Zn,Al-silicate (Si/Zn=150)

From Figs. 5.7-5.9 and Table 5.4, it has been found that Fe(0.2)/H-MFI containing the smallest amount of Brönsted acid sites. As for Zn-containing MFI, it has been found that the increasing order of Brönsted acid amount was Zn(0.2)/H-MFI < H-Zn,Al-silicate (Si/Zn=150) < Zn(1.0)/H-MFI as shown in Figs. 5.10-5.12 and Table 5.4.

5.2 Alkylation of Toluene with Methanol

5.2.1 Effect of Metal Loading Amount in Fe/H-MFI or Zn/H-MFI Catalysts

Figures 5.13 and 5.14 show the catalytic performance on alkylation of toluene with methanol of Fe/H-MFI and Zn/H-MFI catalysts containing Fe or Zn in the range of 0–2 wt.% loading.

From Figures 5.13 and 5.14, it has been found that Fe(0.8)/H-MFI; Fe/H-MFI with Fe loading content of 0.8 wt.% and Zn(1.0)/H-MFI; Zn/H-MFI with Zn loading content of 1.0 wt.% exhibited the best aromatics (Benzene + Ethylbenzene + Xylene + Ethyltoluene) selectivity and xylene selectivity. While Fe(0.2)/H-MFI and Zn/H-MFI provided the highest *p*-xylene distribution but gave the lowest toluene conversion and aromatics selectivity. Of all xylene produced on any amount of Fe or Zn loading, the amount of o-xylene was almost constant while the amount of *p*-xylene was inversely related with that of m-xylene and toluene conversion. This result can be explained that isomerization of *p*-xylene which was the side reaction plays an important role on xylene distribution [5, 54].

5.2.2 Effect of Metal Loading Method Between Incorporation and Ion-exchange

For comparison, H-MFI incorporated with Fe or Zn, H-Fe,Al-silicate or H-Zn,Al-silicate were prepared. The comparative results are shown in Table 5.5. The thermodynamic compositions of xylene isomers at reaction temperature were given in parentheses.

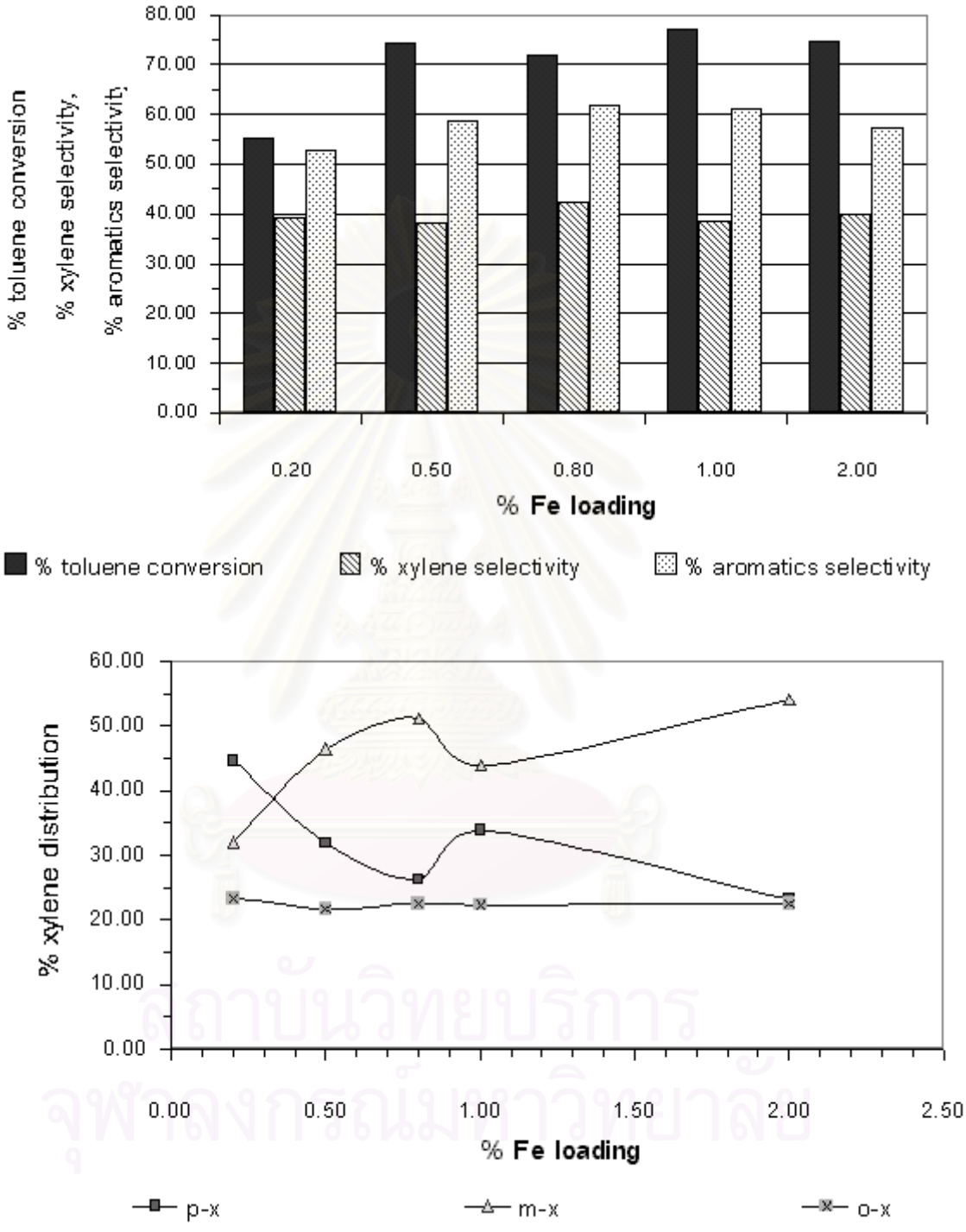

Figure 5.13 Alkylation of Toluene with Methanol on Fe/H-MFI at Various % Fe Loading

(450 ^{o}C, 6000 h^{-1}, 80 min on stream, Methanol/Toluene feed ratio 2.5-3.5 : 1 by wt.)

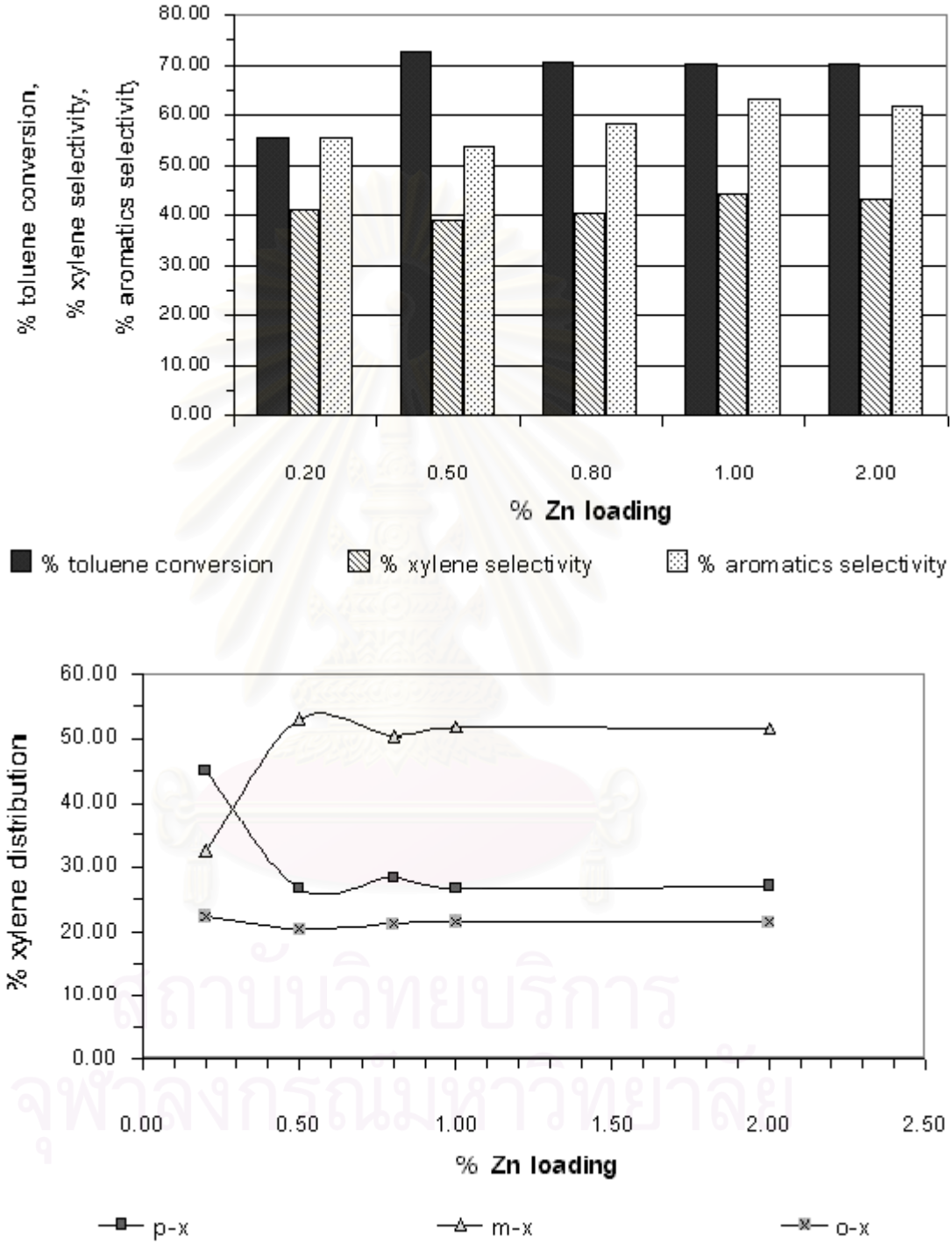

Figure 5.14 Alkylation of Toluene with Methanol on Fe/H-MFI at Various % Zn Loading

(450 ^{o}C, 6000 h^{-1}, 80 min on stream, Methanol/Toluene feed ratio 2.5-3.5 : 1 by wt.)

Table 5.5 Comparison of Catalytic Performance of Prepared Catalysts

(450 ^{o}C, 6000 h^{-1}, 80 min on stream, Methanol/Toluene feed ration 2.5-3.5 : 1 by wt.)

Catalyst	H-MFI	Fe			Zn		
		(0.2)*	(0.8)*	(150)*	(0.2)*	(1.0)*	(150)*
Fe or Zn Observed (wt.%)	0.00	0.20	0.46	0.50	0.19	0.74	0.76
Conversion (%)							
Methanol	90.70	73.06	93.46	93.99	77.73	93.28	93.85
Toluene	66.00	55.10	71.68	70.63	55.54	70.16	72.22
Products Distribution (wt.%)							
C1-C4	40.13	49.41	31.68	31.77	46.68	29.88	27.40
C5-C8	2.04	2.10	2.50	3.99	1.74	3.62	1.83
Benzene	2.18	0.17	1.00	0.51	0.18	1.13	1.02
Toluene	14.62	17.18	12.44	13.25	17.38	14.34	12.16
Ethylbenzene	0.18	0.16	0.28	0.28	0.19	0.32	0.36
Xylene	30.32	20.68	33.62	31.55	22.49	33.88	36.97
Ethyltoluene	8.37	6.76	14.34	13.46	7.51	13.19	16.26
Others	2.18	3.53	4.14	5.21	3.85	3.64	3.99
Xylene Distribution (%)							
p-xylene (21.56)	30.53	44.65	26.27	34.38	45.11	26.67	28.96
m-xylene (53.33)	46.83	32.02	51.20	45.29	32.45	51.70	49.34
o-xylene (25.11)	22.64	23.33	22.53	20.33	22.44	21.62	21.69

* Fe(0.2), Fe(0.8), Fe(150), Zn(0.2), Zn(1.0) and Zn(150) refer to Fe(0.2)/H-MFI, Fe(0.8)/H-MFI, H-Fe,Al-silicate (Si/Fe=150), Zn(0.2)/H-MFI, Zn(1.0)/H-MFI and H-Zn,Al-silicate (Si/Zn=150), respectively.

From Table 5.5, all of the prepared catalysts provided the higher *p*-xylene distribution than that expected from the thermal equilibrium. Both H-Fe,Al-silicate (Si/Fe=150) and H-Zn,Al-silicate (Si/Zn=150) exhibited catalyst activity and xylene selectivity approximately comparable with those of Fe(0.8)/H-MFI and Zn(1.0)/H-MFI with nearly the same amount of the corresponding Fe or Zn. From the results, there is a small amount of benzene product indicating that there is a small degree of toluene

disproportionation which is one type of competitive reactions of toluene alkylation. From Table 5.4 and Table 5.5, it has been found that Fe(0.2)/H-MFI containing the smallest amount of Brönsted acid sites exhibited the highest *p*-xylene selectivity. However, Fe(0.8)/H-MFI having less amount of Brönsted acid sites gave lower *p*-xylene selectivity than H-Fe,Al-silicate (Si/Fe=150). It is suggested that the iron oxide probably formed in case of high Fe loading may contribute to *p*-xylene isomerization and thus less *p*-xylene selectivity was obtained. As for the Zn-containing MFI, it has been found that the increasing order of Brönsted acid amount was inversely related to the *p*-xylene selectivity. Therefore, the moderate Brönsted acid amount should be required to suppress the *p*-xylene isomerization.

The further comparison of *p*-xylene to total xylene between Fe(0.8)/H-MFI and H-Fe,Al-silicate (Si/Fe=150); Zn(1.0)/H-MFI and H-Zn,Al-silicate (Si/Zn=150) at various reaction temperatures were given in Figures 5.15 and 5.16.

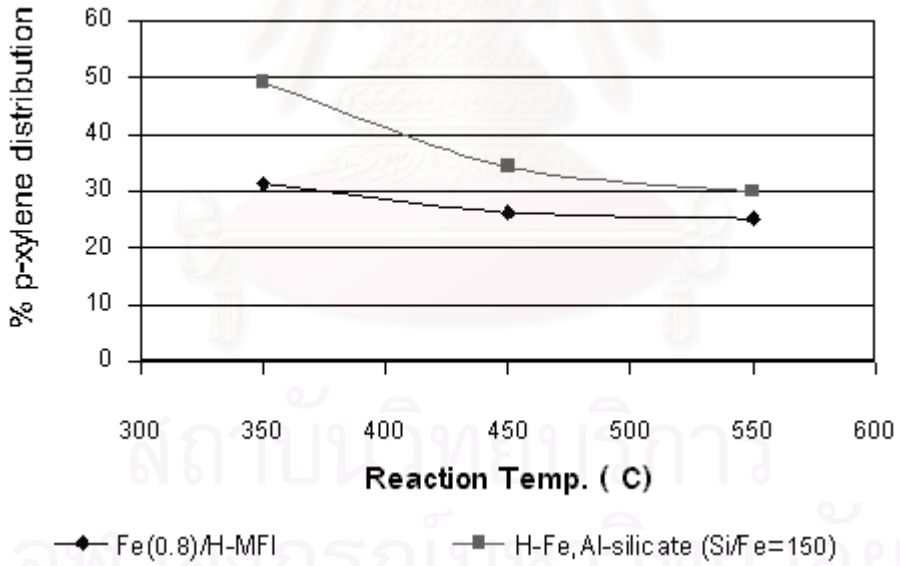

Figure 5.15 Xylene Distribution on Alkylation of Toluene with Methanol of (a) Fe(0.8)/H-MFI and (b) H-Fe,Al-silicate (Si/Fe=150)

(GHSV 6000 h^{-1}, 80 min on stream, Methanol/Toluene feed ratio 2.7-3.3 : 1 by wt.)

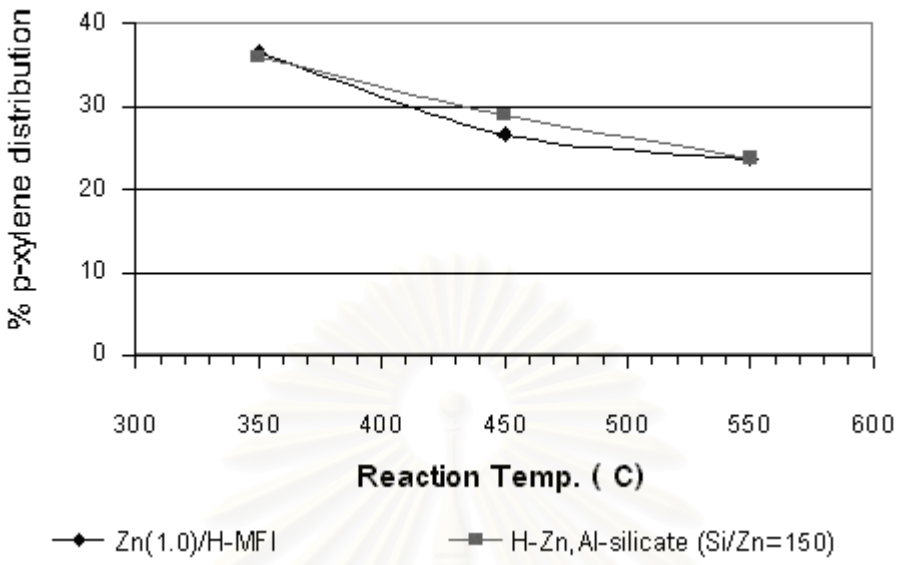

Figure 5.16 Xylene Distribution on Alkylation of Toluene with Methanol of (a) Zn(1.0)/H-MFI and (b) H-Zn,Al-silicate (Si/Zn=150)

(GHSV 6000 h^{-1}, 80 min on stream, Methanol/Toluene feed ratio 2.7-3.3 : 1 by wt.)

The higher *p*-xylene distribution was achieved with H-Fe,Al-silicate (Si/Fe=150) and H-Zn,Al-silicate (Si/Zn=150) at any reaction temperatures and thus less *p*-xylene isomerization than did Fe/H-MFI and Zn/H-MFI. Moreover, H-Fe,Al-silicate and H-Zn,Al-silicate can be prepared in only one-step crystallization and need no post-synthesis treatment by ion-exchange. The results suggested that the modification of the catalytic properties of MFI-type zeolite by loading Fe or Zn as an active component by incorporation method was rather suitable for alkylation of toluene with methanol than ion-exchanged method because of the high distribution of *p*-xylene obtained and the convenience of one-step preparation. Furthermore, the result shows that the *p*-xylene distribution was decreased while m-xylene and o-xylene distribution were increased with the increasing reaction temperature (For the more comparison, see Figs. 5.17 and 5.18).

5.2.3 Effect of Reaction Temperatures, Space Velocities and Times on Stream on Alkylation of Toluene with Methanol

Effect of reaction temperatures, space velocities and times on stream on alkylation of toluene with methanol are shown in Figs. 5.17, 5.18, 5.19, 5.20, 5.21 and 5.22 respectively.

From Figures 5.17 and 5.18, the xylene and aromatics selectivity were increased while *p*-xylene to m-xylene and *p*-xylene to o-xylene ratio were decreased markedly with the increasing reaction temperature. This results show that the progressive of alkylation reaction and the isomerization of *p*-xylene on the external surfaces and narrow pores of catalyst were activated by temperature effect.

From Figures 5.19 and 5.20, the *p*-xylene to m-xylene and *p*-xylene to o-xylene ratio were increased markedly with the increasing GHSV. This can be explained that the higher GHSV provided the shorter contact time between reactants and catalyst and hence the lower degree of *p*-xylene isomerization.

Aromatics selectivity and xylene selectivity are effected by toluene conversion which decreased rapidly with the increasing time-on-stream. Many researchers have clearly shown that the deactivation is mainly due to coke deposition on the catalysts. This idea corresponds with the results as shown in Figures 5.23. Coke deposition on both H-Fe,Al-silicate (Si/Fe=150) and H-Zn,Al-silicate(Si/Zn=150) comprise of a lot of high temperature coke. Figures 5.21(b) and 5.22(b) show the strong influence of catalyst deactivation on *p*-, *m*- and *o*-xylene distribution. It can be suggested that the distribution of xylenes depends on toluene conversion. The increase of *p*-xylene with time-on-stream reflects the suppression of xylene isomerization caused by coke deposition. Choudhary et. al. [55-57] have suggested that the increased shape selectivity was attributed mostly to an increase in the intracrystalline diffusional resistance because of the coke

deposition both at the external surface and in the catalyst channels, causing partial or complete blockage of some of the channels.

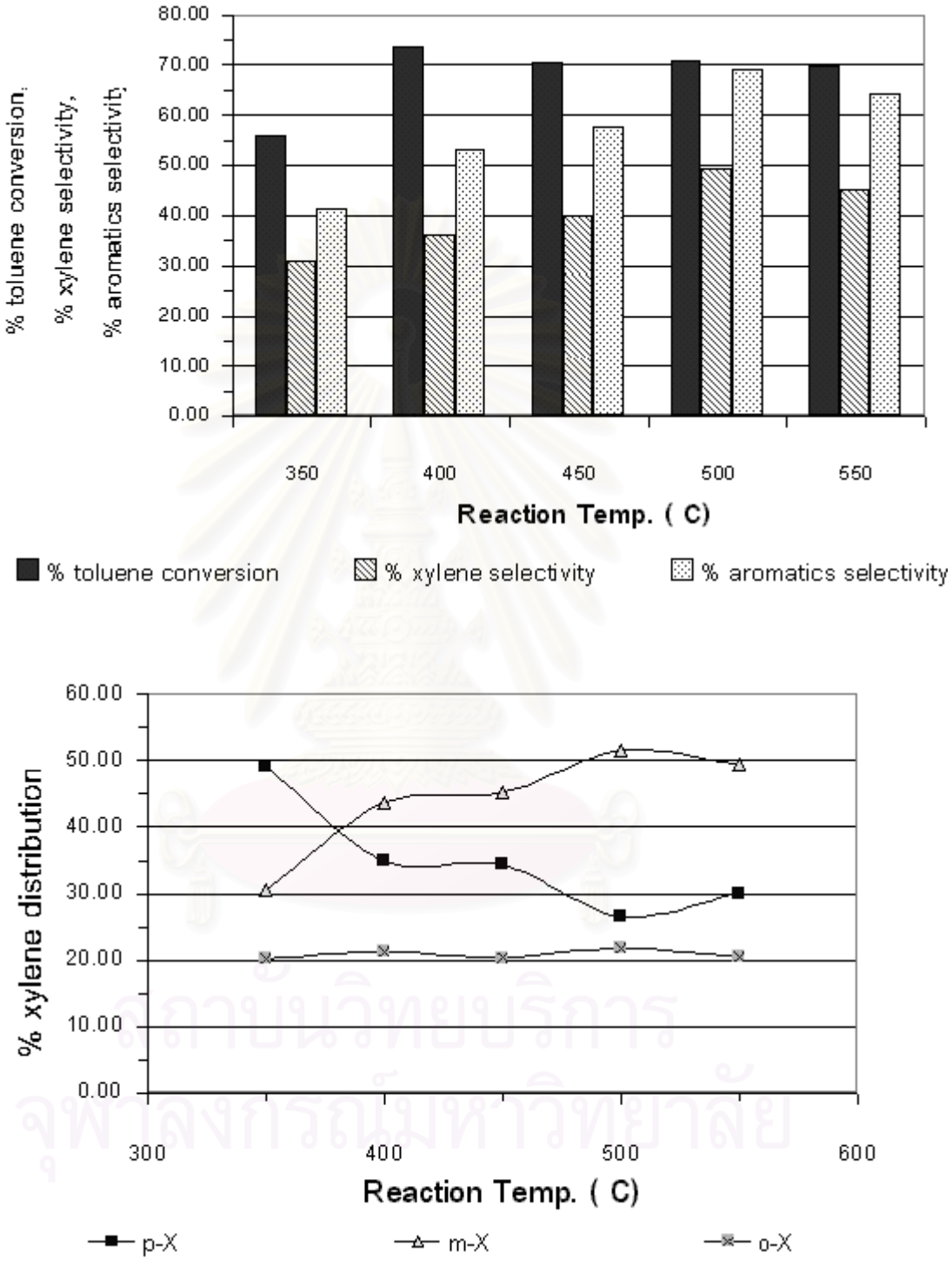

Figure 5.17 Alkylation of Toluene with Methanol on H-Fe,Al-silicate (Si/Fe=150) at Various Reaction Temperatures

(GHSV 6000 h^{-1}, 80 min on stream, Methanol/Toluene feed ratio 2.7-3.3 : 1 by wt.)

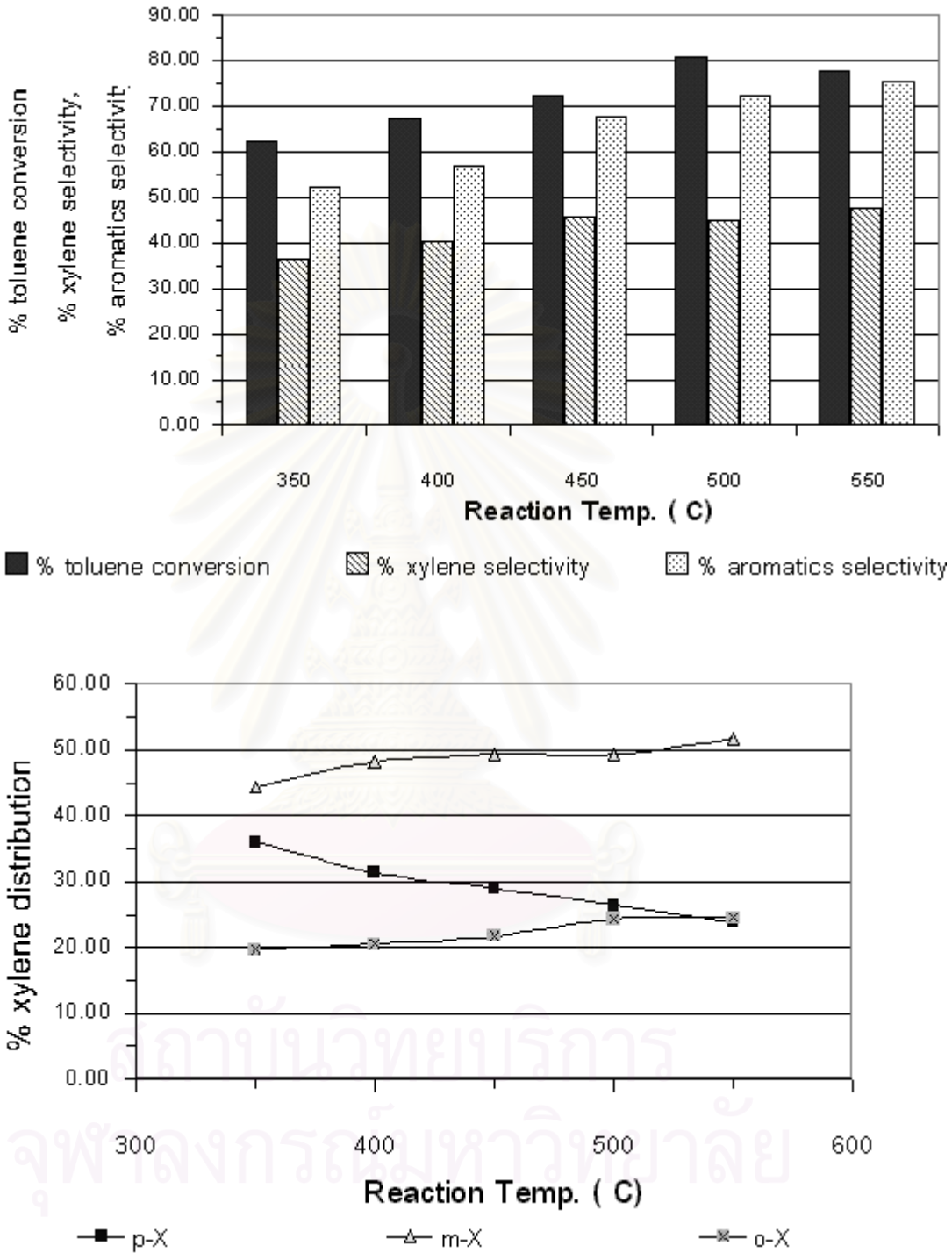

Figure 5.18 Alkylation of Toluene with Methanol on H-Zn,Al-silicate (Si/Zn=150) at Various Reaction Temperatures

(GHSV 6000 h^{-1}, 80 min on stream, Methanol/Toluene feed ratio 2.7-3.2 : 1 by wt.)

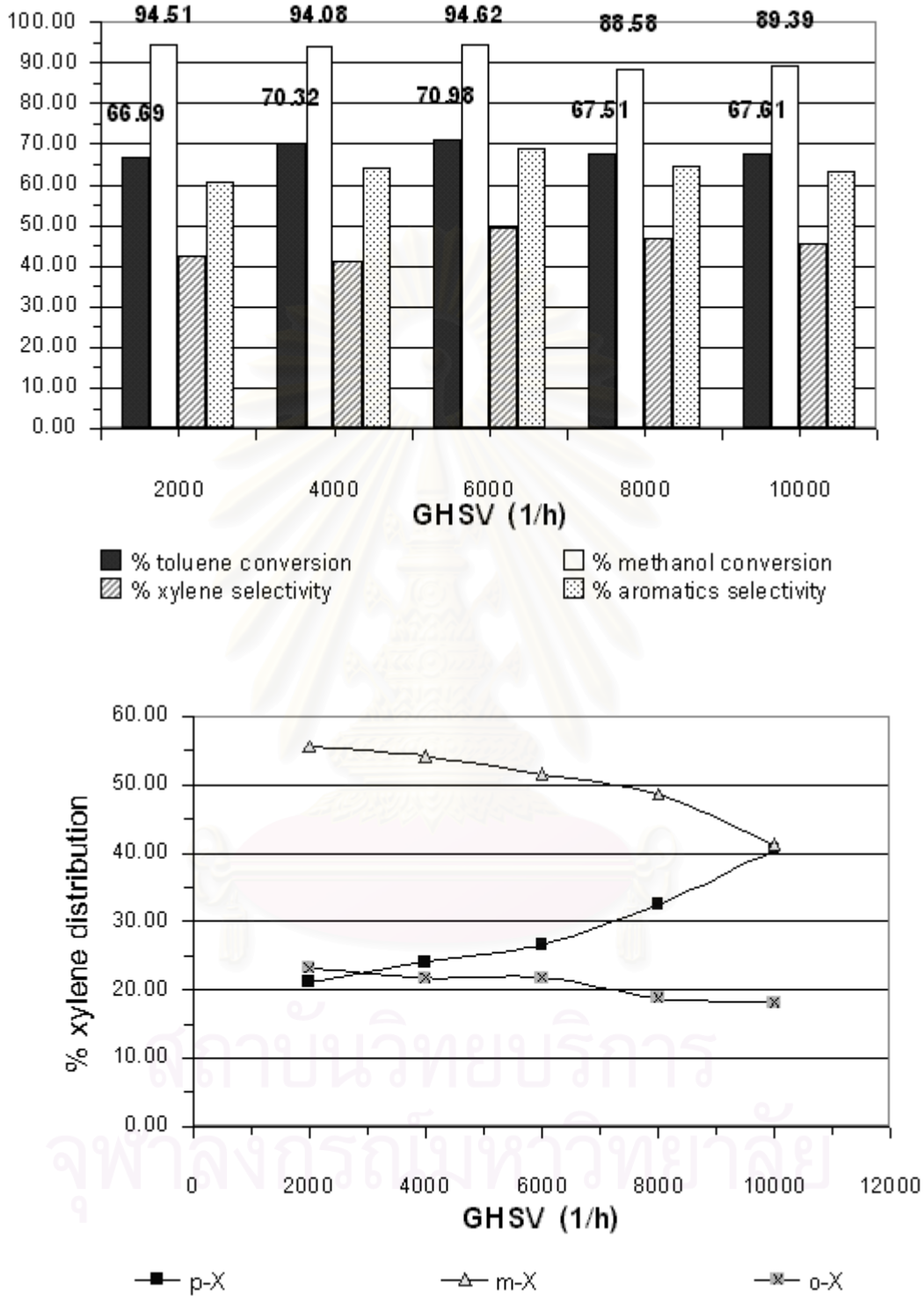

Figure 5.19 Alkylation of Toluene with Methanol on H-Fe,Al-silicate (Si/Fe=150) at Various Space Velocities

(500 ^{o}C, 80 min on stream, Methanol/Toluene feed ratio 2.7-3.2 : 1 by wt.)

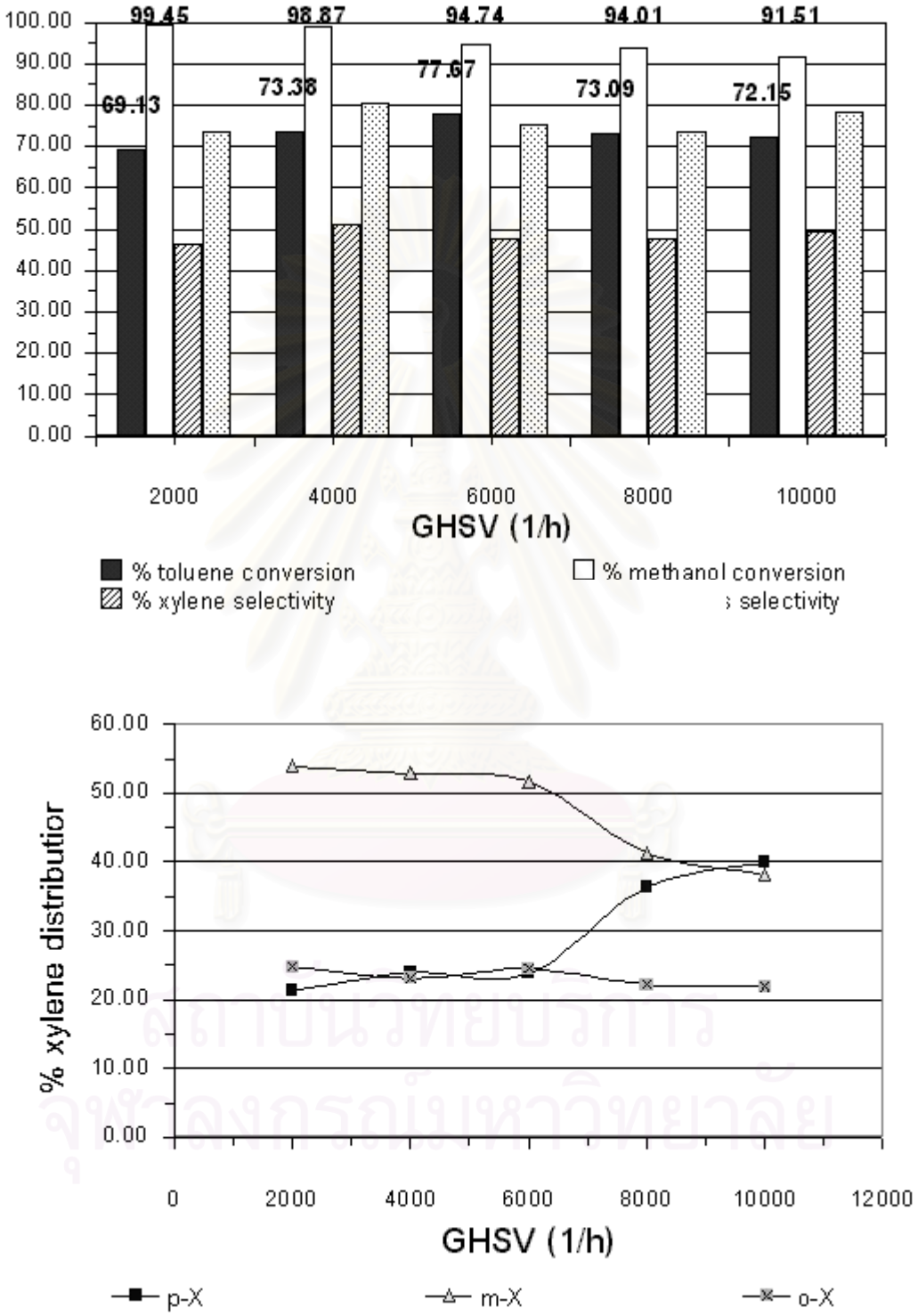

Figure 5.20 Alkylation of Toluene with Methanol on H-Zn,Al-silicate (Si/Zn=150) at Various Space Velocities

(550 ^{o}C, 80 min on stream, Methanol/Toluene feed ratio 2.7-3.2 : 1 by wt.)

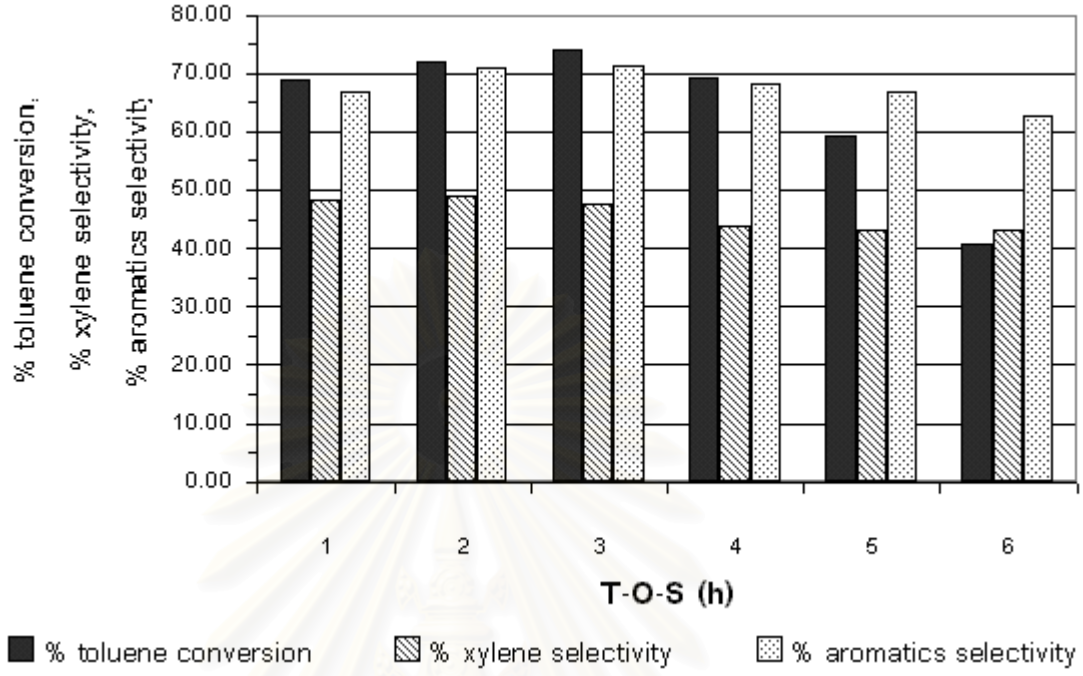

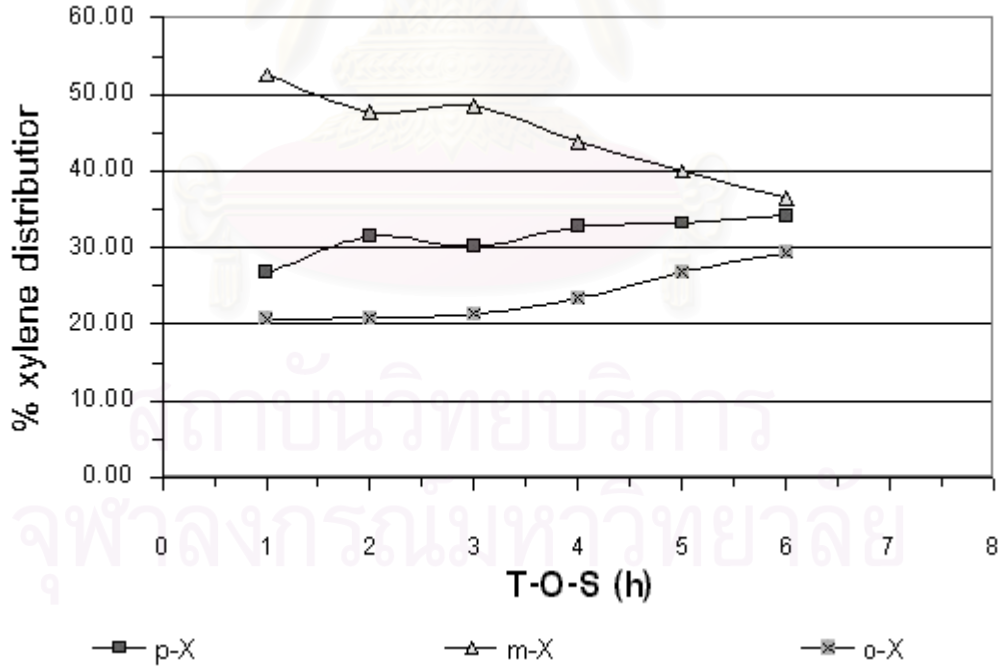

Figure 5.21 Alkylation of Toluene with Methanol on H-Fe,Al-silicate (Si/Zn=150) at Various Time-on-Stream

(550 ^{o}C, GHSV 4000 h^{-1}, Methanol/Toluene feed ratio 2.7-3.2 : 1 by wt.)

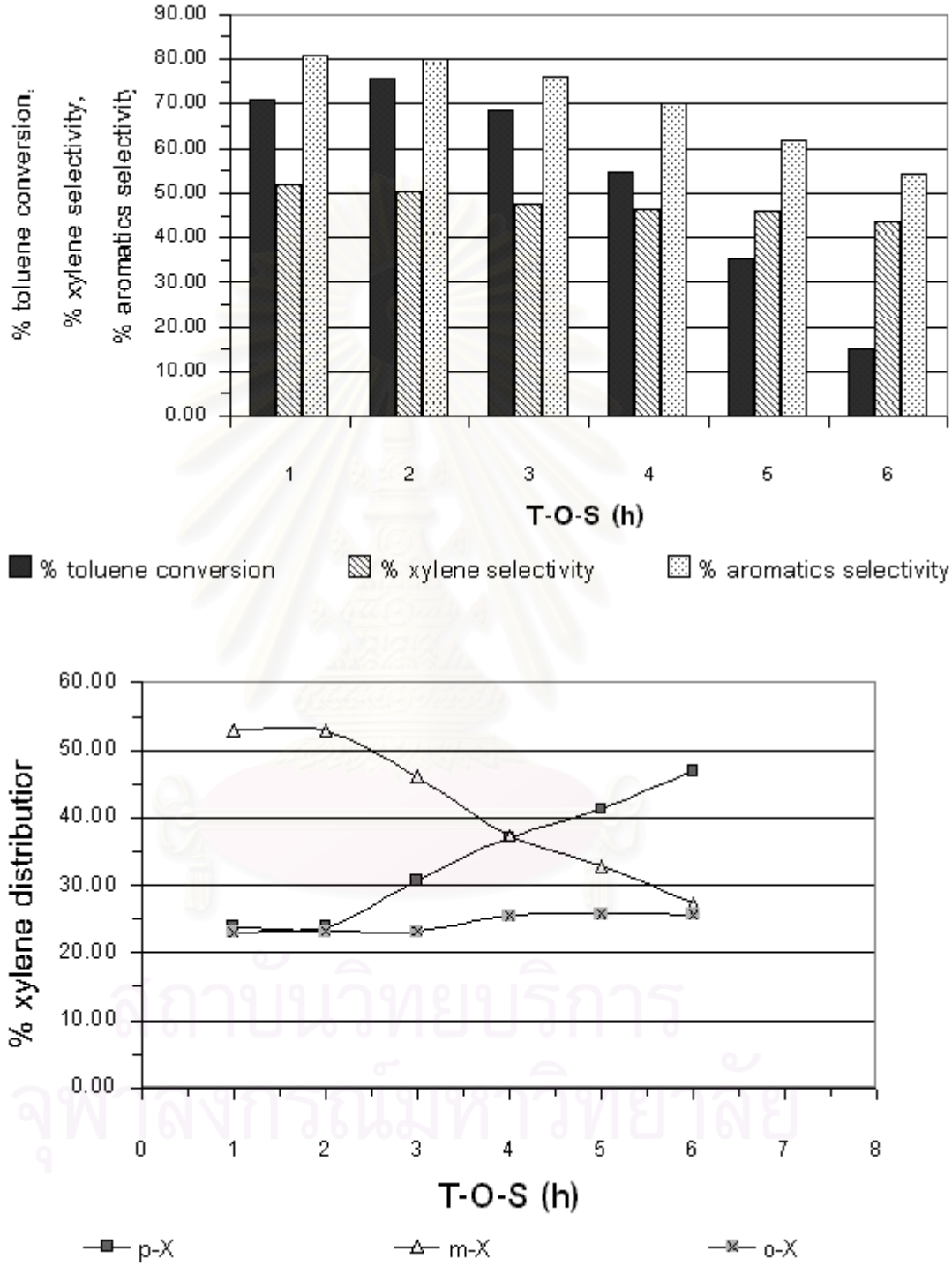

Figure 5.22 Alkylation of Toluene with Methanol on H-Zn,Al-silicate (Si/Fe=150) at Various Time-on-Stream

(500 ^{o}C, GHSV 6000 h^{-1}, Methanol/Toluene feed ratio 2.7-3.2 : 1 by wt.)

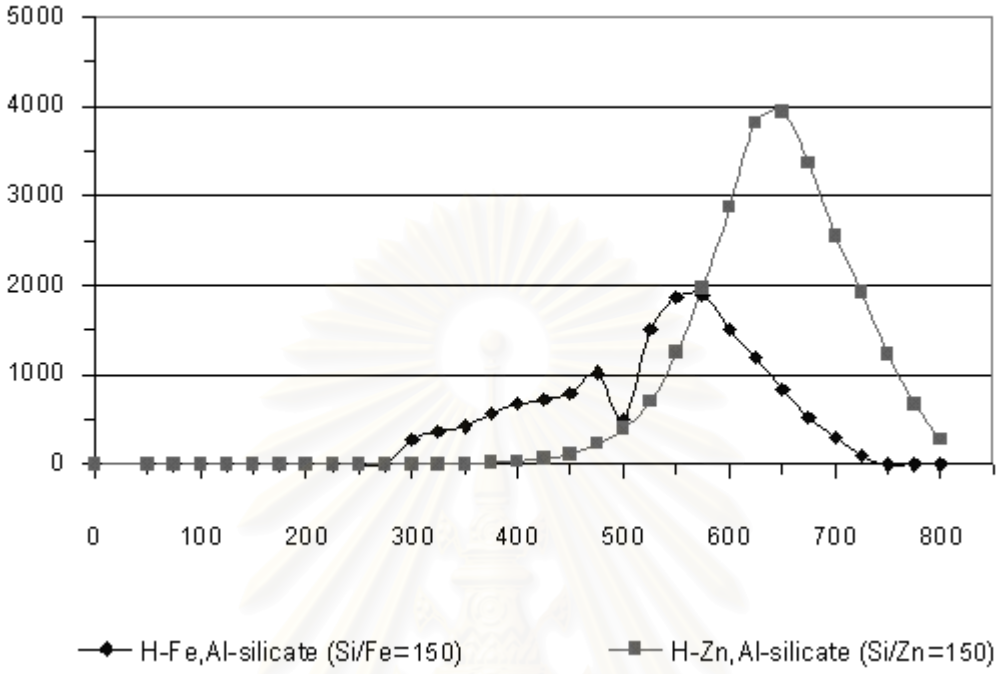

Figure 5.23 Temperature Programmed Oxidation of H-Fe,Al-silicate (Si/Fe=150) and H-Zn,Al-silicate (Si/Zn=150)

CHAPTER VI

CONCLUSIONS AND RECOMMENDATIONS

6.1 Conclusions

The alkylation of toluene with methanol was investigated on Fe or Zn containing MFI-type zeolite catalysts. Fe or Zn was introduced to the zeolite catalyst either by incorporation or by ion-exchanged method. The results obtained lead to the following conclusions.

1. The weaker Brönsted acid strength on MFI-type zeolite catalysts gave the higher *p*-xylene distribution, because the isomerization of *p*-isomer produced primarily was considerably suppressed.
2. The modification of the catalytic properties of MFI-type zeolite by loading Fe or Zn as an active component by incorporation method, Al in zeolite framework would be substituted by Fe or Zn and generated the weaker Brönsted acid strength which provide the lower isomerization of *p*-xylene and thus the higher *p*-xylene distribution was obtained from toluene methylation with methanol.
3. The isomerization of *p*-xylene may readily occur on Fe or Zn agglomerates dispersed on the external surface of the catalyst in case of the high loading amount of metal.
4. The *p*-xylene selectivity would be promoted by decreasing of reaction temperature or increasing of space velocity in order to reduce the degree of *p*-xylene isomerization or increasing of time-on-stream in order to increase shape selectivity caused by coke deposition.

6.2 Recommendations

1. Further study in detail of the oxidation state of Fe or Zn species on the surface of MFI catalyst.

2. Study of crystal size effect of zeolite MFI to *p*-xylene selectivity in alkylation *o*-toluene with methanol.

3. Study of *p*-xylene selectivity in case of the same catalysts but different reaction such as disproportionation reaction and in case of tha same reaction but different of catalysts.

4. Compare catalytic performance of alkylation of toluene with methanol reaction with liquid phase and gas phase of reactants

REFERENCES

1. S. Mater, M.J. Mirbach, and H.A. Tayim, Catalysis in Petrochemical Processes, Kluwer Academic Publisher, Dordrecht, Netherlands, 1989.
2. C.T-W. Chu, and D. Chang, *J. Phys. Chem.*, **89** (1985), 1569.
3. R.J. Arganger, and G.R. Londolt, US Patent 3702886, 1972.
4. W.W. Kaeding, C. Chu, L.B. Young, B. Weistein, and S.A. Butter, *J. Catal.*, **67** (1981), 159.
5. T. Yashima, Y. Sakaguchi, and S. Namba, *Stud. Surf. Sci. Catal.*, **7** (1981), 739.
6. J. Weitkamp, Int. Symp. in Zeolite Catalalysis, Siofok, Hungary, Acta Phys. Chem., (1985), 271.
7. J.L. Sotelo, M.A. Uguina, J.L. Valverde, and D.P. Serrano, *Ind. Eng. Chem. Res.*, **32** (1993), 2548.
8. T. Yashima, K. Sato, T. Hayasaka, and N. Hara, *J. Catal.*, **26** (1972), 303.
9. H. Itoh, A. Miyamoto, and Y. Murakami, *J. Catal.*, **64** (1980), 284.
10. H. Itoh, T. Hattori, K. Suzuki, and Y. Murakami, *J. Catal.*, **79** (1983), 21.
11. C.D. Chang, and A.J. Silvestri, *J. Catal.*, **47** (1977), 249.
12. G. Paparatto, E. Moretti, G. Leofanti, and F. Gatti, *J. Catal.*, **105** (1987), 227.
13. N.Y. Chen, *J. Catal.*, **114** (1988), 17.
14. D. Franenkel, and M. Levy, *J. Catal.*, **118** (1989), 10.
15. J.H. Kim, S. Namba, and T. Yashima, *Bull. Chem. Soc. Jpn.*, **61** (1988), 1051.
16. J.-H. Kim, S. Namba, and T. Yashima, *Zeolites*, **11** (1991), 59.
17. F. Lonyi, J. Engelhardt, and D. Kallo, *Zeolites*, **11** (1991), 169.
18. T. Inui, H. Nagata, O. Yamase, H. Matsuda, T. Kuroda, M. Yoshikawa, T. Takeguchi, and A. Miyamoto, *Appl. Catal.*, **24** (1986) 257.
19. G. Mirth, and J.A. Lercher, *J. Catal.*, **132** (1991), 244.

20. P.A. Parikh, N. Subramanyum, Y.S. Bhat, and A.B. Halgeri, *Catal. Lett.*, **14** (1992), 107.

21. M.A. Uguina, D.P. Serrano, R. Grieken, and S. Venes, *Appl. Catal.*, **99** (1993), 97.

22. V. Bhandarkar, and S. Bhatia, *Zeolites*, **14** (1994), 439.

23. P. Smirniotis, and E. Rukenstien, *Ind. Eng. Chem. Res.*, **34** (1995), 1517.

24. G. Mirth, H.D. Wanzenboeck, and J.A. Lercher, *Stud. Surf. Sci. Catal.*, **94** (1995), 449.

25. J.G. Wang, Y.W. Li, S.Y. Chen, and S.Y. Peng, *Zeolites*, **15** (1995), 288.

26. Y.S. Bhat, J. Das, K.V. Rao, and A.B. Halgeri, *J. Catal.*, **159** (1996), 369.

27. S. Bordiga, R. Buzzoni, F. Geobaldo, C. Lamberti, E. Giamello, A. Zecchina, G. Leofanti, G. Petrini, G. Tozzola, and G. Vlaic, *J. Catal.*, **158** (1996), 486.

28. H. Berndt, G. Lietz, B. Lucke, and J. Volter, *Appl. Catal.*, **146** (1996), 351.

29. R. Szostak, Molecular Sieves Principle of Synthesis and Identification, Van Nostrand Reinhold, New York, 1989.

30. W.O. Haag, R.M. Lago, and P.B. Weiss, *Nature*, **309** (1984), 589.

31. D.H. Olsen, G.T. Kokotailo, and S.L. Lawton, *J. Phys. Chem.*, **85** (1981), 2238.

32. F. Liebau, Structural Chemistry of Silicates, Springer-Verlag, Berlin, 1985.

33. W.M. Meier, D.H. Olsen, Atlas of Zeolite Structure Type, International Zeolite Association, IZA, Zurich, 1978.

34. E.M. Flanign, J.M. Bennett, R.W. Grose, J.P. Cohen, R.L. Patton, and R.M. Kirchne, *Nature*, **271** (1978), 512.

35. J.R. Anderson, K. Foger, T. Mole, R.A. Rajiadhyaksha, J.V. Sanders, *J. Catal.*, **58** (1979), 114.

36. T. Sano, K. Fujisawa, and H. Higiwara, *Stud. Surf. Sci. Catal.*, **34** (1987), 74.

37. D. Barthoment, Zeolites Science and Technology, Matinus Nighoff Publishers, The Hauge, 1984.

38. K. Tanabe, M. Misona, Y. Ona, and H. Hattori, *Stud. Surf. Sci. Catal.*, **51** (1989), 142.

39. V.S. Nayak, and V.R. Choudhary, *Appl. Catal.*, **4** (1982), 333.

40. V.S. nayak, and V.R. Choudhary, *Appl. Catal.*, **10** (1984), 137.

41. J. Dwyer, *Disc. Faraday Soc.*, **72** (1981), 376.

42. S.M. Csicsery, *Zeolites*, 4 (1984), 202.

43. E.G. Derouane, New Aspects of Molecular Shape Selectivity, Catalysis by Zeolites, (B. Lmelik, et al.), Elsevier, Amterdam, 1980.

44. D.W. Breck, Zeolite Molecular Sieves, Wiley, New York, 1974.

45. T. Inui, O. Yamase, K. Fukada, A. Itoh, J. tarumoto, N. Morinaga, T. Hagiwara, and T. takegami, Proc. 8th Congress on catalysis, West Berlin, 1984.

46. T. Inui, Zeolite Synthesis (ACS Symposium Series 398), Amer. Chem. Soc., Washington D.C. (1989), 479.

47. S.K. Yong and S.A. Wha, *Microporous and Mesoporous Materials*, **30** (1999), 283

48. Meier, Olson and Baerlocher, Atlas of Zeolite Structure Types, (1996), 525.

49. F. Pal, B.N. Janos, K. Kristof, and V. Gyorgy, *Appl. Catal.*, **145** (1996), 155.

50. H.G. Karge, *Microporous Materials*, **22** (1998), 547.

51. J. Connerton, R. Joyner, and M. Padley, *J. Chem. Soc. Faraday Trans.*, **91** (1995), 1841.

52. M. Campbell, M. Bibby, M. Coddington, F. Howe, and H. Meinhold, *J. Catal.*, **161** (1996), 358.

53. H.G. Karge, *Microporous Materials*, **22** (1998), 547.

54. G. Paparatto, G. de Alberti, G. Leofanti and M. Padovan, *Stud. Surf. Sci. Catal.*, **41** (1989), 225.

55. V.R. Choudhary, P. Devadas, A.K. Kinage, C. Sivadinayana and M. Guisnet, *J. Catal.*, **158** (1996), 537.

56. V.R. Choudhary, C. Sivadinayana, A.K. Kinage, P. Devadas and M. Guisnet, *Appl. Catal.*, **136** (1996), 125.

57. V.R. Choudhary, P. Devadas, A.K. Kinage, and M. Guisnet, *Zeolites*, **18** (1997), 188.

58. A. Man and P. Amorn, Principles and Techniques of Instrumental Analysis, Chulalongkorn Publisher, 1994.

LIST OF PUBLICATIONS

1. The Proceeding of Regional Symposium on Chemical Engineering, Manila, Philippines, 1998.

2. Journal of Science Faculty, Chiang Mai University, Thailand, 1999.

3. The 8th Asian Pacific Confederation of Chemical Engineering, Seoul, Korea, 1999.

4. 2nd Asia-Pacific Congress on Catalysis (APCAT 2000), Sydney, Australia, 2000.

5. Korean Journal of Chemical Engineering, Korean, 2000.

APPENDICES

APPENDIX A

SAMPLE OF CALCULATIONS

A-1 Calculation of Metal Used for Catalyst Preparation

The calculations are based on weight of "Sodium Silicate" ($Na_2OSiO_2.H_2O$) in G2 and S2 solutions.

Using Sodium Silicate 69.00 (g) with 45.00 (g) of water as a G2 and S2 solutions.

Molecular Weight of Si = 28.0855
Molecular Weight of SiO_2 = 60.0843
Weight Percent of SiO_2 in Sodium Silicate = 28.5

Mole of Si used = wt. x (%) x (M.W. of Si) x (1 mole)
100 (M.W. of SiO_2) (M.W. of Si)
= 69.00 x (28.50/100) x (1/60.0843)
= 0.3273 (mole)

• To prepare MFI catalyst at Si/Al atomic ratio of 40 by using $AlCl_3$ for aluminum source. (Adding in G1 and S1 solutions)

Molecular Weight of Al = 26.9815
Molecular Weight of $AlCl_3$ = 133.3405

Mole of Al required = 0.3273/40 = 8.125×10^{-3} (mole)
Mole of $AlCl_3$ required = $1/1 \times 8.125 \times 10^{-3} = 8.125 \times 10^{-3}$ (mole)
Amount of $AlCl_3$ used = $8.125 \times 10^{-3} \times 133.3405$ = 1.0911 (g)

• To prepare Fe,Al-silicate with Si/Fe atomic ratio of 150 by using $Fe(NO_3)_3.9H_2O$ for iron source. (Adding in G1 and S1 solutions)

Molecular Weight of Fe = 55.8470
Molecular Weight of $Fe(NO_3)_3.9H_2O$ = 399.8470

Mole of Fe required = 0.3273/150 = 2.182×10^{-3} (mole)
Mole of $Fe(NO_3)_3.9H_2O$ required = $1/1 \times 2.182 \times 10^{-3} = 2.182 \times 10^{-3}$ (mole)
Amount of $Fe(NO_3)_3.9H_2O$ used = $2.182 \times 10^{-3} \times 399.8470$ = 0.8725 (g)

• To prepare Zn,Al-silicate with Si/Zn atomic ratio of 150 by using $Zn(NO_3)_2.6H_2O$ for zinc source. (Adding in G1 and S1 solutions)

Molecular Weight of Zn = 65.37000

Molecular Weight of $Zn(NO_3)_2.6H_2O$ = 297.3700

Mole of Zn required = $0.3273/150 = 2.182 \times 10^{-3}$ (mole)

Mole of $Zn(NO_3)_2.6H_2O$ = $1/1 \times 2.182 \times 10^{-3} = 2.182 \times 10^{-3}$ (mole)

Amount of $Zn(NO_3)_2.6H_2O$ used = $2.182 \times 10^{-3} \times 297.3700 =$ <u>0.6489 (g)</u>

Amount of Al, Fe and Zn used in catalyst preparation at different ratios calculate as described above.

A-2 Calculation of Metal Loading in Ion-exchanged MFI Catalysts

• To prepare Fe(0.8)/H-MFI, Fe/H-MFI with Fe loading content of 0.80 wt.%

Amount of Fe loading = 0.80 (wt.%)

H-MFI used = 3.00 (g)

So that, Fe/(3.00 + Fe) = 0.80/100

Thus, Fe used = (0.80 x 3.00)/(100 - 0.80) (g)

$Fe(NO_3)_3.9H_2O$ used = <u>0.0242 (g)</u>

Amount of Fe and Zn in Fe/H-MFI and Zn/H-MFI at different % loading calculate as described above.

A-3 Calculation of Volumetric Flow Rate

The catalyst used 0.25 (g)

Packed catalyst into quartz reactor (inside diameter = 0.60 cm.)

Determine the average high of catalyst bed = H (cm.)

So that, Volume of catalyst bed = $\pi \times (0.30)^2 \times H$ (cm^3)

Used Gas Hourly Space Velocity (GHSV) = 6000 (h^{-1})

$$GHSV = \frac{\text{Volumetric flow rate}}{\text{Volume of catalyst bed}}$$

Thus, Volumetric flow rate = GHSV x Volume of catalyst bed

= $6000 \times \pi \times (0.30)^2 \times H$ (cm^3/h)

= $(6000 \times \pi \times 0.30^2 \times H)/60$ ($cm^3/min.$)

A-4 Calculation of Conversion and Product Distribution

For example
Catalyst: H-Fe,Al-silicate (Si/Fe = 150)
Reaction Condition: Catalyst wt. = 0.2499 (g), Reaction Temp. = 500 (^{o}C),
GHSV = 6000 (h^{-1}), Time on Stream = 90 (min.)

Data
Feed (From OV-1 Column)
Table A-1

Species I	Area
Methanol	224243.5
Toluene	262789.0

Product (From OV-1 Column)
Table A-2

Species I	Area
C1-C4 (Methanol free)	136563.0
Methanol	12161.5
C5-C8	6313.5
Benzene	3512.0
Toluene	76324.5
Ethylbenzene	1534.5
(p+m)Xylene	162331.0
o-Xylene	45638.0
Ethyltoluene	80296.5
Others	18968.0

Xylene Distribution (From Bentone Column)
Table A-3

Xylene isomer	Area	% Area
p-Xylene	161408.5	25.76
m-Xylene	325259.0	51.90
o-Xylene	139983.0	22.34

Calculation
• The roughly method to separate area of (p+m)Xylene in OV-1 column.
From Table A-2 and A-3, area of (p+m)Xylene in OV-1 column can be divided to

$$p\text{-Xylene in OV-1} = 162331.0 \times \frac{25.76}{(25.76 + 51.90)} = 53845.6$$

$$m\text{-Xylene in OV-1} = 162331.0 \times \frac{51.90}{(25.76 + 51.90)} = 108485.4$$

• Calculation of Conversion

$$\% \text{ Conversion of species I} = \frac{\text{I(in)} - \text{I(out)}}{\text{I(in)}} \times 100$$

From Table A-1 and A-2, we can conclude that

Methanol conversion (%) $= \frac{(224243.5 - 12161.5)}{224243.5} \times 100$

$= \underline{94.62}$

Toluene conversion (%) $= \frac{(262789 - 76324.5)}{262789} \times 100$

$= \underline{70.96}$

• Calculation of Product Distribution

$$\% \text{ Product distribution of species I} = \frac{(A_I / F_I)}{(\text{Sum. of } A_I / F_I)} \times 100$$

When A_I and F_I refer to area and corrective factor of species I, respectively. (For list of F_I see Appendix B)

Calculation of product distribution are shown in Table A-4.

Table A-4

Species I	Area	F	A/F	% wt.
C1-C4 (Methanol free)	136563.0	1.275	107108.235	20.13
Methanol	12161.5	0.348	34946.839	6.57
C5-C8	6313.5	1.000	6313.500	1.19
Benzene	3512.0	0.698	5031.519	0.95
Toluene	76324.5	1.102	69259.982	13.02
Ethylbenzene	1534.5	0.977	1570.624	0.30
p-Xylene	53845.6	0.955	56382.827	10.60
m-Xylene	108485.4	0.994	109140.241	20.52
o-Xylene	45638.0	0.987	46239.108	8.69
Ethyltoluene	80296.5	1.043	76986.098	14.47
Others	18968.0	1.000	18968.000	3.57

APPENDIX B

LIST OF CORRECTIVE FACTOR

List of Corrective Factor
(Calculate from OV-1 Column in GC-14A)

Compound	Corrective factor, F
Methanol	0.348
Methane	1.329
Ethane	1.321
Ethylene	1.307
Propane	1.328
Propene	1.240
Butane	1.242
Butene	1.159
Pentane	1.000
Pentene	0.970
n-Hexane	1.040
n-Hexene	0.673
n-Heptane	1.025
n-Octane	1.197
Benzene	0.698
Toluene	1.102
Ethylbenzene	0.977
p-Xylene	0.955
m-Xylene	0.994
o-Xylene	0.987
p-Ethyltoluene	0.905
m-Ethyltoluene	1.186
o-Ethyltoluene	1.038

* F_I of OV-1 column in GC-14A calculate as described in previous study [58.]

VITA

Mr. Thana Punsupsawat was born on March 28, 1973 in Bangkok, Thailand. He graduated Bachelor's Degree of Science from Department of Chemical Technology, Chulalongkorn University in 1995. Then, he has continued studying in Doctoral degree of Engineering from the department of Chemical Engineering, Chulalongkorn University since May, 1995.